AN ABSTRACT OF THE THESIS OF

Kenneth D. Bomben for the degree of Doctor of Philosophy in Chemistry presented on November 11, 1980.

Title: Photoelectron Spectroscopy of Small Molecules

Abstract approved: Redacted for Privacy
(T. Darrah Thomas)

The photoelectron spectra of a series of halogenated molecules have been investigated in the gas phase. Both core-ionization energies and Auger kinetic energies were measured to probe the nature of the interaction that holds a core electron to the molecule.

It was found that satellite structure (shake) could be used to predict the amplitude attenuation in the Br_2 EXAFS spectrum. Inclusion of multielectron processes into the theory that predicts the EXAFS amplitude provides a more accurate representation of the EXAFS spectrum if certain assumptions about the threshold of shake are valid.

The satellites can be used to investigate the nature of the transitions themselves. In the case of argon, the transitions arise from Rydberg processes that excite a 3p valence electron to the 4p or 5p.

In addition, the shake structure allows a measurement of the relaxation energy. The difference between the average energy of a spectrum, including shake, and the energy of the main peak in that spectrum is equal to the

difference between the Koopmans' theorem "frozen orbital" state and the fully relaxed state. This is the total relaxation. Difference spectra can then be used to get at the extra-atomic relaxation. Comparison with the values of extra-atomic relaxation arrived at via other methods shows that this method yields comparable results.

Investigation of the extra-atomic relaxation energy by means of the Auger parameter was found to yield information on the nature of electronegativity. Quantitative and qualitative comparisons of the relative values of extra-atomic relaxation as well as of initial-state effects (chemical shifts) lead to conclusions that are in excellent accord with chemical experience.

The correlation between core-ionization potentials and gas-phase acidities breaks down for certain compounds. It was found that the failure arises from the inability of certain aromatic compounds to undergo the same geometric rearrangent upon protonation as their aliphatic analogs.

Other experiments into the nature of the dipole of ClF have indicated that, contrary to chemical intuititon and theoretical evidence, the negative end of the dipole may be on the chlorine atom. An investigation of the charge distribution, corrected for relaxation effects, shows that this conclusion is not supported and that the more recent experimental results are correct.

An attempt was made to measure the difference between

the core-ionization energy of a diatomic molecule and a monatomic dissociation product. While difficulties in experimental procedure made it impossible to measure the core-ionization energy of the atom, an estimate of the magnitude of the relative extra-atomic energy was made.

Photoelectron Spectroscopy of Small Molecules

by

Kenneth D. Bomben

A THESIS

submitted to

Oregon State University

in partial fulfillment of
the requirements for the
degree of

Doctor of Philosophy

Completed November 11, 1980

Commencement June 1981

APPROVED:

Redacted for Privacy

Professor of Chemistry
in charge of major

Redacted for Privacy

Chairman of the Department of Chemistry

Redacted for Privacy

Dean of the Graduate School

Date thesis is presented November 11, 1980

Typed by Rand Dow for Kenneth D. Bomben

DEDICATION

To my father,

while he never lived to see it completed, he never doubted that I could do it. I dedicate this work to him.

ACKNOWLEDGEMENTS

There are a great many people who have contributed to this work in word, thought and action. Some of them deserve special mention.

First, to the graduate students who shared lab and office space; Dr. Steven Smith, Dr. Scott Chambers and Mr. Gary Nolan. The time spent in discussion and exchange of ideas with each of you has added to my understanding of Chemistry and the nature of the physical world.

Special thanks are due to those undergraduates who, in learning, also taught; Mr. Pat Sitton, Mr. George Traugh, Mr. Ed Aitken, Mr. Loren Lucason and Mr. Mark Ungs. Your contribution to my education cannot be overestimated.

I owe the post-doctoral and visiting fellows a thanks for conversations and discussions that aided the course of this research; Drs. Seppo and Helena Aksela, Dr. James Jen, Dr. Mahinder Bahl, Dr. James Gimzewski, Dr. Leon Ungier and Dr. Peter Weightman. The truly international flavor that you added to the time I spent here shall not be forgotten.

Of special importance was the influence of Dr. T. Darrah Thomas, whose ability to cut to the heart of any problem makes Physical Chemistry seem easy. Of all the thanks I owe, the one I owe you is the hardest to put into words and the most important. Without your influence and guidance, I could not have accomplished what I did.

There have been outside contributions to this research. In particular, I wish to thank Dr. Arthur Ashe, III and Dr. Frank Larkins for suggesting or improving a research problem and Dr. Joseph Nibler for providing some of the chemicals used.

There are others who deserve mention, in particular Mr. John Archibald and Mr. Doyle Woodrow. Their hands are evident in the construction and design of several projects. Thanks are also due to Mr. Rand Dow whose computer printed this thesis and whose understanding of the little beasties known as computers has been of incalculatable assistance.

I gratefully acknowledge the support of the Department of Chemistry and of the National Science Foundation.

To the fellow students and friends who were important in this endeavor, your fellowship has lent much to my self-confidence. To Chris, Thom, Howard, Rich, Arnie, Scott, Krys, Ron and Ed, thanks.

My family has been important in seeing me through. My mother and my in-laws have had a confidence in my ability that never waivered. To my wife, Carol, who has stood by me through the tough times with love and understanding, you have helped more than I can say, thank you is somehow not enough. I trust that you understand.

TABLE OF CONTENTS

VI. APPENDICES

LIST OF FIGURES

LIST OF TABLES

PHOTOELECTRON SPECTROSCOPY OF SMALL MOLECULES

I. GENERAL INTRODUCTION

Photoelectron spectroscopy (PES) has its origins embedded in a physical principle that has been understood for seventy-five years -- the photoelectric effect. First observed accidentally by Hertz[1] in 1887, the effect was explained by Einstein[2] in 1905 by the use of the concept of quanta of energy. A photon, impinging on a metal surface, can cause the emission of an electron only if the photon has sufficient energy to overcome the energy that holds the electron to the metal. To a good approximation, this energy corresponds to the ionization energy of the orbital from which the electron is removed. With the introduction of the quantum concept of electrons in atoms and molecules in the mid-1920's, it became clear that investigation of orbital energies would lead to a better understanding of a variety of chemical and physical phenomena. However, it was necessary to wait until the 1960's and the development of the technology to measure electron energies to high resolution before chemists became aware of the potential of PES.

The bombardment of atoms or molecules with photons of sufficient energy can cause the ejection of an electron from any energy level in the sample, valence or core.

Since each atom has a unique set of such energy levels, PES can be used as an analytical probe for each atom in a surface or molecule. The valence region of molecules is being investigated via ultraviolet photoelectron spectroscopy (UPS) thanks to the pioneering work of Turner[3]. The study of core levels has been the primary concern of X-ray photoelectron spectroscopy (XPS) and was developed through the work of Siegbahn and colleagues[4,5] at the same time as UPS. (The basic concept of XPS was conceived as early as 1914[6].) Although the core levels studied by XPS are not greatly affected by changes in the chemical environment of the atom, the small chemical shifts that are observed between one molecule and a free atom or between a molecule and a reference molecule are of considerable chemical interest.

It is possible to separate these chemical shifts into two components, one arising from the initial charge distribution in the molecule, and the other from rearrangement of charge during ionization. These both depend upon the chemical environment and allow XPS to probe into other physical and chemical parameters. (See Chapter II, Section A.)

Another process of interest is the manner in which the excited sample loses energy. The Auger effect, discovered in 1923[7], occurs when an atom or molecule with a core vacancy loses energy by electron emission. Auger electron spectroscopy (AES) is used to study shifts in Auger

energies between a molecule and either a free atom or a reference molecule. These shifts can also be separated into ground-state and final-state components. Since the Auger process is different from the photoionization process, a comparison of the shifts arrived at via XPS and those of AES allows, by means of the Auger parameter, a separation of initial- and final-state effects. (See Chapter II, Section C.)

In addition to the primary core-ionization, additional electronic excitations can occur simultaneously. These are observed as satellite lines on the low-kinetic-energy side of the primary peak. Ejection of a core electron causes valence shell excitations to unoccupied bound or continuum states. The terms "shakeup" and "shakeoff" have been used to describe these processes. Study of these processes in molecules is accomplished more readily in the gas phase than in the solid phase because the latter has higher backgrounds, extrinsic energy loss structures, and charging effects to confuse the investigator. The one drawback is that intensities are low in the gas phase. (See Chapter II, Section B.)

An outgoing electron, treated as a plane wave, can interact with other atoms in the molecule and create back-scattered plane waves that constructively and destructively interfere with the outgoing wave. This leads to oscillations in the photon absorption cross section, which may be

observed via the technique of extended X-ray absorption fine structure (EXAFS) spectroscopy. The inelastic processes of shakeup and shakeoff also generate EXAFS spectra of their own, shifted in energy from the elastic EXAFS by an amount equal to the excitation energy of the ion. The total EXAFS should then be the sum over the individual processes. The interference between the primary EXAFS process and the secondary processes should lead to a reduction in the EXAFS amplitude. One of the goals of this research was to measure the XPS spectrum of Br_2 and determine the EXAFS amplitude reduction factor. (See Chapter II, Section B.)

It may be possible to get direct measurements of the final-state or relaxation effects if comparisons are made between gaseous and condensed phases of atoms. For example:

$$I_2(g) \iff 2I(g)$$
$$M(s) \iff M(g)$$

In these comparisons, and other similar ones, the initial-state contribution to the relative ionization energies should be close to zero and any chemical shift should be entirely due to the final-state contributions. However, most such reactions require high temperatures in order to maintain a concentration of the rare species sufficient to measure its core-ionization potential. (See Chapter II,

Section D.) Another of the directions of this research has been to construct such a high temperature device. (Also see Appendix C.)

This research has also been directed toward the construction and operation of a hollow-anode X-ray source capable of 1500 watts. This source enhanced the counting rates in our experiments as much as ten-fold over the previous 100 watt source[8]. (See Appendix A.) Additionally, to ensure the safe operation of this new source, a safety device was designed and incorporated into the spectrometer. (See Appendix B.)

II. THEORETICAL FRAMEWORK

A. IONIZATION ENERGY

Schematically, an atom, in its ground state, with a kinetic energy of kT, is placed in a radiation field. At some time, t, a photon with energy hν enters the vicinity of the atom. There is a probability that the photon will be absorbed.

Three important processes that can remove photons from a beam of electromagnetic radiation are pair production, the Compton effect, and the photoelectric effect. For photon energies up to 5000 electron volts (5 keV) the only important interaction is the photoelectric effect. In addition, only the photoelectric effect occurs with the dipole-interaction ejection of an electron.

Knowledge of the photon energy and measurement of the kinetic energy of the ejected photoelectron leads, via conservation of energy, to the energy with which the ejected electron was held to the atom, the ionization energy, E_i, of the atom, a[9].

$$h\nu - KE = E_i(a) + r_I \qquad \text{(II.1)}$$

KE is the kinetic energy of the ejected electron, the energy that the electron carries away, and is determined from the focus voltage and geometry of the spectrometer. r_I is the recoil energy of the ion, the energy imparted to

the nuclear system by conservation of momentum. The recoil term is small since it is proportional to the ratio of the mass of the electron to the mass of the ion, m_e/m_I, and even in the extreme case of hydrogen is only about 0.03%. Nonetheless, r_I is accounted for in the calculations reported here. E_i is then easily determined experimentally.

E_i may also be determined theoretically, by calculating the difference between the energy of the initial state and the energy of the final state. One such method makes use of the Hartree-Fock self-consistent field (ΔSCF) calculation[10]. (It should be mentioned that this method has deficiencies due to inadequate treatment of the correlation energy.) It is possible, with the use of Koopmans' theorem[11], to approximate the ionization potential by a calculation of the initial state of the energy level of interest. However, these calculations require that the energy so calculated be the energy of that shell in the ground state. This is the so-called "frozen orbital approximation" and as such ignores the fact that the electrons in the remaining atomic shells can relax toward the core hole and provide a stabilization energy to the ion being formed. Hence the theoretical Koopmans' theorem ionization energy, E_{KT}, (which is equal to the orbital energy, but with opposite sign; $-\varepsilon$) is different from the experimental atomic ionization energy, $E_i(a)$, by

R_i, the intra-atomic rearrangement energy, also called the intra-atomic relaxation energy.

$$E_i(a) = E_{KT} - R_i \qquad \text{(II.2)}$$

This relaxation energy has been calculated by Gelius[12]. Its magnitude turns out to be 75 to 85% of the square root of the final energy of the ion, when both quantities are expressed in eV. We will use Equation II.2 as a close approximation to the ionization energy of an isolated atom.

In molecules, the atom being probed is affected by two additional considerations. First, the interaction of the atom with its neighbors causes a change in atomic levels, ΔE_{KT}, which essentially is a perturbation of E_{KT} due to molecular geometry and competition for electrons with the surrounding atoms. Second, upon photoionization, the electronic distribution of the neighboring atoms adjusts to provide additional stabilization to the core hole. This is the extra-atomic relaxation energy, R_e, or the polarization energy. The relationship between experimental and theoretical ionization energies for a molecule, m, is

$$E_i(m) = E_{KT} + \Delta E_{KT} - R_i - R_e \qquad \text{(II.3)}.$$

Hedin and Johansson[13] have derived explicit relations describing relaxation in the final state. Davis and Shirley[14] have developed methods for using Equation II.3 for correcting core-level binding energy shifts for

relaxation effects.

It is possible to measure absolute ionization energies[15], but it is customary to look instead at the shifts in energy between the atom of interest in the molecule and a reference compound. In general, the shift in ionization energies, ΔE_i, between the compound of interest and a reference compound can be represented as

$$\Delta E_i = \Delta E_{KT} - \Delta R \qquad \text{(II.4)}$$

where ΔE_{KT} reflects the difference in the initial-state charge distribution between compound and reference and ΔR is the difference in extra-atomic relaxation between compound and reference. Note that both E_{KT} and R_i cancel because they are measures of the atom and are not changed within a molecular structure. Further note that the remaining parameters are measures of electronic charge distributions and electronic response to an introduced charge in molecules. ΔE_{KT} is a reflection of the competition for electrons between atoms in a molecule and represents the response of the ground-state, or initial-state, charge distribution to the change in molecular potential between compounds. This initial-state charge distribution is also called the chemical shift, denoted ΔV. ΔR represents rearrangement of electron distribution to accommodate the creation of the core hole. This is a measure of the polarizability difference between compound

and reference.

B. SHAKE ENERGY

1. Description of Shake

In addition to one-electron excitation of a core electron to the continuum, multielectron excitations can occur. These are processes analogous to the Franck-Condon excitation of vibrational states during an electronic transition. Condon[16] predicted such satellite structure in electronic spectra in 1928.

Within the framework of the orbital approximation, the final states resulting from one-electron and two-electron excitations are depicted in Figure II.1. The process on the left depicts the final state following a one-electron core ionization, while the representation on the right shows a two-electron final state with both a core hole and an excited valence electron. If ε_v' is a bound state, the process is termed "shakeup" (monopole excitation). If ε_v' is a continuum state, the process is termed "shakeoff" (monopole ionization). Collectively, these processes are termed "shake".

The core electron ejected via the one-electron excitation will have a kinetic energy greater than that of the electron ejected via the two-electron excitation by an amount equal to the energy of excitation, $\varepsilon_v' - \varepsilon_u'$. This

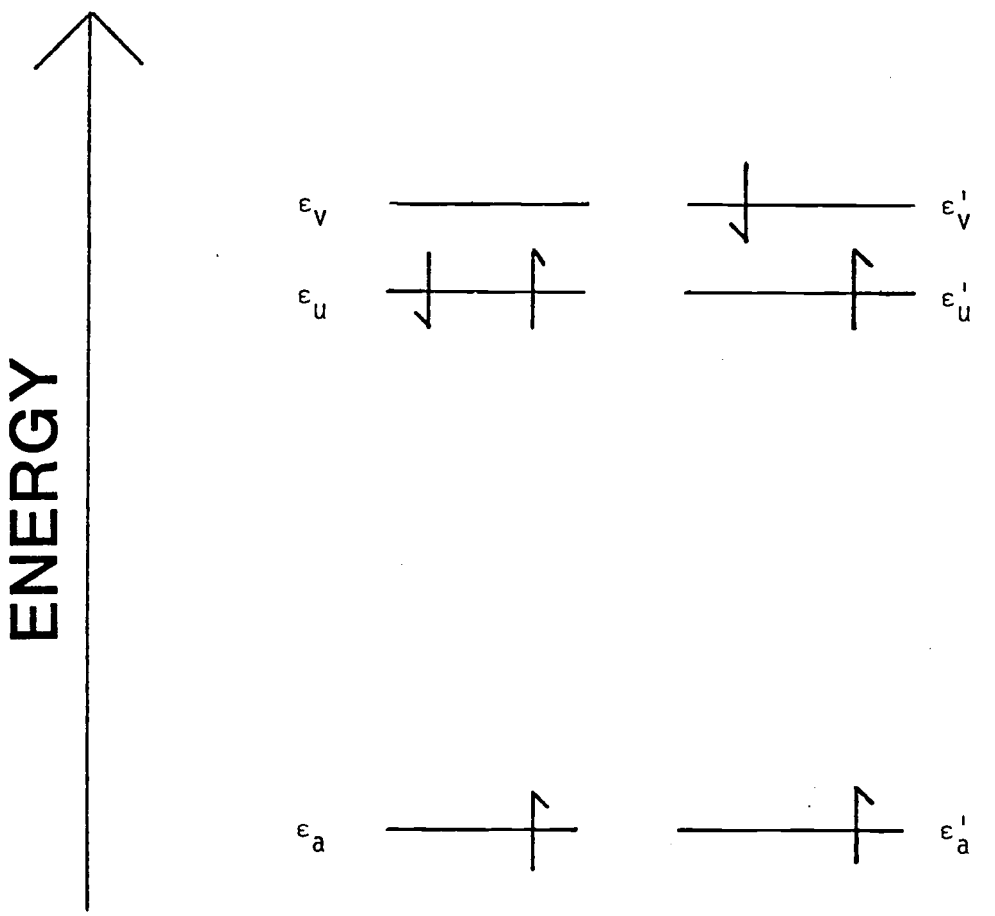

FIGURE II.1

Orbital representation of the final state of a one-electron process with a core hole (left) and a two-electron process with a core hole plus an excited valence electron (right).

gives rise to satellite lines in the photoelectron spectrum on the low-kinetic-energy side of the one-electron, or primary, line.

The theory of electron shake was first developed by Feinberg[17] and Migdal[18] for beta decay and was based on the sudden approximation, which requires that a finite change in the Hamiltonian of the electronic system occur suddenly in a time that is short compared to all relevant time periods. The wave function remains unchanged during a sudden change of the potential. The sudden approximation assumes that the initial and final states are well defined and that the ejected electron is of sufficient energy that its interaction with the ion is negligible. Martin and Shirley[19], in a study of transition probabilities, have shown that the sudden approximation and the limit of the dipole approximation at high photoelectron energies give the same results.

Within the sudden approximation, the shake probabality is independent of the mechanism that produces the inner-shell vacancy. Only the principal quantum numbers change, the spin and angular momentum cannot change. In photoionization, because the dipole interaction is involved, the total change is $\Delta L = \pm 1$. The extra monopole excitation does not alter the angular momentum further.

The use of the sudden approximation was then applied to electron shake in Auger processes by Wolfsberg and

Perlman[20], to photoionization by Carlson et al.[21-23] and to electron impact by Åberg[24]. Martin and Shirley[19] derived a general expression for the photoelectric cross section in the dipole approximation using single determinant wave functions.

The shake structure arises from processes that are intrinsic to the photoelectron event. The spectra as measured, however, contain contributions from other processes including inelastic scattering. Certain precautions can be taken to minimize these events and the details of these manipulations are outlined in Chapter IV, Section B and in Appendix E, Part 2.

The shake transitions can be used as probes of other molecular parameters. Specifically, as outlined below, an examination of shake structures and energetics can lead to a prediction of EXAFS amplitude attenuation and an estimate of the relative polarizability of atoms in molecules.

2. Relationship to EXAFS

Photoejection of an electron from an atom can occur over all 4π stereradians. In molecules, certain of these paths are blocked by the presence of adjacent nuclei. These nuclei backscatter the outgoing electron plane wave causing constructive and destructive interference that gives rise to oscillations in the X-ray absorption coefficient above the absorption edge. The technique of

extended X-ray absorption fine structure (EXAFS) analysis[25] allows the observation of these oscillations as a function of photon energy. Although theory has been successful in describing the overall shape of the EXAFS spectra, the predictions of the EXAFS amplitude are not in quantitative agreement with those found experimentally.

In a study of the EXAFS spectrum of Br_2, Kincaid and Eisenberger[26] found the experimental amplitude of the EXAFS oscillations to be about half of that calculated theoretically. More recent measurements by Stern, Heald and Bunker[27] show that there is no discrepancy for photon energies close to the absorption edge ($k < 5$ Å^{-1}) but that, at higher photon energies, the experimental amplitude was 20% lower than the theoretical value.

It was suggested[26,28,29] that the theoretical amplitudes are higher than those observed experimentally because the theory did not include multielectron processes -- valence-shell excitations during core-hole production, or shake, whose effects are seen as satellite structure in the photoelectron spectrum.

Lee and Beni[29] pointed out that shake gives rise to EXAFS shifted in energy from the main spectrum by an amount equal to the excitation energy of the ion. The total EXAFS is a sum of these individual contributions; there should, therefore, be a relationship between the satellites of the photoelectron spectrum and the amplitude attenuation of the

EXAFS spectrum. They suggested that shakeoff electrons are spread over such a wide range of energies that any EXAFS feature associated with the process will be smeared out. Using shakeup data from neon, they concluded that the contribution to the EXAFS spectrum from shakeup is negligible. Their overall conclusion was that the calculated EXAFS amplitude should be multiplied by the relative weight of the main peak (0.74 for Ne) before comparison is made to experimental data. Empirically, they found that a factor of 0.62 gave reasonably good agreement between theory and the experimental results for Br_2 available at the time.

Rehr, Stern, Martin and Davidson[30] have considered the role of shake in the EXAFS spectrum of bromine in more detail. From Hartree-Fock-Roothaan calculations, they conclude that only 64% of the core ionizations in Br_2 lead to the ground state of the ion. Although this result is in good agreement with the empirical factor of 0.62 found by Lee and Beni, they note that there is no compelling argument for ignoring the contributions from multielectron excitations. When they include estimates for shake, the calculated EXAFS attenuation factor becomes 0.7 ± 0.04, somewhat higher than Lee and Beni's value and lower than the most recent experimental results.

The normalized EXAFS spectrum, X, is defined by Stern[31] in terms of the X-ray-absorption coefficient, μ, as

$$X = (\mu - \mu_o)/\mu_o \qquad \text{(II.5)}$$

where μ_o is the atomic absorption coefficient. For molecules with only one significant interatomic distance (e. g. Br_2 and $GeCl_4$) a number of authors[32-35] have shown that X may be represented as

$$X_o(k) = (|f_k|/kR^2)\sin(2kR + 2\delta_o(k))x \exp(-\gamma R - 2\sigma^2k^2) \qquad \text{(II.6)}$$

where k is the wave vector of the outgoing electron, R is the interatomic distance, f_k is the backscattering amplitude, σ^2 is the mean-square fluctuation in R due to molecular vibration, $\delta(k)$ is an appropriate phase shift and $\exp(-\gamma R)$ is a decay factor to account for absorption of the electron as it travels through the molecule.

Rehr *et al.* have modified Equation II.6 to take account of multielectron excitations, each of which leads to a new EXAFS spectrum, $X_n(k)$. The primary effect of these processes is a shift, ΔE_n, in the energy of the EXAFS oscillations. This shift can be used to calculate $X_n(k)$ if the EXAFS of the primary process, $X_o(k)$ is known.

$$X_n(k) \approx X_o(k^2 - 2\Delta E_n)^{\frac{1}{2}} \qquad \text{(II.7)}$$

The total EXAFS, X, is

$$X = \sum_n S_n^2 X_n(k) \qquad \text{(II.8)}$$

where S_n^2 is the probablitity of occurrence of $X_n(k)$[36].

If one assumes that only the sine factor of equation II.6 varies rapidly with k and that all other terms remain essentially constant, then one may approximate the attenuation of the EXAFS amplitude with the attenuation of the sine factor. Then, setting $\delta_n(k) = \delta_o(k)$, as Rehr *et al.* have done, and defining a relative phase shift, $\Phi_n(k)$ as

$$\Phi_n(k) = 2R((k^2 - 2\Delta E_n)^{\frac{1}{2}} - k) \qquad \text{(II.9)}$$

X can be written as

$$X = |A(k)|(((|f_k|/kR^2)\sin(2kR + 2\delta(k) + \Phi(k))x \exp(-\gamma R - 2\sigma^2k^2) \qquad \text{(II.10)}$$

where the amplitude reduction factor, $|A(k)|$, and the phase shift are determined from the expression

$$|A(k)|\exp(i\Phi(k)) = \sum_n S_n^2 \exp(i\phi_n(k)) \qquad \text{(II.11)}.$$

If the S_n^2 values are known as a function of ΔE_n, then $|A(k)|$ can be calculated from equation II.11. We have measured the positions and intensities associated with the satellite structure to get S_n^2 as a function of ΔE for Br_2. The interpretation of the relationship of shake and EXAFS is discussed in Appendix E, Part 2, in a reprint entitled "Extended-x-ray-absorption fine-structure attenuation in Br_2: Relationship to satellites in the x-ray photoelectron spectrum."

3. Relationship to Relaxation

According to the Manne-Åberg sum rule[37], the average energy over the photoelectron spectrum, taken over the entire spectrum, is equal to the Koopmans' theorem energy. The difference between this and the true ionization energy is the relaxation energy as defined by Equation II.2. (Additional discussion of the relaxation energy can be found in the next section of this thesis.) Alternatively, taking the position of the main peak as zero energy and averaging over the spectrum generates the relaxation energy directly.

C. AUGER ENERGY

1. The Auger Process

Following the formation of a core hole, the ion can de-excite via two pathways. The radiative (X-ray) process occurs when an outer-shell electron fills the core vacancy while the energy is lost via a photon. The non-radiative (Auger) process occurs when, instead of photon production, the energy is carried away by a second electron being ejected into the continuum of the ion. The predominant process is the Auger process (named for Pierre Auger[7]) in all cases except those involving the K shell of atoms whose Z is greater than 30 or in the L shell of very heavy

elements[38].

The Auger process can be represented as

$$A^{*+} \rightarrow A^{++} + e^{-} \qquad \text{(II.12)}$$

where A^{*+} represents an atom with a core hole and A^{++} the final ion, which may or may not have core vacancies. The process is further represented in Figure II.2 for a typical KLL Auger transition. All Auger transitions are simultaneous two-electron Coulombic readjustments to the initial core hole. All possible transitions are allowed, making Auger spectra line rich.

The kinetic energy of an Auger electron is independent of the radiation used to excite the core hole as long as the ejected core electron has sufficient energy to leave the vicinity of the atom before the Auger process begins. Any three orbitals can be involved, so long as the energy difference between the initial and final states indicates that the transition is energetically possible, i. e. the total energy must be positive. In addition, the Auger process is dependent upon the energy of the levels involved so that a chemical shift may be observed between two different molecules, analogous to the chemical shift observed in photoionization.

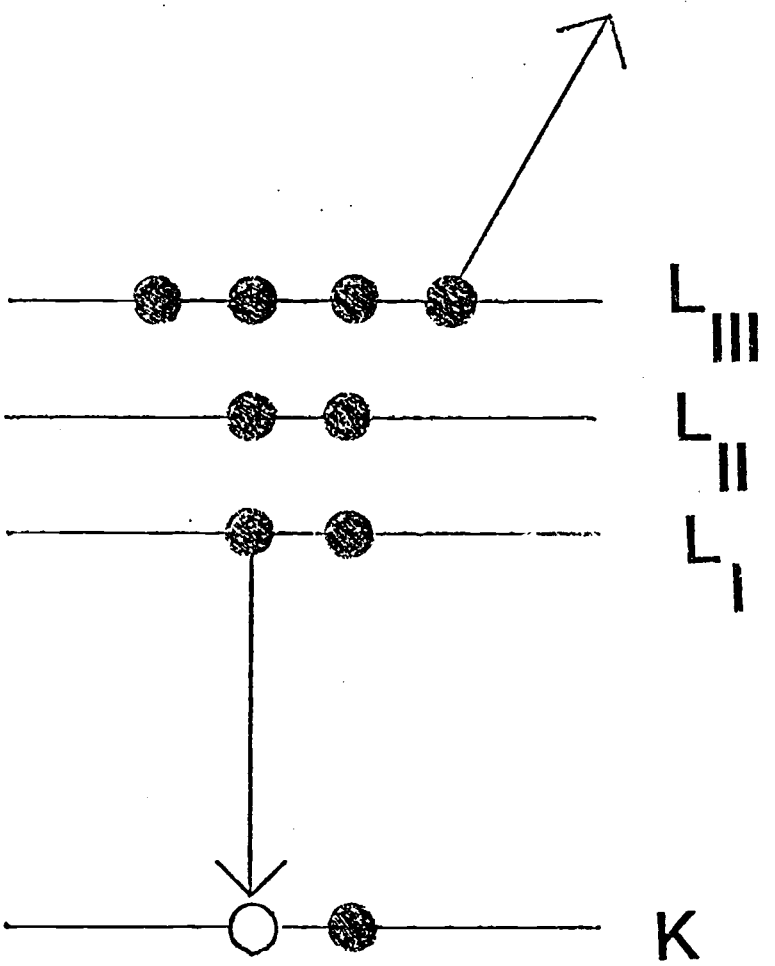

FIGURE II.2

Orbital representation of a KL_IL_{III} Auger process.

2. The Auger parameter

Early ideas on the magnitude of the Auger chemical shifts held that they should be similar to the photoelectron chemical shifts and in the same direction. Discrepancies were first observed in solids in 1972 on sodium salts[39] and in 1973 on oxidized magnesium surfaces[40]. Early gas phase work showed similar discrepancies[41-44]. These failures arose because the early views were based entirely on changes in ground-state energies and did not consider extra-atomic relaxation.

For an Auger process, the kinetic energy of the ejected electron will be the difference between the intital- and final-state energies. Limiting this discussion to core-type Auger lines and following the treatments of Shirley[45], we may write the KLL Auger energy, E_A, for an atom as

$$E_A(a) = E_i(K^+) - 2E_i(L^+) - F(x) + R_s \qquad \text{(II.13)}.$$

$$= E_{KT}(K) - R_i(K^+) - 2E_{KT}(L) + 2R_i(L^+) - F(x) - R_s \qquad \text{(II.14)}$$

$E_i(S)$ is the ionization energy of the level indicated and $E_{KT}(S)$ is the corresponding Koopmans' theorem energy. $F(x)$ is an electron-electron interaction term made necessary by the double electron vacancy in the final state and R_s is a

intra-atomic "static" relaxation energy for the L shell that arises because of rearrangement of the passive electrons on the first ionization.

For a molecule, the equation of interest is

$$E_A(m) = E_{KT}(K) - \Delta E_{KT}(K) - 2E_{KT}(L) + 2\Delta E_{KT}(L) - R_i(K^+) + 2R_i(L^+) - F(x) - R_s + R_e(L^+L^+) - R_e(K^+) \quad \text{(II.15)}$$

where $R_e(K^+)$ is the extra-atomic relaxation energy associated with the formation of the hole in the K shell and $R_e(L^+L^+)$ is the extra-atomic relaxation energy associated with the double vacancy in the L shell.

Once again, upon taking the difference between a molecule and an atom (or, in a more general derivation, between a molecule and a reference molecule) the atomic terms (R_s, $F(x)$, E_{KT} and R_i) all cancel with the following result

$$\Delta E_A = \Delta E_{KT}(K) - 2\Delta E_{KT}(L) + R_e(L^+L^+) - R_e(K^+) \quad \text{(II.16)}.$$

Note that in a conductor, the polarization energy should be[46]

$$R_e = (e^2/2r)(1-1/\varepsilon) \quad \text{(II.17)}$$

where e is the charge on the electron, r is the radius of minimum electron screening and ε is the dielectric

constant. If one assumes a charged sphere model, then $\Delta E_{KT}(K)$ and $\Delta E_{KT}(L)$ are identical (experimentally they are nearly the same). Further, to the extent that r for a one-electron hole is the same as that for a two-electron hole, $R_e(K^+)$ and $R_e(L^+L^+)$ differ by a factor of four. Hence

$$\Delta E_A = -\Delta E_{KT} + 3\Delta R \qquad \text{(II.18)}$$

(Note that this equation has been generalized by assuming an R_e relative to a reference compound and replacing with the more general ΔR term, as was done in Equation II.4.)

The approach used to arrive at Equation II.18 is that of Wagner[47]. A variety of other approaches[45,48,49] also arrive at the same result.

A comparison of Equation II.18 with Equation II.4 shows the differences and similarities between ΔE_i and ΔE_A. Clearly the early ideas on the magnitude of the Auger chemical shift were in error.

It is now possible to define the relative Auger parameter, $\Delta\alpha$, as the sum of the relative ionization energies (Equation II.4) and the relative Auger energies (Equation II.18)

$$\Delta\alpha \equiv \Delta E_i + \Delta E_A = 2\Delta R \qquad \text{(II.19)}.$$

The Auger parameter is then characteristic of a chemical and physical state and is easily measured. It is independ-

ent of reference level and is entirely an effect of extra-atomic relaxation.

Via appropriate recombination with either Equation II.4 or II.18, the chemical shift, ΔE_{KT}, may be deduced, providing that there are no reference level problems, as in solids. It should be noted that both ΔE_{KT} and ΔR are measures of the ability of a molecule to accept additional charge at the ionization site, as was discussed in Section A of this chapter.

D. RELAXATION ENERGY

1. The Auger Parameter

As outlined in previous sections of this chapter, two types of relaxation can be differentiated in molecules. The first is intra-atomic relaxation and is a measure of the ability of the atom to respond to core ionization. The second, extra-atomic relaxation, is a measure of the ability of the molecule to respond to the removal of an electron from the atom being probed. By use of the Auger parameter, it is possible to arrive at relative extra-atomic relaxation energies. In the following discussions, whenever relaxation is mentioned, it is to be understood that only the extra-atomic relaxation is being discussed, unless otherwise explicitly stated.

Evaluation of the Auger parameter, via Equation II.19, by simultaneous measurement of the relative ionization

potentials and the relative Auger kinetic energies leads directly to the relative relaxation energies. An experimental study of a variety of chlorine containing compounds was undertaken and is reported in Appendix E, Part 3. This study concluded that the Auger parameter was a useful technique for the determination of ΔR and, hence, ΔE_{KT}. It is important to verify the values of ΔR obtained in this manner.

Smith[50] employed gas phase acidities and basicities as a probe of the relaxa- tion. It may also be possible that, in a comparison of atomic versus condensed states, relaxation energies may be measured directly. Finally, it is possible to make use of the Manne-Åberg sum rule[37] to get an estimate of the relaxation energy. The latter two methods are to be discussed in the following segments.

2. Atomic versus condensed states

The most accurate experimental values are of core-ionization energies for free atoms (e. g. Ne[15], Ar[15,51] and Kr[5]). In these cases, the measurements are free of uncertainties in reference levels, charging effects and extra-atomic relaxation. In addition, the most accurate theoretical calculations are for free atoms[52,53].

It is of considerable interest, then, to compare theory and experiment and, at the same time, to examine the change in core-ionization energy between a free atom and a

condensed phase of the same atom. (e. g. I(g):I_2(g) or M(g):M(s) where M is any metal.) In addition, evaluation of ΔE_i between atomic, diatomic and polyatomic species (e. g. S_2(g):S_8(g))[54] should be of importance.

In systems such as those mentioned above, there is no change in oxidation number. To first order, the ground-state-potential model[55] would predict zero difference in the core ionization between the two species. To the extent that this approximation is correct, any differences that do exist should be largely due to relaxation. Hence, a comparison of the core-ionization potentials of the species should provide an alternative method of measuring the relaxation energy. Verification of the validity of this outlook was attempted during the course of this research, and is discussed in Chapter IV, Section C. However, no conclusion could be reached.

3. Manne-Åberg sum rule

The Manne-Åberg sum rule[37] states that the average energy of a core-ionization spectrum, taken over the entire spectrum, is the ionization energy if no relaxation takes place. The difference between the average energy of the total spectrum and the energy of the main peak is then the relaxation energy.

Measurement of the average energy of a spectrum, E_{ave}, is attained in our experiments by subtracting the Al $K\alpha_{3,4}$

satellite contribution from the entire spectrum, then summing over the number of data channels, n, in the spectrum

$$E_{ave} = \frac{\sum_{j=1}^{n} E_j c_j}{\sum_{j=1}^{n} c_j} \qquad \text{(II.20)}.$$

E_j is the energy of the j^{th} channel and c_j is the number of counts in the j^{th} channel. If the energy of the peak channel is taken to be zero, then E_{ave} is R_e. Otherwise

$$R_e = E_{ave} - E_{peak} \qquad \text{(II.21)}.$$

If, instead, the averaging is done over a difference spectrum (subtracting the spectrum of a reference compound from the spectrum of the sample, with the main peaks of both spectra superimposed), then the relative relaxation energy is obtained.

$$\Delta R = E_{ave}(\text{sample}) - E_{ave}(\text{reference}) \qquad \text{(II.22)}$$

In this manner, it is possible to check the values of extra-atomic relaxation, arrived at via different procedures, for consistency.

A large part of this research has been directed toward the measurement of the relative relaxation energies of a variety of compounds in the manners outlined above, In the next chapter, and in Appendix E, Part 3, the results and

conclusions of these investigations will be explored.

III. EXPERIMENTAL

A. ORIGIN OF SAMPLES

The compounds used in this investigation came from a variety of sources. All commercially obtained samples were used without further purification.

Arsabenzene and phosphabenzene were synthesized by Ashe according to the methods described elsewhere[56] and were used without further purification. Phosphine was prepared by Sitton[57] via the reaction of calcium phosphide and water and purified by distillation under vacuum. Arsine and some trimethylarsine were obtained from a colleague[58] and some additional trimethyarsine was purchased from Strem Chemicals. Bromine was obtained from Mallinkrodt, as were the chlorine-substituted methanes (CH_3Cl, CH_2Cl_2, $CHCl_3$ and CCl_4). The chlorine-fluorine substituted methanes were obtained from Matheson, as were the acid gases (HCl and HI), noble gases (Ar and Ne for calibration) and chlorine gas. ClF was purchased from Ozark Mahoning. Iodine was obtained from Merck.

B. PROCEDURES FOR GENERATING SPECTRA

XPS spectra were obtained using the Oregon State University cylindrical mirror analyser, shown in cross section in Figure III.1. Two X-ray sources were employed in the course of this work. The X-ray source of Smith[8] was used

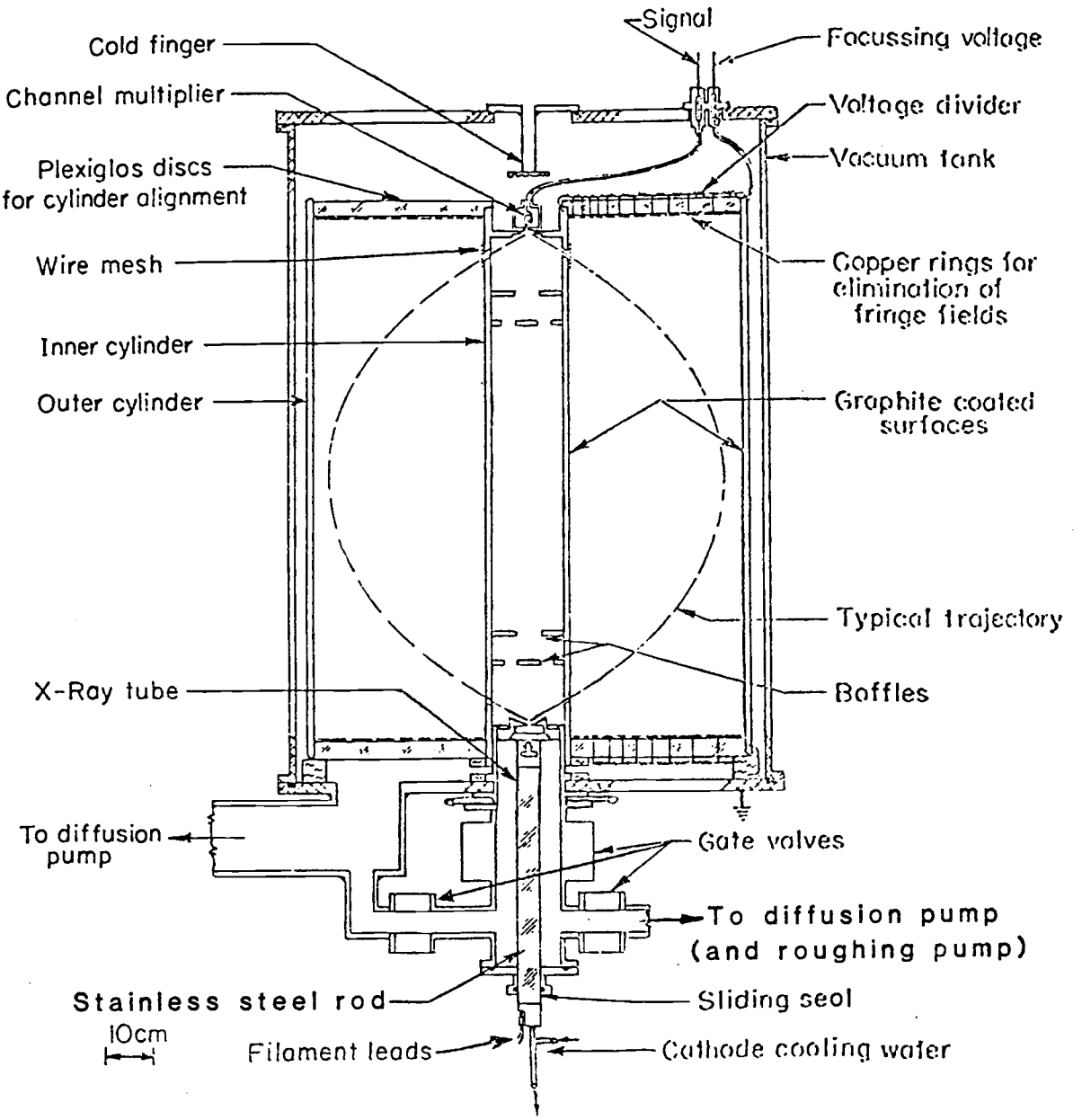

FIGURE III.1

Oregon State University Cylindrical Mirror Analyzer, in cross section. (Modified from Reference 59.)

initially and was replaced by the X-ray source described in Appendix A. All data were taken with either Al $K\alpha_{1,2}$ or Ag $L\alpha_1$ radiation. A tripod was used on top of the X-ray gun to minimize background features, predominantly from the carbon 1s line.

Gaseous samples and neon calibrant entered through the stainless steel needle valves of the gas manifold. A schematic representation of the gas handling system is depicted in Figure III.2.

Those samples in pressurized containers were first passed through a regulator valve. Liquid samples under pressure or corrosive samples were also passed through a regulator specifically selected for the sample involved. Both types of gases were introduced through the sample ports of Figure III.2. Samples that were liquids with sufficient vapor pressure at room temperature were placed in a glass ampule and attached directly under a needle valve at the short line.

The vapor pressure of iodine at room temperature is not sufficient to carry appreciable vapor into the sample cell from the short-line gas manifold, so a small container with a hole in the top was placed in the sample cell on top of the X-ray tube. This provided sufficient I_2 vapor for experimental purposes but no pressure measuring device within the spectrometer noted any pressure increase while the container was in place.

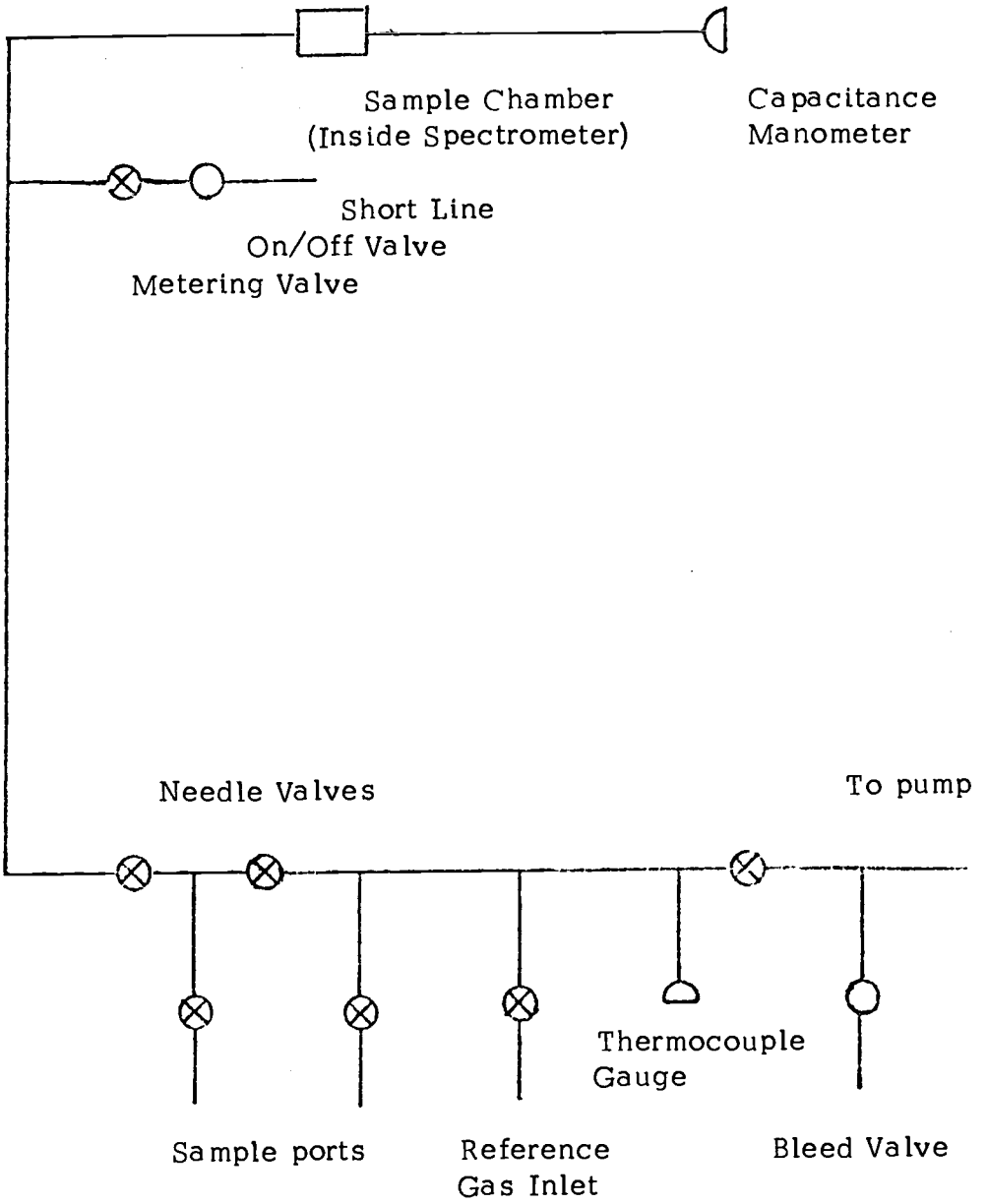

FIGURE III.2

Schematic of the Gas-Handling Manifold

Measurement of Cl_2 and ClF were made after enough gas had passed through the sample cell and no evidence of impurities remained. Without such pretreatment, reaction of the sample gas with substances adsorbed on surfaces within the spectrometer would give rise to impurity peaks in the spectrum.

The duration of individual experiments ranged from tens of minutes to several days, depending upon X-ray source performance, sample pressure, the spacing of the peaks to be resolved and the intensity of the satellite peaks (if any) being measured. The data collection systems employed involved two computers that interfaced with the electron detector and the focusing voltage supply. When interfaced to the PDP-9 computer, using the PESCAN programs of T. D. Thomas[57], four different regions of the spectrum could be scanned sequentially and repetitively. Interfaced to the MINC-11 computer, using the PSCAN5 program of T. D. Thomas[57], eight different areas could be measured in the same manner.

In order to improve the statistical accuracy of the data in the shake regions, where intensity is low, the spectra were taken in two segments, split between the main peak and the first shakeup transitions. Data in the shake regions were counted ten times longer and the data in both regions were normalized to one another before combination to provide one continuous spectrum.

The focusing voltage is measured, during the course of the experiment, at the beginning and end channel of each region as well as at a channel near the tip of each peak, using a differential voltmeter (Julie Research Labs, Model TD-1000) or its replacement, a digital voltmeter (Fluke, Model 8502A). Peak positions are determined by least-squares fitting with Voigt functions[60]. Neon is introduced simultaneously for use as a calibrant.

The neon 1s ionization energy is accurately know[15] (870.312 ± 0.017 eV) as is the 2s ionization energy[61,62] (48.476 ± 0.002 eV). Smith[63] has discussed the uncertainties and errors associated with this calibration scheme, which allows accurate measurement of the absolute values of either the ionization energy or the kinetic energy.

Fitting, as outlined above, is usually done without constraints. The calibration program corrects for both the recoil of the ion and any relativistic effects[64].

In cases where the fits and calibrations obtained via this method proved to be inadequate (e. g. closely spaced peaks), a more versatile least-squares program was used[65]. Spectra were then fit to Gaussian functions with an exponential tail and a linear background. The tails are added to the low kinetic energy side of the peak and are included to account for a variety of energy loss phenomena.

C. DATA MANIPULATION

Additional data manipulation was performed on some of the spectra, particularily for the Br_2 experiment and the Cl_2, ClF, and HCl series of experiments. Linear background subtractions, X-ray satellite corrections as well as data smoothing and data matching to exponentials were employed. The programs required for these proceedures are outlined, briefly, in Appendix D. Where significant, details of these manipulations accompany the appropriate discussions of this dissertation.

IV. RESULTS AND DISCUSSION

A. ARGON

The photoelectron spectrum in the Ar 2p region was measured in two segments, split between the main peak and the first shake transition. The counting time per channel in the shake region was ten times that in the region of the main peak during the course of the experiment. Figure IV.1 shows both the shake and main peak data as they were collected as well as the data in the shake region normalized to the data in the region of the main peak to provide one continuous spectrum.

As discussed in Chapter II, Section B, the measured spectrum contains contributions not only from the intrinsic one-electron and multielectron processes, but also from extrinsic inelastic scattering. These effects arise by interaction of the outgoing electron with the gas molecules or with the walls of the sample chamber. It is possible to minimize the effects due to scattering from other gas molecules by keeping the sample pressure low, thereby reducing the number of collisions. In the case of Ar, and for the molecules discussed in Section B of this chapter, the pressure dependence of the spectrum was investigated in the range from about 0.1 to 25 Pa, as measured by a capacitance manometer connected to the sample chamber. Below 3 Pa, the spectrum is pressure independent,

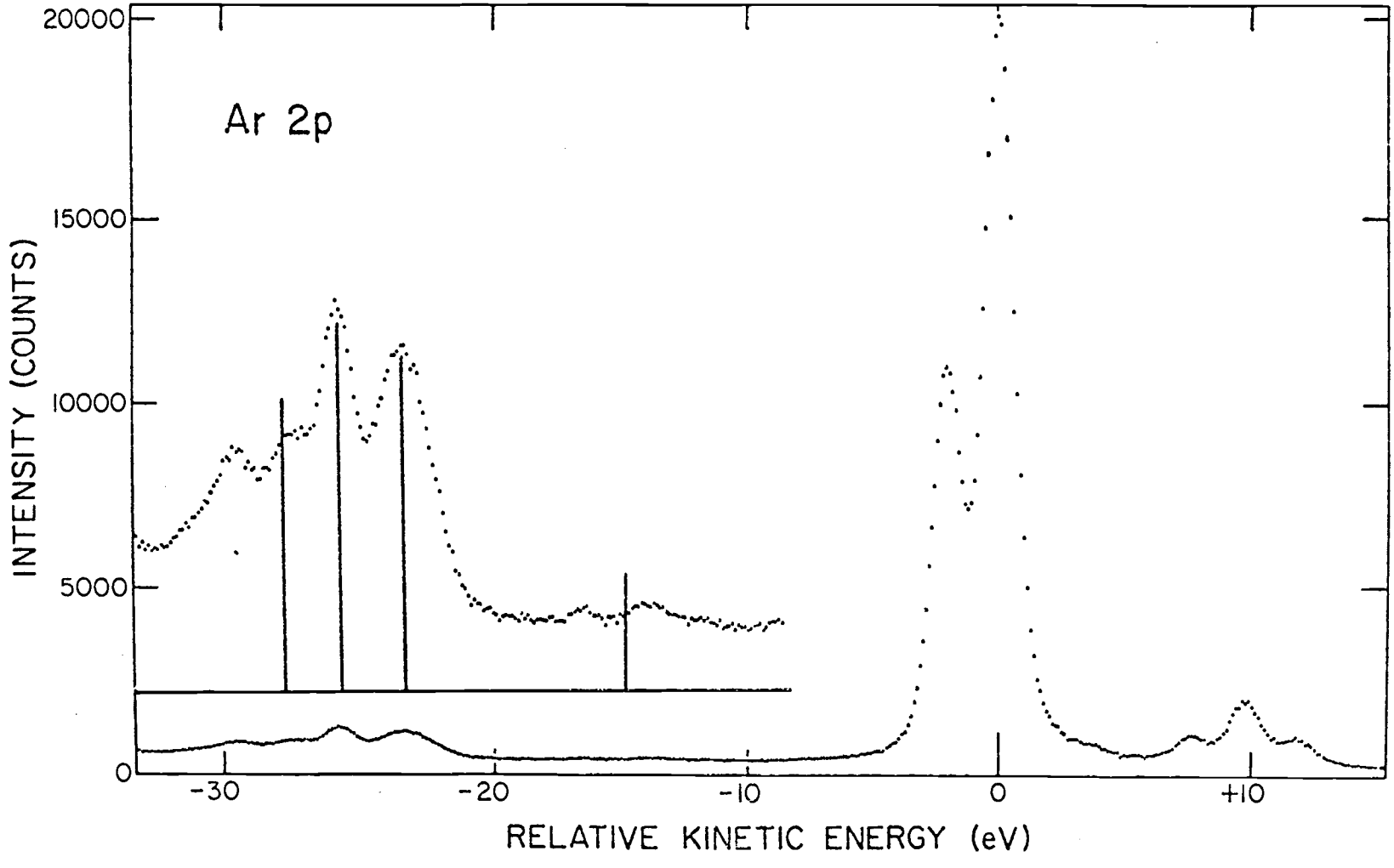

FIGURE IV.1
Argon 2p plus shake spectrum

indicating that there are no contributions from electrons that scatter inelastically from the gas molecules. The data of Figure IV.1, and the data of Section B of this chapter, were taken at pressures between 0.5 and 1 Pa.

In Figure IV.1, the horizontal line beneath the satellite spectrum represents the background, as estimated by averaging over the high-kinetic-energy side of the $K\alpha_{3,4}$ satellites. Vertical lines indicate the positions and approximate heights of the peaks reported in the spectrum of Spears, Fishbeck and Carlson[66]. Agreement is satisfactory, considering the statistics of their data. The relative areas, relative energies and widths are reported in Table IV.1.

An expanded plot of the shake region is shown in Figure IV.2. The solid curves are least-squares fits to Gaussian functions for the data. The sloping linear background was constrained to pass through the data at the right and left hand egdes of the data shown.

The satellites arise largely from the promotion of a 3p electron in argon to the np shell ($n \geq 4$). The possible states are those that result from the coupling of a 2p core hole with a 3p hole and an np electron. The monopole selection rules require that only those states whose angular momentum, J, is 3/2 contribute to the shake structure that arises during ionization of the $2p_{3/2}$ shell and that only those with J=1/2 contribute during ionization of the $2p_{1/2}$

TABLE IV.1

Argon 2p plus shake

Ar		Relative area	Relative energy (eV)	FWHM (eV)
$2p_{3/2}$		1	0	1.52
$2p_{1/2}$		0.526	-2.14	1.52
SHAKE	1	0.062	-23.67	2.57
	2	0.037	-26.26	1.47
	3	0.017	-28.00	1.70
	4	0.030	-30.25	2.46

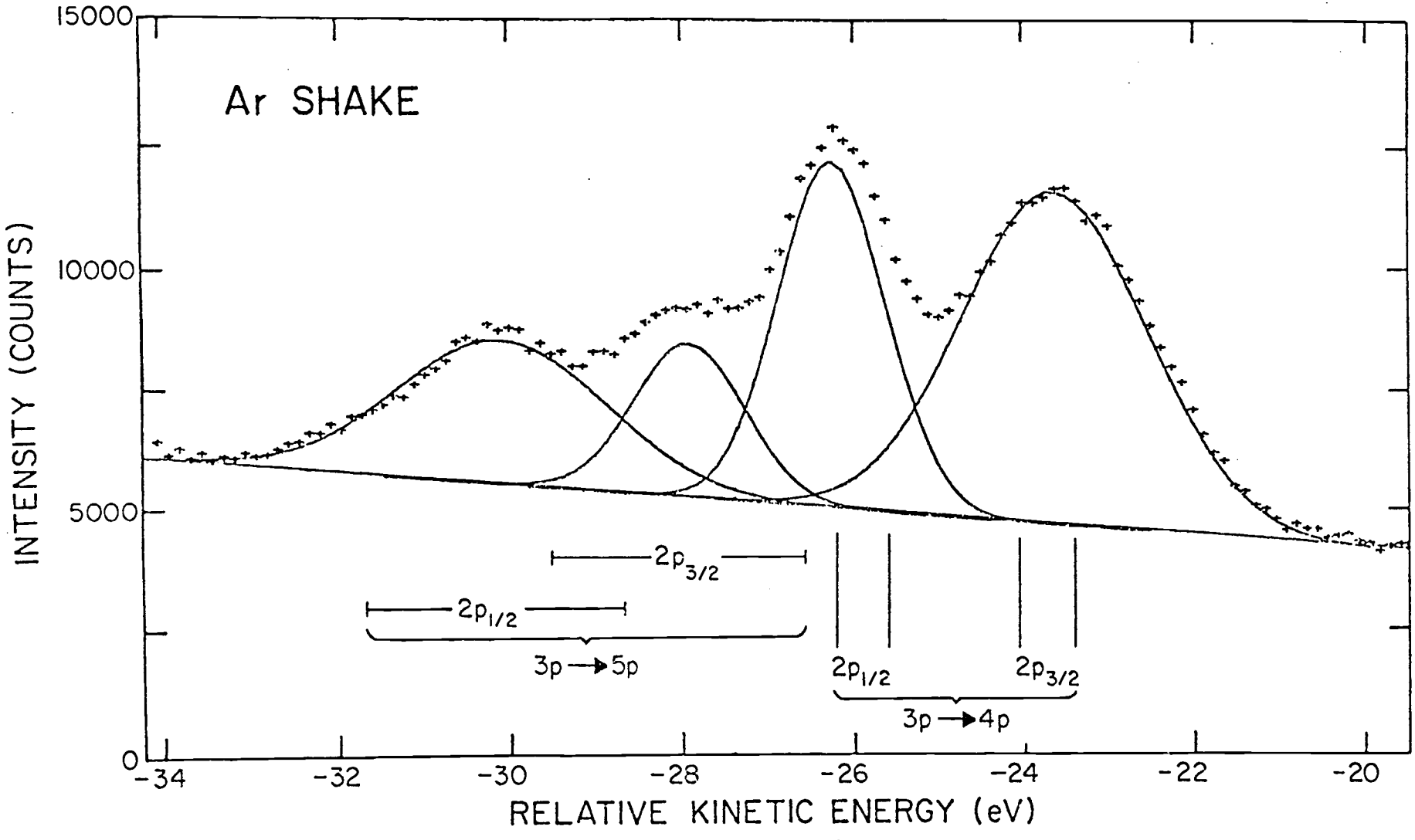

FIGURE IV.2

Expanded Argon Shake Spectrum

shell.

If the coupling between the 2p hole and either the 3p hole or the np electron is weak, then the monopole selection rule applies to the valence configuration as well as to the total configuration. Hence the $3p^6$ (J=0) to $3p^5np$ (J=0) gives rise to two transitions for each n depending upon whether the $3p^5$ configuration is coupled to $^2P_{3/2}$ or $^2P_{1/2}$. It is possible to estimate the energies of these transitions by making use of the equivalent-cores approximation[67]. K^+ is the equivalent-core species for Ar and, according to Moore[68], for n = 4 the energies are 23.53 and 24.15 eV in K^+. Theis pair of energies will appear twice, separated by the energy difference between the $2p_{3/2}$ and the $2p_{1/2}$ core holes.

The position of the K^+ 3p to 4p transitions are indicated in Figure IV.2. The agreement is reasonably good considering that this approach ignores the coupling between the core hole and the valence electrons and considering the possible deficienies in the use of the equivalent-cores approximation.

In addition, the range of energies that might be expected for the 3p to 5p transitions in K^+ are also indicated in Figure IV.2. These correspond well to the two leftmost peaks. The shakeoff portion of the spectrum (not shown in Figures IV.1 or IV.2) is obscured by a rising background and a carbon 1s contamination originating from

graphite on the spectrometer walls. The small feature between the main peak and the 3p-to-4p satellite of Figure IV.1 is probably the $K\alpha_{3,4}$ satellite of the shake spectrum.

In conclusion, the main features of the Ar spectrum are readily understood in terms of the excitation of the outermost (3p) electrons to those Rydberg states that are allowed by the monopole selection rules. This description is entirely consistent with the neon 1s shake spectrum[69] in which the principal transitions are found to be 2p to 3p and 2p to 4p.

A more complete theoretical analysis of this spectrum is being carried out by Dyall and Larkins[70]. The combined theoretical and experimental results will be reported elsewhere.

B. CHLORINE, CHLORINE MONOFLUORIDE AND HYDROGEN CHLORIDE

1. Relaxation via the Auger parameter

Table IV.2 reports the relative relaxation energies for chlorine in Cl_2 and ClF, as determined by the Auger parameter (Chapter II, Section C), with HCl as the reference compound. As can be readily seen, relaxation has a large effect in Cl_2, as expected, because of the high polarizability of chlorine (compared to hydrogen). Note also that because chlorine attracts electrons more strongly than hydrogen does, there is a corresponding increase in

TABLE IV.2

Core-ionization and KLL Auger kinetic energies for Cl_2, ClF and HCl (eV).

Compound	$2p_{3/2}$	$2p_{1/2}$	KLL	ΔR	ΔV
Cl_2	209.45	207.82	2373.72	1.10	1.54
ClF	210.83	209.18	2370.73	0.28	2.08
HCl	209.01	207.38	2371.98	0	0

ΔV. These conclusions are in agreement with those obtained by Smith and Thomas[50] in a comparison of the core-ionization energies and gas phase acidities of CH_3COOH and $CH_2ClCOOH$.

In the Cl_2:ClF comparison, replacement of fluorine by the more polarizable chlorine increases the relaxation energy, again as expected. Further, the ΔV value for ClF is larger than that of Cl_2, indicating that fluorine withdraws electrons from chlorine. (This will be discussed further in Part 2.)

It should be noted that, in halogenated methanes[48] and in halogenated carboxylic acids[50], where the probe is separated from the halogen by one or more carbon atoms, $\Delta V_F = \Delta V_{Cl} = \Delta V_{Br}$. This effective equalization of initial-state effects when the halogens are no longer adjacent makes the relaxation effect the sole influence. This is completely in accord with the view expressed by Hiroaka *et al.*[71], that the relative gas-phase acidities of the halogenated carboxylic acids are dictated by the relative polarizabilities of the halogens.

2. Dipole Moment of ClF

It is chemically reasonable to expect that, in ClF, the charge distribution is $Cl^{\delta+}F^{\delta-}$. However, Flygare and co-workers[72,73] proposed, on the basis of molecular Zeeman measurements, that the polarity was $Cl^{\delta-}F^{\delta+}$. To shed light

on this question, Carroll and Thomas[74] measured the core-ionization energies in Cl_2, F_2 and ClF. They found that the shift in core-ionization energies between ClF, Cl_2 and F_2 was consistent with the configuration $Cl^{\delta+}F^{\delta-}$. However, the effect of relaxation was not taken into account in their interpretation. Since chlorine is considerably more polarizable than fluorine, the shifts they measured might have been entirely due to relaxation effects rather than initial-state charge distribution. Although other experiments[75-77] have shown that the charge distribution is $Cl^{\delta+}F^{\delta-}$, as expected, it is of interest to determine whether the ionization-energy shifts, when corrected for relaxation, agree.

As was noted in Part 1, the larger value of ΔV for ClF compared to Cl_2 in Table IV.2 indicates that fluorine withdraws electrons from the chlorine. This implies that, in keeping with chemical intuition and the recent dipole measurements, the charge distribution is, in fact, $Cl^{\delta+}F^{\delta-}$.

3. Relaxation via the Manne-Åberg sum rule

The 2p photoionization spectra for Ar, Cl_2, HCl and ClF are shown, plotted on a logarithmic scale, in Figure IV.3. Because of a misalignment of the spectrometer, the resolution in the Cl 2p spectra was not sufficient to show any separation in the spin-orbit doublet. The misalignment was corrected before the Ar spectrum was run. Since any

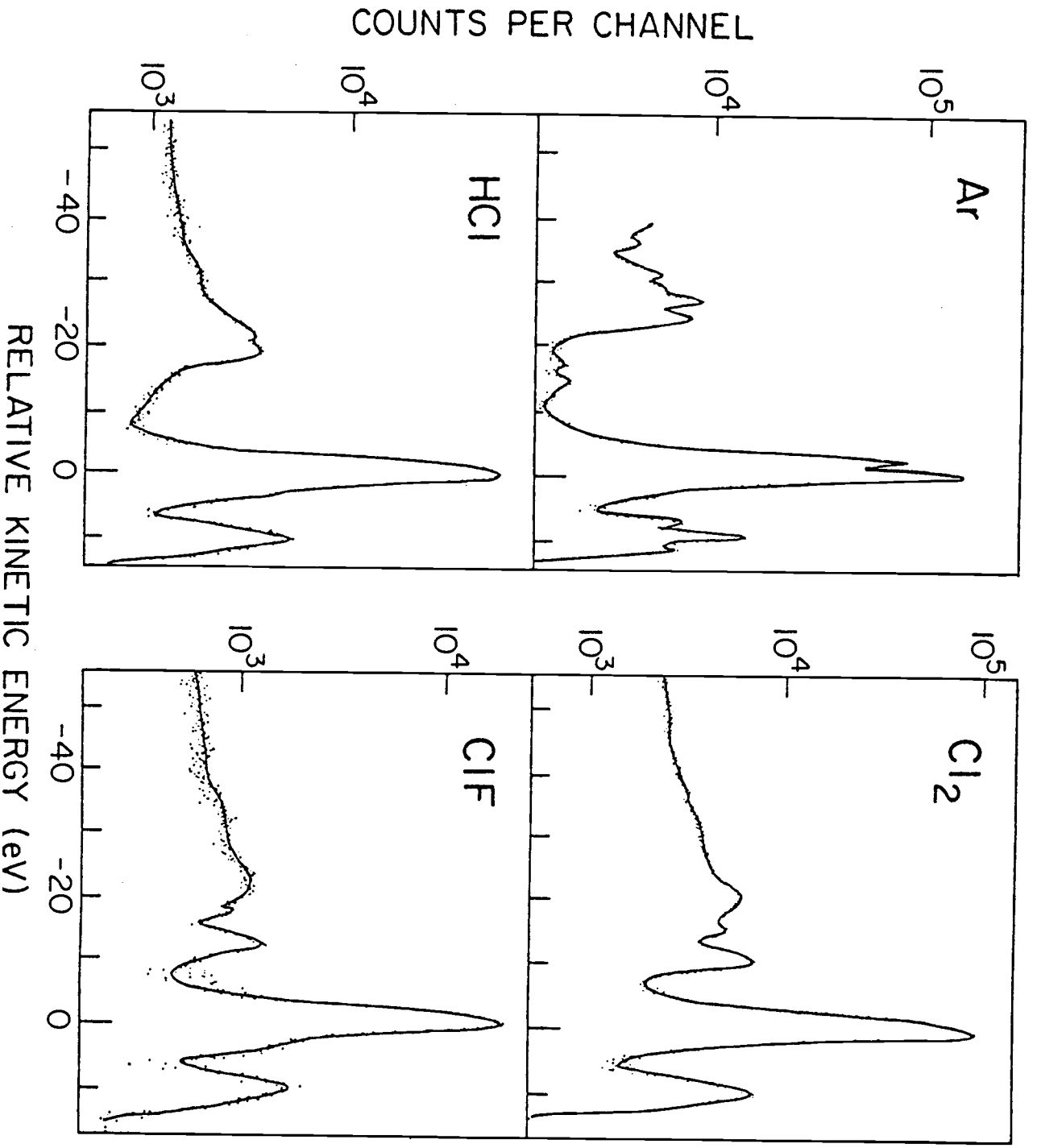

FIGURE IV.3

Ar 2p and Cl 2p Photoionization Spectra

conclusions to be drawn from this part of this work do not depend upon resolution, the chlorine spectra were not repeated.

A discussion of the argon spectrum can be found in Section A of this chapter. Suffice it to recall that the shake transitions were all attributed to Rydberg transitions. The HCl spectrum bears a strong resemblance to the Ar spectrum. HCl is not only isoelectronic with Ar but can be viewed as a slightly perturbed Ar, the perturbation being the withdrawal of a proton from the Ar nucleus. It is not surprising, therefore, that the two spectra are similar. The principal peaks in the HCl spectrum almost certainly represent transitions that begin in molecular orbitals with strong Cl 3p character ($3p_\sigma$ and $3p_\pi$) and end in an orbital with strong Cl np character (np_σ and np_π). This is also analogous to the shakeup transitions in HF[78], where the $F(2p_\pi)$ to $F(3p_\pi)$ and $F(4p_\pi)$, and $F(2p_\sigma)$ to $F(3p_\sigma)$ are strong. Thus, to a large extent, the HCl shakeup spectrum is an atomic one.

The Cl_2 and ClF spectra differ from those of HCl and Ar by the appearance of a strong peak with a shake energy significantly lower than seen in the atomic cases. In Cl_2 the lowest unoccupied molecular orbital is the $3p_\sigma$ antibonding orbital. The transition is then $3p_\sigma$ bonding to $3p_\sigma$ antibonding. Using CNDO/2 wave functions, and following the proceedure discussed by Chambers and Thomas[79] the

intensity for this transition, relative to the main peak, is calculated to be 7.3% in Cl_2 and 6.0% in ClF. The experimental values are 9.6% and 6.8%, respectively. Similar calculations indicate that other transitions to the $3p_\sigma$ antibonding orbital are much weaker. Because of the limited basis set used in these calculations plus the fact that all of the low-lying π orbitals are occupied in Cl_2, no intensity is predicted for transitions involving π electrons. While the CNDO/2 wave functions do not, in general, give accurate predictions of the intensities, they should give a reliable guide for the prediction of the character of the strongest transition.

The σ to σ^* transitions arise because of charge transfer from the spectator chlorine to the core-ionized chlorine during ionization. This statement is supported by the following arguments. For the highest occupied σ orbital, the wave function is, to a good approximation, composed almost entirely of $3p_\sigma$ orbitals contributed to equally from the two chlorine atoms. Representing the atomic wave functions as Φ_A and Φ_B and ignoring the overlap between orbitals on different atoms, the molecular wave function becomes

$$\Psi_\sigma = (\Phi_A - \Phi_B)/(2)^{\frac{1}{2}} \qquad \text{(IV.1)}.$$

For the core-ionized species, the contributions are no longer equal and the wave function becomes

$$\psi_\sigma' = a\phi_A' - b\phi_B' \qquad \text{(IV.2)}$$

for the bonding orbital and

$$\psi_\sigma'^* = b\phi_A' + a\phi_B' \qquad \text{(IV.3)}$$

for the antibonding orbital. The coefficients can be related if it is assumed that the atomic orbitals are normalized and that the overlap between orbitals on different atoms is zero. This leads to the requirement that is $a^2 + b^2 = 1$. If we ignore the changes to the atomic orbitals that are caused by the core ionization and set $\phi = \phi'$, then we may easily calculate the shakeup and ground-state intensities. The ratio, R, of shakeup to ground-state intensity, is

$$R = |\langle\psi_\sigma|\psi_\sigma'^*\rangle|^2 / |\langle\psi_\sigma|\psi_\sigma'\rangle|^2 \qquad \text{(IV.4)}$$

$$= (1 - 2ab)^2/(1 + 2ab)^2 \qquad \text{(IV.5)}.$$

When a = b, corresponding to no charge transfer, R = 0. If the charge transfer during core ionization is complete, (e. g. a = 1, b = 0), then R = 1 and there is equal intensity in both peaks. Thus, the greater the charge transfer, or relaxation, during core ionization, the greater the shake intensity. While the above discussion has focussed on the σ to σ^* transition, similar arguments should apply to the other molecular orbitals. Because the vacant orbitals of proper symmetry are at higher energies, the corresponding

transitions also lie at higher energies. Thus, the strong, extra peak in the Cl_2 and ClF spectra of Figure IV.2 corresponds to the σ to σ^* transition while the higher energy peaks are obscured by other shake features. In order to better show these features, difference spectra were generated. For these spectra, corrections were made to the data to account for a variety of problems. The details of these corrections are outlined below.

The calculation of the relaxation energy from the shake and difference spectra is sensitive to background and other corrections. Contributions to the spectrum from the Al $K\alpha_{3,4}$ satellites were removed by subtracting from each data channel 9.0% of the counts in the channel 10.7 eV lower in kinetic energy. This procedure should work satisfactorily in the shake region, where the overall resolution is low. It fails to correctly eliminate the $K\alpha_{3,4}$ peak itself, since the procedure treats the satellite as a single peak, whereas it is, in fact, two peaks. To compensate for the oscillating spectrum that resulted on the high-energy side of the main peak, part of the corrected data on the high- energy side of the main peak was replaced by a smooth exponential tail. The parameters of the tail were chosen to match the main peak in slope and height at a point 3.1 eV above the main peak. This procedure also eliminated shoulders on the high-energy side of the HCl and ClF peaks, which we believe were due to some

impurity. The tail was continued until it dropped below one count per channel. All channels to higher kinetic energy were assumed to have zero counts. The added tail can be seen in the difference spectrum as a region with no statistical fluctuations.

In addition, corrections were made for the portions of the shake spectrum that could not be observed because of interference from the chlorine 2s peaks and for inelastic processes associated with the main peak that were not accounted for by the pressure dependence measurements.

It is possible for electrons to inelastically scatter from the walls of the gas cell and from the analyzer slits, giving rise to a broad background on the low-kinetic-energy side of the main peak. Such a background is indistinguishable from shake. To account for this, the Cl_2 spectrum is used to give an approximate measure of this background for comparison with the other spectra.

For this background, we have chosen a sloping straight line which goes to zero at the point to the right of the main peak where the added smooth tail goes to zero. The slope of the line was chosen so that the energy average over the entire spectrum, with the main peak set equal to zero energy, was equal to the relaxation energy in Cl_2, in keeping with the Manne-Åberg sum rule[37]. The difference between Desclaux's value[52] for the Koopmans' theorem energy and the fully relaxed energy according to Huang *et al.*[53]

gives 11.0 eV for the atomic relaxation energy. To this we add 1.8 eV, calculated by Martin and Davidson[80], for the extra-atomic relaxation. The slope of the background line in Cl_2 was chosen so that the spectrum remaining after background subtraction had an average energy of 12.8 eV. The intersection of this line with our data falls in a region where the shakeoff spectrum is obscured by the Cl 2s spectrum and its satellites. To account for this part of the spectrum, which we cannot measure, an additional 167 eV of exponential tail was added to the data, normalzed to the height of the leftmost points of the data, The slope of the added tail is the same as that for the data, which falls exponentially in that region.

Since the goal is to determine the relaxation energies in HCl and ClF relative to that in Cl_2, it is not possible to use the same method to estimate the sloping backgrounds for the these compounds. An attempt was made to correct the slope found appropriate for Cl_2 for the different total counts in the other spectra. The difference spectra generated by this procedeure showed a nearly constant, nonzero remnant in the shakeoff region, with the Cl_2 higher than the other two. Additionally, the relative relaxation energies calculated using these spectra were not reasonable. While it is possible that the shakeoff intensity for Cl_2 is different from that of HCl or ClF, it does not seem reasonable that these spectra should differ by a nearly

constant amount over a wide range of energies. It is more likely that the true difference at high energy loss is zero and that this procedure overestimates the background for HCl and ClF in the shakeoff region.

Instead, the slope were chosen so that the average intensities in the first 100 channels of the data in the shakeoff region was the same in all three spectra after normalization. The resulting difference spectra are shown in Figure IV.4. The relative extra-atomic relaxation energies obtained by calculating the average over these difference spectra are given in Table IV.3. For comparison, the relaxation energies determined from the Auger parameter are included. The agreement ranges from excellent to satisfactory.

The results arrived at above depend upon the choice of total relaxation energy for Cl_2, which is uncertain by one or two electron volts. To investigate the effect of this uncertainty on the calculated extra-atomic relaxation energies, the calculations were repeated using an assumed total relaxation energy for Cl_2 of 11.0 ev instead of 12.8 eV. This is also reported in Table IV.3, and it is obvious that the choice of the total relaxation energy value does not affect the qualitative conclusions that can be drawn.

In the difference spectra of Figure IV.3, the main peaks contribute essentially nothing to the energy average. The energies are small here and, because the peak is nearly

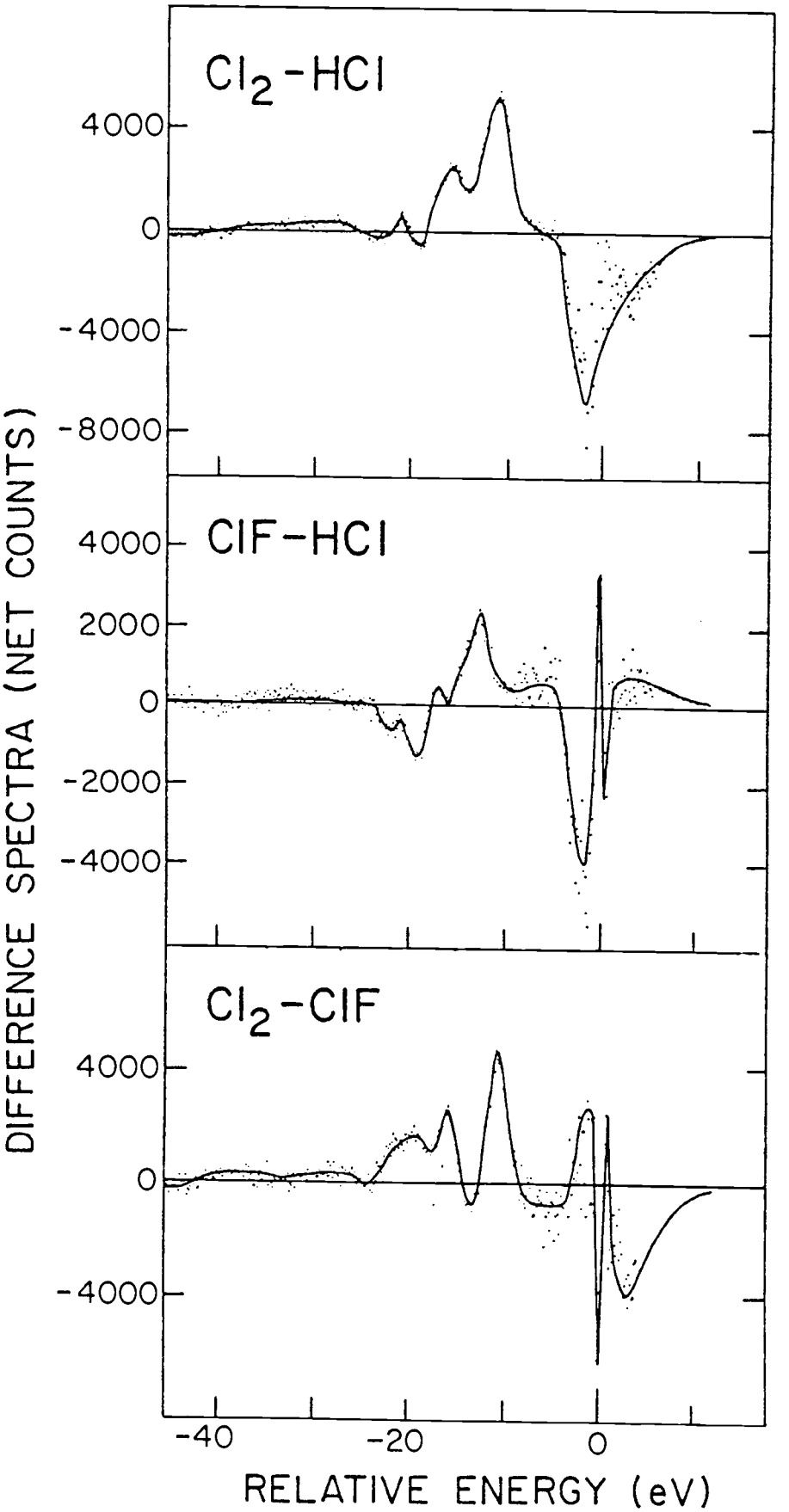

FIGURE IV.4
Cl 2p Difference Spectra

TABLE IV.3

Relative Relaxation Energies (eV)

Method / Compound	Auger	Shake	
		E_{ave} = 12.8	E_{ave} = 11.0
Cl_2 - HCl	1.10	1.10	1.17
Cl_2 - ClF	0.82	1.04	1.03
HCl - ClF	-0.28	-0.05	-0.13

symmetrically distributed about zero, tend to cancel. In the Cl_2:HCl spectra, the data are everywhere positive, except for the region of the main peak, implying a larger extra-atomic relaxation energy in Cl_2 than in HCl. This result is expected and is in agreement with what has been measured using the Auger parameter. For ClF:HCl, the difference spectrum is positive at medium energies and weakly negative at higher energies. In the energy averaging, the higher energy combined with the weaker peak nearly compensates for the lower energy and stronger peak. The relaxation-energy difference is small. This result is also in accord with the Auger parameter data and with the conclusion that there is little difference between the polarizabilities of H and F. The Cl_2:ClF difference spectrum similarily shows that chlorine is more polarizable than fluorine, as expected.

In conclusion, the relaxation due to the chlorine is significantly greater than that due to an adjacent hydrogen or fluorine, and the relaxation due to fluorine differs only slightly from that due to the hydrogen. These results are consistent with the polarizability of these substances, and in complete agreement with the conclusions drawn from the relaxation energies arrived at via the Auger parameter.

C. HYDROGEN IODIDE AND IODINE

As discussed in Chapter II, Section D, an alternative measurement of relaxation energies may be possible if comparisons can be made between atomic and condensed states of atoms. An investigation of the $I_2(g) <=> 2I(g)$ equilibrium was attempted using the oven described in Appendix C. Unfortunately, a variety of difficulties, primarily associated with the introduction of the sample gas, did not allow us to measure the core-ionization energy of iodine atom.

However, measurement of the core-ionization energy and $M_{4,5}N_{4,5}N_{4,5}$ Auger energy of I_2 and HI was accomplished and, together with the values of ΔR and ΔV, relative to HI, are reported in Table IV.4. For comparison, ΔR for Cl_2:HCl was 1.10 eV and ΔV was 1.54 eV (See Table IV.2). Because the probe changes from Cl to I, this comparison may be misleading as both polarizability and distance change. Nonetheless, some conclusions can be drawn.

A large, positive ΔV for I_2 relative to HI indicates that the iodine attracts electrons more strongly than does hydrogen, as seems reasonable. In addition, The value of ΔR shows the high polarizability of iodine compared to hydrogen, also as expected.

Despite the failure of the attempt to study the I atom, it is possible to arrive at an estimate of the

TABLE IV.4

Core-ionization and KLL Auger kinetic energies for HI and I_2 (eV).

Compound	$3d_{5/2}$	$3d_{3/2}$	$M_{45}N_{45}N_{45}$	ΔR	ΔV
I_2	627.62	639.11	504.42	0	0
HI	627.35	638.80	506.74	1.00	0.69

relative core-ionization energy. Comparison with existing experimental and theoretical information is tabulated in Table IV.5 for two halogen-containing systems. In the left column, the difference between the ionization energies of the diatomic halogens and the hydrogen halides are presented. Note the change in sign as the series progresses. The estimates of the differences between diatomic and atomic halogens are shown in the right column. The first three values are averages of values calculated by Martin and Davidson[80]. If the progression in this column is assumed to be similar to that of the left column, an estimate of the relative core-ionization energy for I_2:I would be -0.8 eV.

The relative $M_{4,5}N_{4,5}N_{4,5}$ Auger energy has been measured for I_2:I[83] as 3.25 $\pm$ 0.10 eV. Combining this with the estimate of -0.8 eV for the ionization-energy shift gives the relaxation energy as 1.2 eV and the chemical shift as 0.4 eV. As discussed in Chapter II, Section D, to first order in the ground-state-potential model, ΔV is expected to be zero. This discrepancy seems somewhat larger than can be explained by experimental uncertainty and implies that either the extrapolation attempted in Table IV.5 is not valid, or that higher orders of the ground-state-potential model must be used to arrive at a more accurate estimate of ΔV.

As a final comment, the measurement of the atomic

TABLE IV.5

Relative Core-ionization Energies (eV)

X =	X_2 - HX	X_2 - X
F	2.49[a] (1s)	-2.7[e]
Cl	0.44[b] ($2p_{3/2}$)	-1.2[e]
Br	0.04[c] ($3p_{3/2}$)	-1.0[e]
I	-0.31[d] ($3d_{5/2}$)	-0.8[f]

a From Reference 15 and Reference 80.

b From Reference 47.

c From Reference 81.

d This work.

e From Reference 79.

f Estimate - see text.

core-ionization spectrum is complicated by the coupling of the core hole with the unfilled 5p shell of I. Since we were attempting to measure the 3d shift, the coupling gives rise to a multiplicity of states in the atomic spectrum. If the temperature in the oven is sufficient to cause equal concentrations of diatomic and atomic iodine, the diatomic peak will add to the confusion, making deconvolution difficult.

D. OTHER MOLECULES

In addition to the work outlined above, three related areas were investigated. The previously published[48,84,85] accounts of this research can be found in Appendix E of this dissertation.

Appendix E, Part 1 examines the failure of the correlation of core-binding energy and gas-phase bascitity or proton affinity for two molecules, arsabenzene and phosphabenzene. The anomalously low basicity of these compounds was investigated via XPS and the results support the view that the low basicity is due to the inability of the aromatic compounds to undergo the same geometric rearrangement on protonation as their aliphatic analogs.

In Appendix E, Part 2 the relationship between the EXAFS amplitude attenuation and the XPS shake spectrum of Br_2 was investigated. While, given certain assumptions about the threshold of shakeup, there is agreement between

the amplitude attenuation calculated on the basis of the XPS experiment and that observed in the most recent EXAFS experiments, if the assumptions are not valid (and there is at least a suspicion that they are not[86]) then agreement is poor. The role of multielectron excitations in the EXAFS spectrum would still seem to require further investigation.

Appendix E, Part 3 reports the investigation of the role of initial- and final-state effects on electronegativity. The results agree with chemical experience and theoretical calculations and show that substituent polarizability increases in the order $H \approx F < CH_3 \leq Cl < Br$. Additionally, the chemical shift increases in the order $CH_3 < H < Br < Cl < F$ if the substituent is attached directly to the probe and $CH_3 < H < Br \approx Cl \approx F$ if the substituent is remote from the site.

V. REFERENCES AND FOOTNOTES

1. H. Hertz, Ann. Physik, 31, 983 (1877).

2. A. Einstein, ibid., 17, 132 (1905).

3. D. W. Turner and M. L. Al-Joboury, J. Chem. Phys., 37, 3007 (1962).

4. K. Siegbahn, C. Nordling, A. Fahlman, R. Nordberg, K. Hamrin, J. Hedman, G. Johansson, T. Bergmark, S. E. Karlsson, J. Lindgren and B. Lindgren, "ESCA -- Atomic, Molecular and Solid State Structure Studied by Means of Electron Spectroscopy", Almqvist and Wiksells, Upsalla, Sweden, 1967.

5. K. Siegbahn, C. Nordling, G. Johansson, J. Hedman, P. F. Heden, K. Hamrin, U. Gelius, T. Bergmark, L. O. Werme, R. Manne and Y. Baer, "ESCA Applied to Free Molecules", North Holland Publishing Co., Amsterdam, Holland, 1969.

6. H. Robinson and W. F. Rawlinson, Phil. Mag, 28, 277 (1914).

7. M. P. Auger, a) Compt. Rend., 180, 65 (1925)
   b) J. de Phys. Radium, 6, 205 (1925)
   c) Compt. Rend., 182, 773 (1926)
   d) ibid., 182, 1215 (1926).

8. S. R. Smith, "Gas Phase X-Ray Photoelectron Spectroscopy of Compounds Containing Multiply-Bonded Oxygen", Ph. D. Thesis, Oregon State University, 1977.

9. For condensed-phase samples, the work functions of the spectrometer and of the sample enter into equation II.1.

10. See any text on atomic or molecular orbital calculations. For example, I. N. Levine, "Quantum Chemistry", 2nd ed., Allyn and Bacon, Inc., Boston, 1974, pp. 347-353.

11. T. Koopmans, Physica, 1, 104 (1934).

12. U. Gelius, Phys. Scripta, 9, 133 (1974).

13. L. Hedin and A. Johansson, J. Phys. B, Ser. 2, 2 (1969).

14. D. W. Davis and D. W. Shirley, Chem. Phys. Lett., 15, 185 (1972).

15. T. D. Thomas and R. W. Shaw, Jr., J. Elec. Spec. Rel. Phen., 5, 1081 (1974).

16. E. U. Condon, Phys. Rev., 32, 858 (1928).

17. E. L. Feinberg, J. Phys. (U.S.S.R.), 4, 423 (1941).

18. A. Migdal, ibid., 4, 449 (1941).

19. R. L. Martin and D. A. Shirley, J. Chem. Phys., 64, 3685 (1976).

20. M. Wolfsberg and M. L. Perlman, Phys. Rev., 99, 1833 (1955).

21. M. O. Krause, M. L. Vestal, W. H. Johnson and T. A. Carlson, Phys. Rev., 133, A385 (1964).

22. T. A. Carlson and M. O. Krause, ibid., 137, A1655 (1965).

23. T. A. Carlson, C. W. Nestor, Jr., T. C. Tucker and F. B. Malik, ibid., 169, 27 (1968).

24. T. Åberg, ibid., 156, 35 (1967).

25. P. Eisenberger and B. M. Kincaid, Science, 200, 1441 (1978).

26. B. M. Kincaid and P. Eisenberger, Phys. Rev. Lett., 34, 1361 (1975).

27. E. A. Stern, S. M. Heald and B. Bunker, ibid., 42, 1372 (1979).

28. J. J. Rehr, E. A. Stern and M. Brown, unpublished.

29. P. A. Lee and G. Beni, Phys. Rev., B15, 2862, (1977).

30. J. J. Rehr, E. A. Stern, R. L. Martin and E. P. Davidson, ibid., B17, 560 (1978).

31. E. A. Stern, ibid., B10, 3027 (1974).

32. D. E. Sayers, F. W. Lytle and E. A. Stern, in "Advances in X-Ray Analysis", B. L. Henke, J. B. Newkirk and G. R. Mallett (eds.), Plenum Press, New York, 13, 248 (1970).

33. D. E. Sayers, E. A. Stern and F. W. Lytle, Phys. Rev. Lett., 27, 1204 (1971).

34. C. A. Ashley and S. Doniach, Phys. Rev., B11, 1279 (1975).

35. P. A. Lee and J. B. Pendry, ibid., B11, 2795 (1975).

36. The use of S_n^2 for probability follows the notation of Reference 30. S_n is the monopole matrix element between the Koopmans'-theorem state and the final, ionic state. The probability for population of the state is the square of this matrix element.

37. R. Manne and T. Åberg, Chem. Phys. Lett., 7, 282 (1970).

38. T. A. Carlson, "Photoelectron and Auger Spectroscopy", Plenum Press, New York, 1975, p. 279.

39. C. D. Wagner, Anal. Chem., 44, 967 (1972).

40. C. D. Wagner and P. Biloen, Surface Sci., 35, 82 (1973).

41. L. Asplund, P. Kelfve, H. Siegbahn, O. Goscinski, H. Fellner-Feldegg, K. Hamrin, B. Blomster and K. Siegbahn, Chem. Phys. Lett., 40, 353 (1976).

42. W. E. Moddeman, "Auger Spectroscopy of Simple Gaseous Molecules", ORNL-TM-3017 1970.

43. R. W. Shaw, Jr., and T. D. Thomas, Phys. Rev., A11, 1491 (1975).

44. W. B. Perry and W. L. Jolly, Chem. Phys. Lett., 23, 529 (1973).

45. D. A. Shirley, Phys. Rev. A, 7, 1520 (1973).

46. N. F. Mott and R. W. Gurney, "Electronic Processes in Ionic Crystals", Clarendon Press, Oxford, 1948.

47. C. D. Wagner, Faraday Disc., Chem. Soc., 60, 291 (1975).

48. E. J. Aitken, M. K. Bahl, K. D. Bomben, J. K. Gimzewski, G. S. Nolan and T. D. Thomas, J. Am. Chem. Soc., 102, 4873 (1980).

49. T. D. Thomas, J. Elec. Spec. Rel. Phen., 20, 117 (1980).

50. S. R. Smith and T. D. Thomas, J. Am. Chem. Soc., 100, 5459 (1978).

51. G. Johansson, J. Hedman, A. Berndtsson and R. Klasson, J. Elec. Spec. Rel. Phen., 2, 295 (1973).

52. J. P. Desclaux, At. Data Nuc. Data Tables, 12, 312 (1973).

53. K.-N. Huang, M. Aoyagi, M. H. Chen, B. Craseman and H. Mark, ibid., 18, 243 (1976).

54. M. S. Banna, D. C. Frost, C. A. McDowell and B. Wallbank, Chem. Phys. Lett., 43, 426 (1976).

55. D. W. Davis and D. W. Shirley, J. Elec. Spec. Rel. Phen., 3, 137 (1974).

56. A. J. Ashe, III, J. Am. Chem. Soc., 93, 3293 (1971).

57. Unpublished research and reports of the research group of T. D. Thomas, Oregon State University.

58. J. W. Nibler, Oregon State University.

59. P. H. Citrin, R. W. Shaw, Jr., and T. D. Thomas, in "Electron Spectroscopy", D. A. Shirley (Ed.), North Holland Publishing Co., Amsterdam, Holland, 1972, p. 105.

60. J. F. Kielkopf, J. Opt. Soc. Am., 63, 987 (1973).

61. J. C. Boyce, Phys. Rev., 46, 378 (1934).

62. J. A. Bearden, Rev. Mod. Phys., 39, 78 (1967).

63. Reference 8, pp. 36-40.

64. Reference 8, pp. 31-33.

65. The program, GAMET, was provided by B. E. Mills of the Lawrence Berkeley Laboratory.

66. D. P. Spears, H. J. Fishbeck and T. A. Carlson, Phys. Rev. A, 9, 1603 (1974).

67. W. L. Jolly, in "Electron Spectroscopy", D. W. Shirley (Ed.), North Holland Publishing Co., Amsterdam, Holland, 1972, p. 629.

68. C. E. Moore, Natl. Bur. Stand. (U.S.) Cir. No. 469 (1949).

69. S. P. Kowalczyk, L. Ley, R. L. Martin, F. R. McFeely and D. A. Shirley Faraday Disc., Chem. Soc., 60, 7 (1975).

70. K. G. Dyall and F. P. Larkins, Monash University, Australia.

71. K. Hiroaka, R. Yamdagni and P. Kebarle, J. Am. Chem. Soc., 95, 6833 (1973).

72. J. J. Ewing, H. L. Tigelaar and W. H. Flygare, J. Chem. Phys., 56, 1957 (1972).

73. J. McGurk, C. L. Norris, H. L. Tigelaar and W. H. Flygare, ibid., 58, 3118 (1973).

74. T. X. Carroll and T. D. Thomas, ibid., 60, 2186 (1974).

75. S. Green, ibid., 58, 3117 (1973).

76. R. E. Davis and J. S. Muenter, ibid., 57, 2863 (1972).

77. B. Fabricant and J. S. Muenter, ibid., 66, 5274 (1977).

78. R. L. Martin, B. E. Mills and D. A. Shirley, ibid., 64, 3690 (1976).

79. S. A. Chambers and T. D. Thomas, ibid., 67, 2596 (1977).

80. R. L. Martin and E. R. Davidson, Phys. Rev., A, 16, 1341 (1977).

81. T. X. Carroll, R. W. Shaw, Jr., T. D. Thomas, C. Kindle and N. Bartlett, J. Am. Chem. Soc., 96, 1989 (1974).

82. W. B. Perry and W. L. Jolly, Inorg. Chem., 13, 1211 (1974).

83. T. Rantala, J. Vayrynen and S. Aksela, Chem. Phys. Lett., 66, 384 (1979).

84. A. J. Ashe, III, M. K. Bahl, K. D. Bomben, W.-T.Chan, J. K. Gimzewski, P. G. Sitton and T. D. Thomas, J. Am. Chem. Soc., 101, 1764 (1979).

85. K. D. Bomben, M. K. Bahl, J. K. Gimzewski, S. A. Chambers and T. D. Thomas, Phys. Rev. A, 20, 2405 (1979).

86. R. D. Deslattes, private communication

VI. APPENDICES

APPENDIX A. X-RAY GENERATION

1. CRITERIA FOR THE PRODUCTION OF X RAYS

In order to attain accurate measurements of the ionization energy of a sample, X radiation of a known energy must be employed. In most instruments, this is accomplished by electron bombardment of a metal in a vacuum to produce the characteristic X rays of the target. The metals most commonly used are magnesium and aluminum. In both cases, the $K\alpha_{1,2}$ doublet is unresolved but sufficiently narrow for most purposes. The X-ray energy for Al is 1485.582 ± 0.019 eV[1] and for Mg is 1253.619 ± 0.026 eV[2,3] with full widths at half maximum of 0.9 eV and 0.8 eV respectively[4]. The Mg full width at half maximum is smaller than that of Al because the spin-orbit splitting and the atomic linewidth both decrease with atomic number. Resolutions of 0.2 to 0.5 eV have been attained with the Al $K\alpha_{1,2}$ lines by use of a monochromator[5-7],but with a concomitant reduction in intensity. In addition, Ag $L\alpha_1$ radiation is used extensively by this research group. The X-ray energy is 2984.31 ± 0.03 eV[8].

X-ray production via electron bombardment is an inefficient process, about 99.9%[9] of the incident energy being dissipated as heat from from the anode. In order to

avoid anode meltings, the rate of heat removal must set the upper limit on the power levels that can be used.

Additionally, the number of Kα quanta generated is an increasing function of the accelerating voltage (See Figure A.1). The maximum voltage that can be maintained between the filament and the anode is governed by electrode and insulator geometries, surface conditions, and residual gases. Together, the heat removal and high voltage limits define the best possible X-ray production. There are other phenomena that may degrade performance, however. Two such complications occasionally arise in the X-ray sources employed in this work. Surface sputtering of the anode can occur at a bulk temperature well below the melting point if the electrons from the filament are focussed on a small area[11]. This condition can be corrected by increasing the focal area or rotating the anode. Second, deposits arising from the decomposition of residual sample gases and diffusion pump oil eventually coat the anode, reducing X-ray intensity by interacting with both the incoming electrons and the outgoing X rays. Excessive buildup of these deposits requires the removal of the anode for cleaning and polishing.

2. INITIAL X-RAY SOURCE

Two previous X-ray sources have been designed and employed in the spectrometer. Citrin, Shaw and Thomas[12]

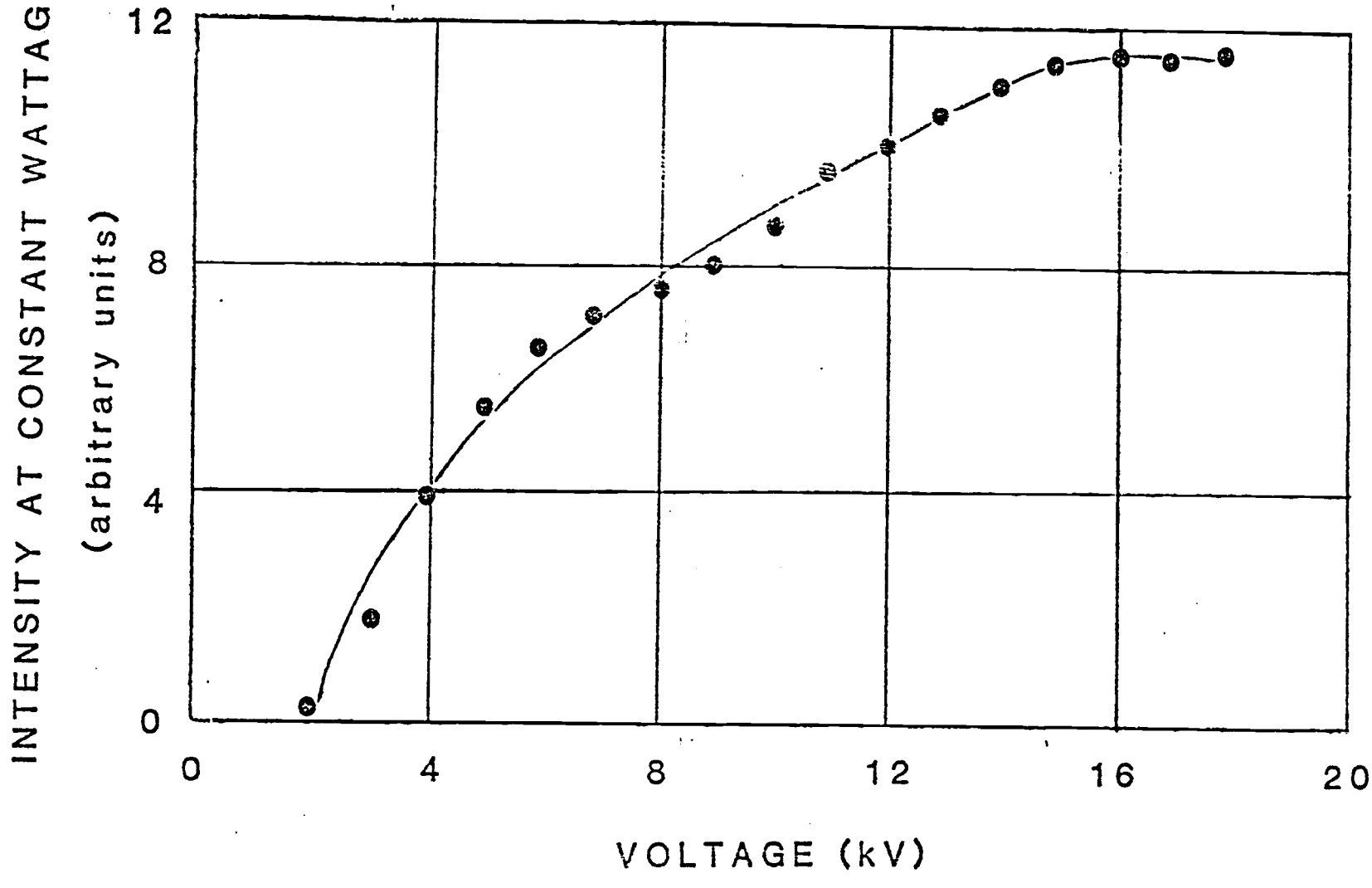

FIGURE A.1

Voltage versus intensity of X rays (From Reference 10).

used a foil that simultaneously served as both anode and X-ray window, allowing efficient use of the produced X rays. Smith[13] designed a finger-shaped anode surrounded by a circular filament with a thin aluminum foil window just above the X-ray generation chamber. Several anode styles were explored for this source, including thin-finger, thick-finger and screw-top anodes. All are described in Smith's dissertation[13].

For gases, the foil-anode source was 20% more efficient (in counts per unit power per unit time) by virtue of the anode/window design that allowed a larger percentage of the X rays produced to irradiate the sample. However, the finger-anode source showed an increased absolute counting rate of 4.3:1[14] and consequently a decrease in the counting time required to attain good experimental statistics. Measurement of gold 4f photoelectrons[14], at a given power level, indicated that, for solids in either a "ring" or "sleeve" mount[12], the foil-anode has an increased counting rate (2.3:1), attributable to the design, and that gold evaporated onto the window surface shows a 10:1 ratio of counting rates, in favor of the foil-anode source.

With an aluminum foil window, the foil-anode source has a maximum operational lifetime of approximately 50 hours at 15 watts. Magnesium foil windows have lifetimes of a few hours only below 10 watts. For aluminum anodes in the finger-anode source, operation at 80 watts can be

maintained for approximately 100 hours. Magnesium anodes, operating at 40 watts, have comparable lifetimes.

Signal-to-background ratios for gases were slightly better for the foil-anode source than for the finger-anode source (1.1:1). For solids, both ring and sleeve mounted, the foil-anode gave a significantly better signal-to-background ratio (4:1).

Smith[13] concluded that for gaseous applications, despite the loss of efficiency and slightly poorer signal-to-background characteristics, the use of the finger-anode source was justifiable because of incresed absolute counting rates and decreased counting times. Longer in-service time was cited as additional support for the use of the finger-anode source.

In lieu of this experience, a new X-ray source was proposed. This new source would be capable of significantly higher power levels and thereby decreased counting times. Preliminary considerations, based upon experience gleaned from the finger-anode source, were assimilated into an initial design by Chambers[14].

3. DESIGN AND DEVELOPMENT OF A NEW X-RAY SOURCE

Several of the considerations and objectives discussed by Smith[13] were imposed upon the new design. Foremost was the method necessary for heat removal from the anode, for, despite precautions, it was possible to melt a thin-finger

or thick-finger anode. It was decided that the most efficient method of heat removal was direct water cooling of a hollow anode.

The anode is a single piece of target material (Figure A.2). The bottom of the anode base is polished smooth to maximize thermal and electrical conductivity across the junction to a copper cooling block. The anode stem, rounded edge, and top are also polished as surface roughness promotes high-voltage breakdowns. The rounded edge and top of the anode serve as the X-ray generation sites. Water is brought to this region from below via a 1/8" stainless steel pipe that nearly contacts the inner surface of the hollow anode. Water flow rates are adjusted so that the heat generated in X-ray production is carried away from the anode before the anode material can achieve temperatures high enough to cause melting.

Figure A.2 shows the detailed assembly of the hollow-anode X-ray source. The anode is attached to a copper cooling block which acts as a further heat sink. A 3/8" copper pipe, soldered into the cooling block, serves the dual function of carrying away heated water and of being the anode high voltage supply line.

The cooling block sits in a Macor insula- tor ("Macor" is a trademark of Dow Corning) with a second Macor insulator acting to keep the anode and cooling block positioned. Outgassing within the X-ray source, a problem

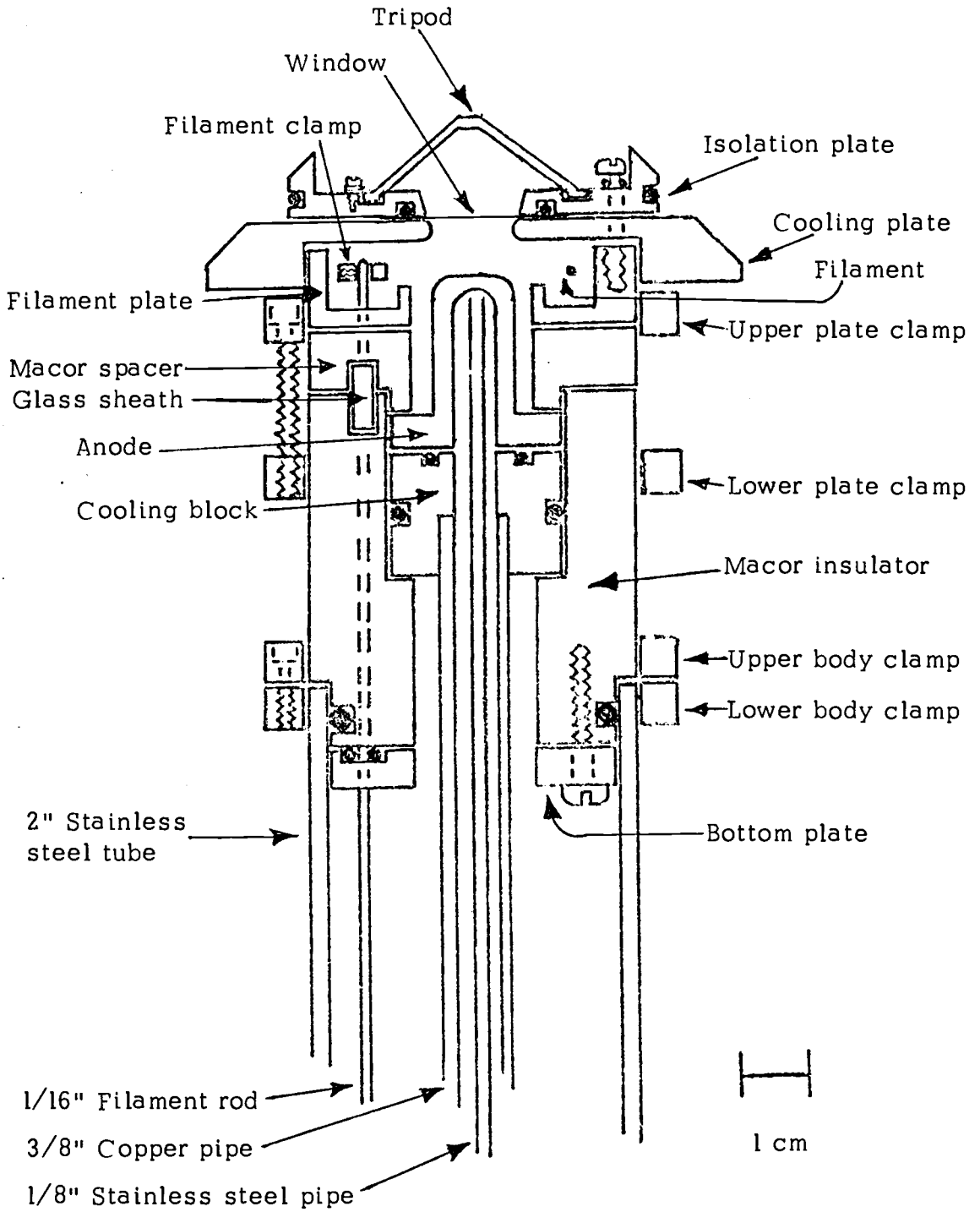

FIGURE A.2

Hollow-Anode X-Ray Tube

that arose whenever the lava insulators in previous sources were exposed to air for a few hours, is virtually eliminated by the use of Macor insulators.

The grounded filament plate rests on top of the second insulator and clamps onto the first insulator which, in turn, is clamped to the stainless steel tube. This last tube has been machined smooth and the entire assembly is introduced into the spectrometer via a sliding seal.

On top of the filament plate, the cooling plate, window, isolation plate and tripod are mounted. These pieces are interchangeably used by the hollow-anode source and the finger-anode source.

The 1/16" filament rods are brought up through the inside of the stainless steel tube and are insulated with Teflon tubing ("Teflon" is a trademark of E. I. DuPont) to prevent arcing to the high voltage power supply (water return pipe). A 9.5 cm wire filament, made of ten mil thick one-percent thoriated tungsten, is clamped onto the top of the rods in a circular configuration around the anode. Since the filament is supported only at its ends, it is subject to distortion while in operation. It is not uncommon for the filament to short circuit to either the filament plate or the bottom of the cooling plate. To avoid accidental contact with the filament plate, two small lava blocks are placed, equally spaced, under the filament wire on the filament plate. The height of the filament

rods can be adjusted externally and judicious choice of position avoids accidental contact with the cooling plate. The filament is usually set at a height such that the rounded edge of the anode is all the filament can "see" over the lip of the filament plate.

4. OPERATIONAL CHARACTERISTICS

The maximum power that can be applied to the hollow-anode X-ray source is determined by the amount of water that can be delivered to the anode tip and by the limitations of the high voltage power supply. The hollow-anode source was designed to operate at a maximum of 1500 watts, the limit of the existing power supply (20 kV, 75 mA). In actual usage, the highest power attained for any length of time has been 850 watts (13 kV, 65mA). Experiments are routinely run at 500 to 750 watts for times in excess of 200 hours with either an aluminum or a silver-coated copper anode. Typical filament currents at these power levels are five to seven amperes.

Once the high voltage desired on the anode has been selected, current is supplied to the filament by means of a power supply with adjustable current and voltage limits. This device, with a feedback loop designed by T. D. Thomas[14], is adjusted for greater control of the current, thereby avoiding breakdown due to accidental overload.

Signal-to-background ratios for the hollow-anode

source are negligibly different from those observed in gases for the finger-anode and window-anode sources. Variations in observed signal-to-background ratios for gases over a period of years with a single X-ray source have led to the conclusion that the minor variation observed between sources may not be statistically significant and that the indvidual sources are indistinguishable in their signal-to-background characteristics.

The hollow-anode source is less efficient than the finger-anode source for X-ray production at equivalent power levels by approximately 15 to 20%. However, since absolute power levels are typically five to eight times higher, the absolute counting rate exceeds those obtained via either the finger-anode or window-anode sources. Net improvements in the counting rate of 10:1 (hollow-anode to finger-anode) have been observed.

5. MODIFICATION OF THE INITIAL DESIGN

Several attempts have been made to improve the efficiency of the hollow-anode X-ray source. Particular attention has been given to window material, anode shape, and filament configuration.

The use of a window causes an attenuation of the X rays produced. The degree of attenuation is determined by both the thickness and atomic composition of the window material. Initially, aluminum foil was used as window

material for Al and Mg X-ray sources. Attenuation of the X-rays by this material ranged from 1.2 for Al to 1.1 for Mg, which was acceptable. However, for Ag X-ray sources, the attenuation was about a factor of four. To remedy this, two new window materials were investigated. Both were inorganic polymers purchased from the Peter J. Schweitzer Division of Kimberley-Clark and know by their trademarks as "Kimfol" and "Kimfone". Kimfol is a polycarbonate and Kimfone is a polysulfonate. While calculations indicated that Kimfol would attenuate X rays less than Kimfone, experience indicated that Kimfone was easier to work with and gave, in general, better results[14]. A thin layer of aluminum coats one side and a layer of graphite is applied to the other to minimize charging effects. The major drawback to the use of plastic windows has been the permeability of the window to chlorine-containing compounds.

Several attempts were made to alter the focusing properties of the electron bombardment system. A thin copper shield was employed such that the window material had no direct line of sight to the filament. However, this shield had adverse effects on the field lines that focused electrons from the filament on the anode. This shield was rejected because of loss of intensity.

Next, a flat-topped anode was tested in the hope that the electrons would focus on a well defined area. While

some surface sputtering occured, indicating a sharp focus, no increase in X-ray intensity was noted. In addition, the use of a ribbon filament with the same cross sectional area as the round filament showed adverse effects upon X-ray production with both the flat-top and rounded-top anodes[14].

Finally, a taller anode was constructed in an attempt to move X-ray production closer to the sample chamber. However, X-ray intensity was reduced, probably because of geometrical inhibition of the illuminated region[14].

6. FUTURE CONSIDERATIONS

In order to take the X-ray gun beyond its present physical limitations and toward the desired goal of 1500 watts of X-ray power, three areas require study. First, the reason for the current upper limit on the high voltage of *ca.* 13.5 to 14 kV must be found. One or more breakdown sites exist somewhere within the X-ray gun itself. It is conceivable that the problem could be associated with the filament leads but it seems more likely, on the basis of observations of "burn" patterns on the insulators, that one of the grounded surfaces is somehow too close to the high voltage. Second, a means of improving the vacuum in the X-ray chamber should be explored. And third, a method for stabilizing the filament both physically and electrically should be investigated. Slow fluctuations in both filament position and emission current are acceptable, however the

rapid pulses or wild "butterflying" that sometimes accompany even the most stable filament should be eliminated.

In addition, new Macor insulators should be made. Elimination of the screw holes that formerly held the filament plate in place should prove worthwhile. The spacer insulator and filament plate can be made into one piece, thereby avoiding the possibility of the filament grounding out when it fluctuates and touches the filament plate. Two foreseeable problems with this suggestion are that the cooling plate and isolation seal will then have to be attached to the insulator, requiring occasional sanding to keep it clean and thereby decreasing the lifetime of the combined piece. The advantages and disadvantages will have to be weighed.

7. X-RAY GUN ASSEMBLY

The following proceedure describes the assembly of the hollow anode X-ray tube. Complete disassembly is seldom necessary; however this can be accomplished by a selective reversal of the steps outlined below.

a.) Grease "O"-ring (#2-129) for the main Macor insulator to stainless steel tube seal and place it in the "O"-ring groove at the bottom of the main Macor insulator.

b.) Grease two "O"-rings (#2-003) for the filament rod feed seals and place them in the "O"-ring grooves on

the top of the bottom plate.

c.) Attach the bottom plate to the bottom of the main Macor insulator. A nylon screw should be used in the screw hole nearest the filament rods. The other screws may be either nylon or stainless steel and all four screws have regular (linear) heads. Lightly fasten all screws, but do not tighten.

d.) Gently insert the 1/16" filament rods through the bottom plate and "O"-rings and through the main Macor insulator. Tighten all screws, but do not use force as the Macor is easily stripped. Cover the exposed filament rods with Teflon tubing.

e.) Place one of the lower circular clamps on top of the stainless steel tube. (Note that the lower circular clamps are tapped, the upper clamps are not.) Make sure that the upper surface of the clamp and the top of the stainless steel tube are flush. Tighten the clamp securely. (Once this clamp has been positioned, it need never be removed.)

f.) Grease the "O"-ring (#2-119) for the cooling block to main Macor insulator seal. Place the "O"-ring in the "O"-ring groove on the side of the cooling block.

g.) Insert the cooling block into the Macor assembly of step d.

h.) Attach the high-voltage clamp to the cooling water pipe, approximately 4.5 cm from the bottom of the

pipe. Rotate the pipe so that the high-voltage lead that comes from the clamp is 180 degrees from the filament rods.

i.) Insert the assembly of step h into the stainless steel tube. Make certain that the assembly is firmly seated.

j.) At the bottom, insert the high voltage lead through the bottom spacer then slide the bottom spacer over the filament rods and Teflon tubing. If necessary, the position of the high voltage clamp can be adjusted so that it fits into the bottom spacer. Align the five screw holes in the bottom spacer with the screw holes in the bottom of the stainless steel tube. (There is only one correct alignment.) Hold the bottom spacer in place with one nylon screw.

k.) At the top, align the main Macor insulator so that the filament rods are not twisted and so that they "fall" straight from the Macor assembly through the bottom spacer.

l.) Set the upper body clamp (the one without the pumpout holes) directly atop the lower clamp on the stainless steel tube. Attach with four hex-head screws.

m.) Securely tighten the upper clamp to the Macor insulator and make sure that the four-hex head screws are tight.

n.) Place a 3/8" Swagelok nut ("Swagelok" is a trademark of the Crawford Fitting Company) with nylon or

Teflon ferrules on the cooling pipe. Insert the 1/8" stainless steel pipe (with heat exchanger "T") into the copper cooling pipe. It is now time to remove the one screw holding the bottom spacer in place, push the spacer up into the stainless steel tube and make the Swagelok connection. Exercise caution, as the nylon ferrules have a tendency to slide off as the connection is being made. (This is perhaps the trickiest part of the whole operation. I have found that it is sometimes necessary to partially screw the Swagelok nut, ferrules and all, onto the heat exchanger "T" then slide that assembly over the copper cooling pipe.) The connection should be leak tight.

o.) When the Swagelok is snug, slide the bottom spacer back into position and secure it there with three nylon screws.

p.) Attach the filament leads to the filament rods.

q.) Attach the hook. The bottom of the X-ray tube is now assembled, procede to the top.

r.) Grease the "O"-ring (#2-012) for the anode to cooling block seal and place it in the groove on the top of the cooling block.

s.) Place 2-cm lengths of glass tubing over the filament rods and into the main Macor insulator.

t.) Attach an anode. Four hex head screws hold it in place.

u.) Set the remaining bottom circular clamp about 2

cm down the body of the main Macor insulator. Clamp it loosely in place.

v.) Set the Macor spacer over the filament rods and anode.

w.) Securely attach the upper plate clamp (with pump-out holes) to the filament plate. The pumpout holes on the clamp should align with the holes in the filament plate. Once this assembly has been completed, it should not be necessary to separate these two pieces, even if the X-ray tube is to be completely disassembled.

x.) Set the assembly from step w over the filament rods and align the plate so that the rods are electrically isolated from the filament plate.

y.) Maintain the alignment of step x while the bottom clamp is loosened and rotated until it aligns with the upper clamp. Fasten the two body clamps together with four regular head screws. Securely tighten the lower clamp to the main Macor insulator. Tighten all screws. (If the alignment of step x is lost during this operation, loosen screws, loosen the lower clamp, reposition, tighten the clamp then tighten all screws.)

z.) Cut a 9.5 cm filament (ten mil, 1% thoriated tungsten wire) and form into a roughly circular shape by bending it around some circular object. The filament is attached to the top of the filament rods by means of the filament clamps. The screws in the filament clamps can be

reached through the pumpout holes in the filament plate.

aa.) Place two lava blocks between the filament and the filament plate. Position the filament (by adjusting the height of the filament rods) so that there is no direct line of sight from the filament to the anode.

bb.) Place the cooling plate on top of the X-ray assembly.

cc.) Cut a window (and, if plastic, spray it with graphite on the side that is not aluminized). Position the window over the hole in the cooling plate.

dd.) Check the "O"-rings on the isolation plate and, if necessary, grease or replace them. If the tripod is to be used, attach it to the isolation plate. Place the isolation plate on top of the X-ray assembly and secure in place with three regular head screws (with "O"-rings). Try to avoid punching holes in the window.

8.REFERENCES AND FOOTNOTES

1. T. D. Thomas and R. W. Shaw, Jr., J. Elec. Spec. Rel. Phen., 5, 1081 (1974).

2. J. A. Bearden, Rev. Mod. Phys., 39, 78 (1967).

3. B. N. Taylor, W. H. Parker and D. N. Langenberg, ibid., 41, 375 (1969).

4. T. A. Carlson, "Photoelectron and Auger Spectroscopy", Plenum Press, New York, 1975, p. 21.

5. U. Gelius, E. Basiler, S. Svenson, T. Bergmark and K. Siegbahn, J. Elec. Spec. Rel. Phen., 2, 405 (1973).

6. K. Siegbahn, D. Hammond, H. Fellner-Feldegg and E. F. Barnett, Science, 176, 245 (1972).

7. Y. Baer, G. Busch and P. Cohn, Rev. Sci. Instr., 46, 466 (1975).

8. R. C. Weast (Ed.), "Handbook of Chemistry and Physics", (50th Ed.) Chemical Rubber Co., Cleveland, (1970).

9. M. Green and U. E. Cosslett, Brit. J. Appl. Phys., (J. Phys. D), 1, 425 (1968).

10. Reference 4, p. 20.

11. N. A. Dyson, "X-rays in Atomic and Nuclear Physics", Longman Group, Ltd., London, 1973, p. 138.

12. P. H. Citrin, R. W. Shaw, Jr. and T. D. Thomas, in "Electron Spectroscopy", D. A. Shirley (Ed.), North Holland Publishing Co., Amsterdam, Holland, 1972, pp. 347-353.

13. S. R. Smith, "Gas Phase X-Ray Photoelectron Spectroscopy of Compounds Containing Multiply-Bonded Oxygen", Ph. D. Thesis, Oregon State University, 1977.

14. Unpublished research and reports of the research group of T. D. Thomas, Oregon State University.

APPENDIX B. SYSTEM/SAFETY STATUS BOARD

The SYSTEM/SAFETY status board was designed to ensure safer operation of the spectrometer and to aid in avoiding anode melting. It is activated by placement in a NIM BIN, attaching the sensor leads that are at the rear and switching the control relay from "Manual" to "NIM BIN Control".

There are three major components associated with the status board; (1) the RELAYS, (2) the SYSTEM sensors and (3) the SAFETY sensors. Their functions and modes of operation are described below. In addition, the function of (4) the HIGH VOLTAGE push-button and (5) the TEST push-button will be described.

1. RELAYS

There are two important relays in the system. In "Manual" mode, the Plexiglas box ("Plexiglas" is a trademark of Rohm and Haas.) has the only functional relay and it is controlled by two microswitches (as described under DOOR and LID). This relay will be referred to as the interior (high-voltage) relay. The second relay is in a small aluminum box just above the Plexiglas safety box. This is a +6 volt relay, powered by the SYSTEM/SAFETY box and, in "NIM BIN Control", it, in turn, powers the interior relay. This second relay will be referred to as the exterior relay.

The exterior relay is controlled by the three system and two safety sensors while in "NIM BIN Control". In "Manual" control, the exterior relay has no function and the interior relay is controlled by the two safety sensors only.

2. SYSTEM SENSORS

The three system sensors are (1) X-RAY COOLING, (2) RING COOLING and (3) VACUUM. Together they ensure that the spectrometer is receiving sufficient water and maintaining good vacuum for safe operation. Their individual functions and modes of operation are described below.

It is possible to bypass all three system sensors, for any number of reasons, by means of the SYSTEMS BYPASS push-button on the NIM module. Upon activation, the bypass maintains itself until the door under the spectrometer is opened. Figure A.3 illustrates the logical equivalent of this bypass. Momentary contact, via the push-button, powers one leg of an OR logic, the output of which powers one leg of an AND logic. The door provides the signal to the other half of the AND and must be "up" in order to get output from the AND. A feedback from the AND powers the second leg of the OR, maintaining output from the OR after momentary contact has ceased. As long as the door is "up" (closed) the bypass remains in effect. Once the door is opened ("down"), the bypass is deactivated and remains

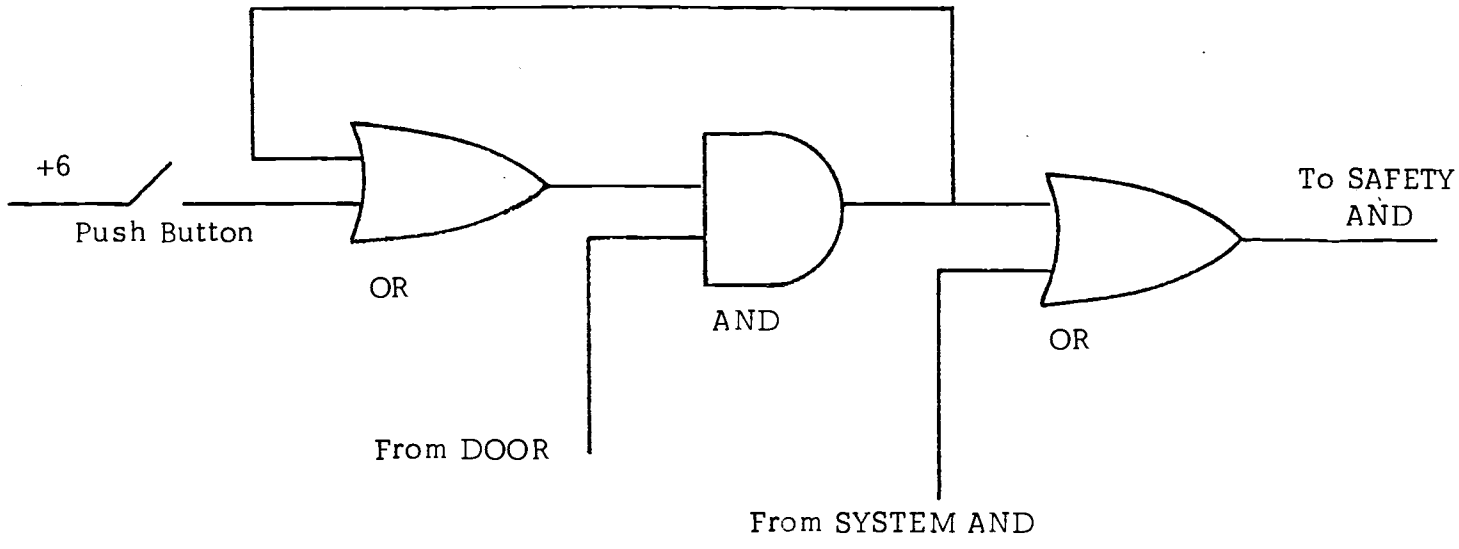

FIGURE A.3

Logical equivalent of the SYSTEM bypass.

deactivated until the button is pushed again.

Output from the AND powers a second OR logic that feeds the SAFETY AND. Output from the normal mode of operation (i. e. output from the SYSTEM AND) powers the other leg of this second OR so that the SAFETY AND cannot differentiate between normal usage and bypass mode.

a. X-RAY WATER

The status board will show green when X-ray cooling exceeds 3/8 gal./min. or approximately 1900 cc/min. (This corresponds to a reading of about 6 at the top of the stainless steel ball in the X-ray water flow meter.) Insufficient flow will show red and will not allow the exterior relay to be thrown, or, if on, will shut off the exterior relay.

Flow is measured by means of a SHUR-FLO automatic interlocking flow switch ("SHUR-FLO" is a trademark of the Hayes Manufacturing Company) that is connected into the status board as shown in Figure A.4. Insufficient flow connects signal to ground and the status board shows red. Adequate flow connects signal to +6 volts and shows green[1-3].

The intent of this device is to ensure sufficient flow of water to cool the anode at 1500 watts and to avoid electrocution is case of a water leak from or through the anode. Since the water cooling pipe is also the high-

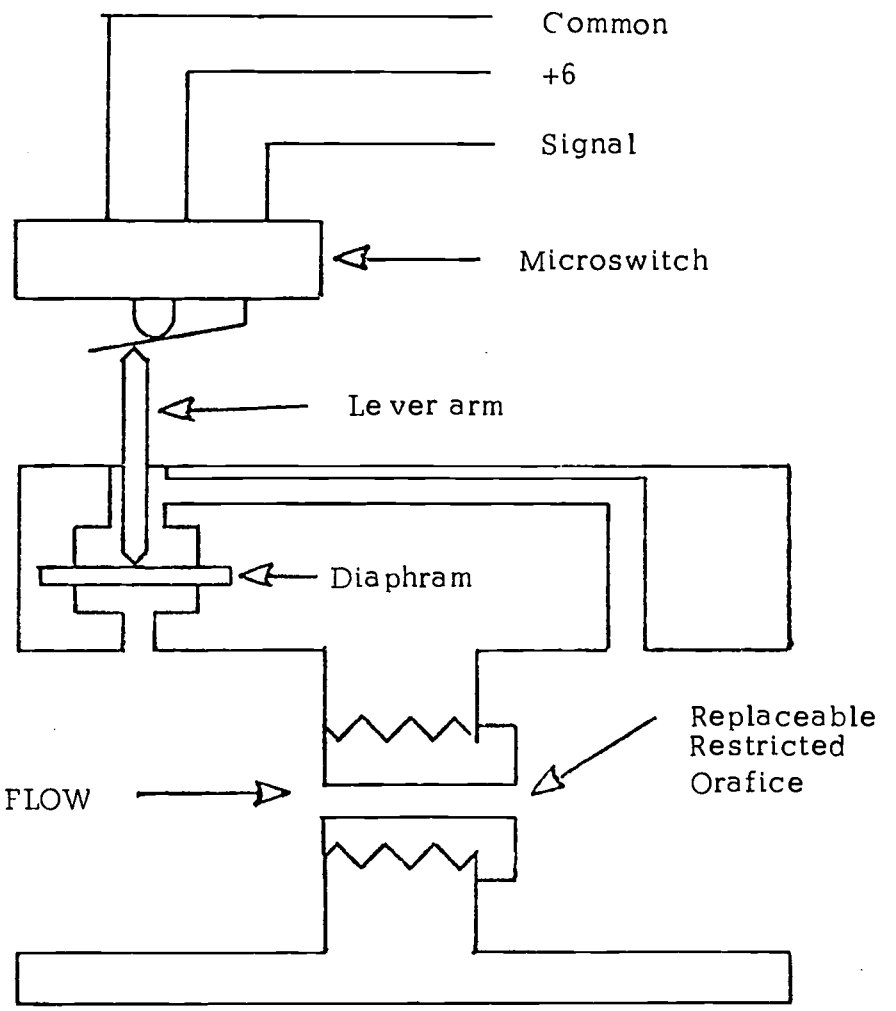

FIGURE A.4

SHUR-FLO, in cross section, with details of flow sensor and signal switching. Not to scale.

voltage supply line, it is possible for any leaking water to be at high voltage also and this device reduces that possibility.

The X-ray status can be bypassed by means of the X-RAY BYPASS push-button, in cases where the prescribed flow rate is too high (as for the window-anode or finger-anode X-ray guns) or unnecessary (as for the electron gun) or if one wishes to run at very low power. The bypass, upon activation, maintains itself until the door under the spectrometer is opened. Figure A.5 illustrates how the system works logically. Momentary contact (push-button) powers one leg of an OR logic, the output of which powers one leg of an AND logic. Since the door provides power to the other leg of the AND, it must be "up" in order to get output from the AND. A feedback loop from the AND to the second leg of the OR maintains power after momentary contact has ceased. As long as the door remains closed ("up"), the bypass is in effect. Once the door goes "down" (opens), the bypass is deactivated and remains deactivated until the button is pushed again.

Output from the AND powers a second OR logic that feeds the SYSTEM AND described earlier. Output from the X-ray water sensor powers the other leg of the second OR so that the SYSTEM AND cannot differentiate between the normal and bypass modes.

The X-ray cooling can also be bypassed as described in

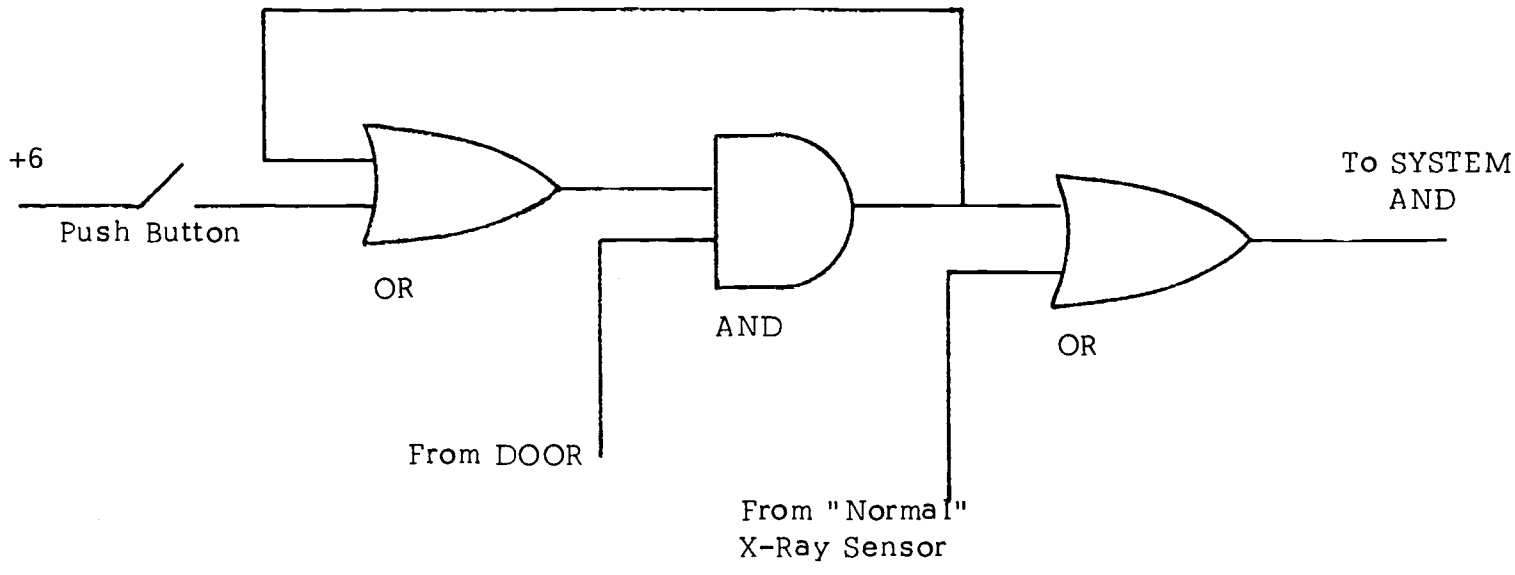

FIGURE A.5

Logical equivalent for the X-Ray Bypass

Part 1 of this appendix, or by switching from "NIM BIN Control" to "Manual" control. The bypass capability should not be used unless it is absolutely necessary, since it is quite simple in any of the bypass modes to melt an anode.

b. RING WATER

The status board will show green when the cooling ring water flow exceeds 1/10 gal./min. or approximately 700 cc/min. (A reading corresponding to about 6 at the top of the black glass ball in the cooling ring flow meter.) Insufficient flow will show red and the exterior relay cannot be turned on, or, if on, will be shut off.

Flow is measured by a SHUR-FLO automatic interlocking flow switch, connected into the status board as shown in Figure A.4. Insufficient flow connects signal to ground and the status board red light glows. Adequate flow connects signal to +6 volts and the green light glows[1-3].

The intent of this device is to ensure sufficient water flow to cool the X-ray head and to avoid overheating and damage to the seals and "O"-rings in the vicinity. Additionally, it protects the spectrometer from heating.

The cooling ring can be bypassed as described in Part 2, or by switching from "NIM BIN Control" to "Manual" control. It is advisable under either bypass condition to have sufficient flow of water into the cooling ring. Additionally, it is possible to heat the vicinity of the

X-ray head by means of current through the filament (See Appendix A) without any water flowing through the cooling ring or X-ray tube. It is probably wisest to avoid this practice and always have adequate flow no matter what the configuration may be.

c. VACUUM

This sensor is currently non-functional but was included so that the status board would show green under acceptable vacuum conditions (say, less than 0.1 Pascal) and red when the vacuum in the X-ray chamber was unsatisfactory. This latter case would not allow the exterior relay to be powered, or, if on, would shut it down. Additionally, it was envisioned that a bad vacuum signal would be used to shut off cooling water to the anode on the assumption that the sudden change in vacuum pressure would be due to a water leak at the anode. While it is hoped that this leak would separately cause the X-ray cooling signal to go red, it is possible that a small leak might not cause sufficient pressure drop to do so.

Currently, the vacuum sensor is attached to a "dummy" switch that can connect it to ground (red) or +6 volts (green)[3]. A second sensor wire, not connected, runs to the spectrometer in the event that a real vacuum sensor is ever connected to the spectrometer. (This wire is the "other" leg of the zip cord that goes to the door microswitch.) One

possible mode of operation would be to have the sensor attached to the ion gauge in the X-ray chamber, however, this implies continuous operation of that gauge while the high voltage is applied.

Vacuum sensitivity can be bypassed as described in Part 2, or by switching from "NIM BIN Control" to "Manual" control. If the sensor is ever connected to a vacuum gauge, it might be advisable to have an external bypass switch included to alleviate the necessity of continual usage of the gauge.

3. SAFETY SENSORS

There are two safety sensors, the DOOR and the LID microswitches. Together, they ensure against accidental electrocution either under the spectrometer or inside the Plexiglas safety box. Their functions are outlined below.

It is not possible to bypass the two safety sensors in either "NIM BIN Control" or "Manual" control as a back-up set of microswitches exist that were not removed when the status board was installed. However, the switches are not redundant as they serve separate functions with identical results[4].

a. DOOR

There are two separate microswitches on the door under the spectrometer. The "old" circuit was not removed so

that in "NIM BIN CONTROL", it would serve as a back-up safety device. In "Manual" mode, the "old" microswitch is the only device that functions. In "NIM BIN Control", the "old" microswitch is responsible for the interior relay[4]. The "new" microswitch operates only in "NIM BIN Control" and is placed such that when the door under the spectrometer is closed and bolted the output signal is connected to +6 volts and shows green. If the door is opened, the "new" microswitch connects signal to ground, shows red and the exterior relay cannot be switched on, or, if on, will be switched off[3].

This device prevents someone from getting under the spectrometer while high voltage is applied. It can be bypassed in "Manual" mode but the "old" microswitch would then control the interior relay and accidents are still avoided. The DOOR control is a primary safety device and should never be circumvented.

b. LID

There are two separate circuits on the lid of the Plexiglas safety box. The "old" microswitch was not removed so that it could function as a back-up safety device while under "NIM BIN Control", or if the SYSTEM/SAFETY device should become non-functional, it could function as it always had. In "Manual" mode, it is the only microswitch that functions. In "NIM BIN Control", the

"old" microswitch is responsible for the interior relay[4]. The "new" switch operates only while in "NIM BIN Control" and is placed such that if the lid of the Plexiglas safety box is raised then the signal is connected to ground and the red light comes on. With the lid properly closed, the signal is connected to +6 volts and the green light is on. When the red light shows, the exterior relay cannot be powered, or, if on, will be turned off.

This device avoids accidental electrocution inside the Plexiglas relay box. It can be bypassed in "Manual" mode, but then the "old" microswitch controls the interior relay and accidents are still avoided. The LID control is a primary safety device and as such should never be disconnected.

4. HIGH VOLTAGE

In "NIM BIN Control", high voltage to the anode is attained by means of the HI VOLT push-button on the NIM module. This activates the exterior relay which, in turn, activates the interior high-voltage relay. High voltage can be turned on and maintained only if the DOOR and LID are green (closed) and the SYSTEM sensors are either all green or bypassed. The logical equivalent of this circuit is shown in Figure A.6. The push-button establishes a momentary contact that, when the three other legs are "up", produces an output from the AND. A feedback loop to the OR

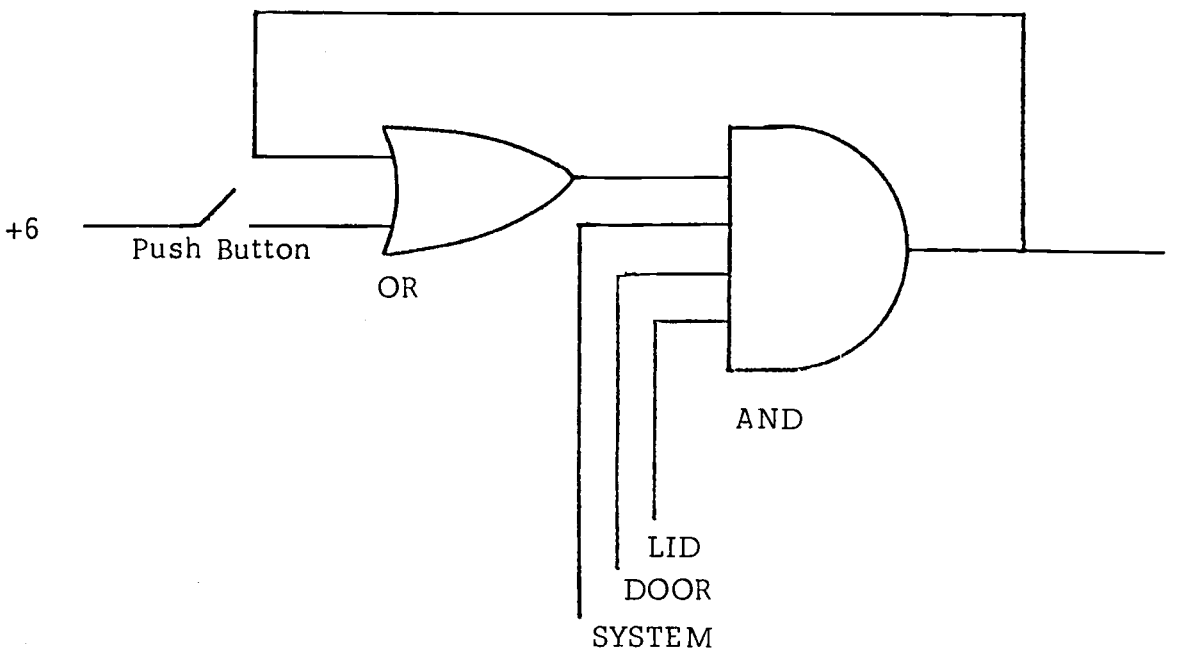

FIGURE A.6

Logical equivalent for the HI VOLT pushbutton

maintains power to the AND after momentary contact has ceased. If any leg goes "down", the high voltage is shut off and remains off until the red condition is corrected and the push-button is depressed again[3].

In "Manual" mode, the interior relay is thrown and high voltage can be generated at the anode only after the green button at the bottom of the Plexiglas safety box is pushed. Contact beyond momentary is maintained by a solenoid.

5. TEST

The TEST push-button powers all lights on the SYSTEM/SAFETY status board to test for burned out lamps. This button can be depressed while the high voltage is on.

6. REFERENCES AND FOOTNOTES

1. A variety of flow rates from 1/10 to 1/2 gal./min. are available by interchanging nozzles in the water flow sensors. (Nozzle No.'s 2838, 2877, 2879, 2880, 2886 and 2887 are also available.) In addition, a blank nozzle (No. 2899) that can be drilled for any flow rate not included in this range is also available.

2. The water flow sensors have a dead band, dependent upon the flow, that causes deactivation to occur at a significantly lower flow than that at which activation occurs. See Folder 2600-40, pp. 10-12.

3. Because of the way the status board was designed, if neither signal is recieved (neither +6 volts nor ground), the green light will be on. A short to ground will, however, show red despite the signal passed by the sensor. It has been suggested that the inputs of the safety circuit be attached to ground through a resistor that is large compared to the output impedance of the +6 volt power supply. Then an accidental disconnect would drive the device to red

rather than green, as a fail safe.

4. If, for some reason, a microswitch on the LID or DOOR should become stuck closed, one of the two following scenarios would occur: (1) If either of the "old" microswitches stuck, the "new" switch would still shut off power to the interior relay (by deactivating the exterior relay), but the interior relay will not return to its "off" position. This is the worst of the two possibilities, as it turns off all warning lights but does not disconnect the high voltage under the spectrometer. Once the "new" microswitch is again closed, the HI VOLT button on the status board must be pushed to reestablish the warning lights. (2) If either "new" microswitch remains closed while the "old" are open, the interior relay will be deactivated, but the exterior relay and high voltage indicator light on the NIM module will remain on. Once the "old" switch is closed again, the interior relay will be thrown immediately (without pushing any buttons). Note that in "Manual" control, only the "old" microswitches are functional and a stuck "new" switch has no effect.

APPENDIX C. THE OVEN

1. DESIGN CONSIDERATIONS

When the initial designs for a high-temperature cell inside the spectrometer were composed, three considerations were of particular importance. First, introduction of the oven into the spectrometer was to be accomplished by attaching the oven to the top of the existing X-ray tube. This allowed for sample manipulation without having to bring the entire spectrometer to atmospheric pressure but created a problem in the method of introduction of the reference and sample gases. Second, bifilar wrap of the heating element was required to minimize magnetic field lines. Third, the heating wire was to be encased in ceramic paper and ceramic cement so as to allow maximum flexibility in the construction of the heater core.

The last consideration, above, also proved the most troublesome, as will be discussed below. The final oven design, along with the sample cell and X-ray tube modifications that were required, is shown in Figure A.7. Note that sample and reference gases are introduced via an inlet pipe that squeeze connects to the top of the oven when the oven is slid into place. Not shown is a referencing pin, which aligns the slits in the oven with the slits in the spectrometer. Also not shown are the filament and

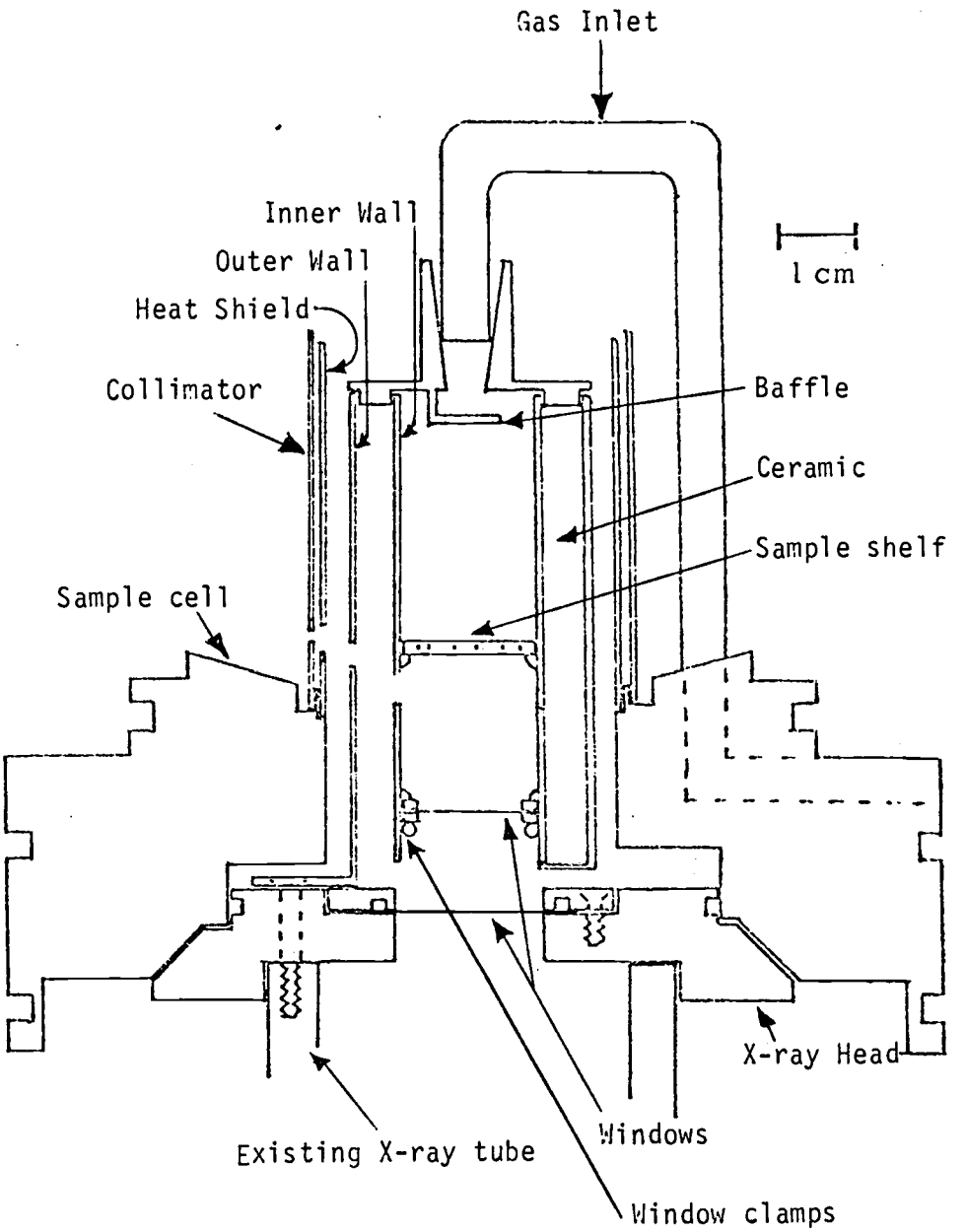

FIGURE A.7

High Temperature Cell

thermocouple leads, the position of the thermocouple nor the fiducial mark for alignment of the slits in the heat shield and collimator with the slits of the spectrometer.

2. CORE CONSTRUCTION

The most difficult and time-consuming operation in the preparation of the oven involves the construction of the heater core. A cylinder of ceramic paper (0.020" thick, obtained from Cotronics Corporation) is fastened to the outside of the inner wall of the oven with wire. A thin layer of ceramic cement (also from Cotronics Corporation) is spread over the ceramic paper. (This is actually a two-step operation; step one spreads cement over the areas that are not covered by the wires that hold the ceramic paper in place, then when the first step has dried, the bands are removed and the paste is applied to the areas that had been covered.) The ceramic paste requires approximately 24 hours to cure, but the process can be speeded up by heating the asssembly at 110 degrees Celsius (°C), for approximately six hours.

When the cement has dried sufficiently, the slit holes are cut in the ceramic shell. The holes should be over-sized so as to minimize any interaction with ejected electrons, and should account for the angle of collection. (While this angle is not important at this step, with each succeding layer of ceramic paper, it becomes increasingly

significant.)

A Nichrome wire wrap (80% Ni, 20% Cr) is made by tightly coiling the wire around a rod with a diameter slightly smaller than the diameter of the inner sleeve. The use of a lathe and screw-drive greatly facilitates this step. When the tension of the wrap is released, the coil will relax to approximately the desired diameter. The wire wrap is placed over the inner ceramic cylinder so that the excess wire is at the top of the oven. Cement the upper half of the wire on the cylinder in place. Gently bend the wire at spots above and below the slits where it will pass one of the slit supports. Cement the lower half in place and count the number of coils that form the inner wrap.

Attach a cylinder of ceramic paper to the outside of the assembly, and lightly cement it in place. If desired, the inner surface of this cylinder can be coated with ceramic paste for better adhesion to the previous layers. Cut out the slits, remembering to correct for the angle.

At the top of the core, unwrap a length of the coiled wire and reverse the direction of the coil. Slide the coil over the ceramic core <u>from the bottom</u> recoiling the length that was unwrapped as you procede. This may take several sessions, as the ceramic is brittle and you may have to reapply the ceramic paste to areas that have taken too much stress. Any protruding bits of ceramic that interfere can be sanded or filed from the surface. When an equal number

of coils has been wrapped around the upper section of the core, cement the wire in place.

Once again, choose a spot to pass the slit supports (but not the same spot as for the inner wrap) and gently bend the wire to pass the slits. It is imperative that no weaknesses in the wire arise because of this bending process or hot spots and breakdowns will occur. The lower section of outer wire can now be cemented in place.

An outer cylinder of ceramic paper is wrapped over the outer wire and cemented into place. The slits are then cut out of this outer layer. At this point, cement should be applied liberally at the top and bottom of the core and along the slits so that no wire can be seen from the outside. The slits are to remain free and oversized.

The assembly is then smoothed to remove any rough or protruding surfaces. Care must be taken to ensure proper separation at the slits; however the core is usually flexible enough so that adjustments can be made once it has been positioned inside the outer wall of the oven. Experience indicates that, upon heating, there is a slight expansion of the ceramic core that tends to firmly position it inside the outer sleeve. This poses no particular problem so long as the slits are carefully attended to.

3. OVEN ASSEMBLY

To assemble the oven, first cut a window roughly the diameter of the inner sleeve. Using three small flathead screws, sandwich the window between the two window clamps. Trim any excess window material from the outside of the assembly and position in the inner sleeve of the oven. Hold the window assembly in place by means of the spring clamp that sits in the three small holes in the inner sleeve.

Slide the inner sleeve assembly into the ceramic core and then slide the ceramic core into the outer sleeve. The sample shelf can be placed in the inner sleeve through the top of the oven. If a sample is to be included, it should be placed inside at this point.

A thermocouple is inserted into the oven by securing two ceramic tubes through the top of the oven and passing one leg of the thermocouple through each of the ceramic tubes. (The thermocouple should be Chromel-Constantan and the ceramic tubes are secured by means of a ceramic-metal cement.) The top of the oven can then be placed over the oven assembly. Ceramic tubes are threaded over the thermocouple legs and attached to the side of the outer sleeve at a slit support.

The electrical connections are made via four wire clamps set in epoxy at the top of the X-ray plate. The

epoxy also acts to help isolate the X-ray chamber from the tank. Wires then pass from the clamps, through the epoxy into the X-ray chamber where they are attached to electrical leads from the outside of the spectrometer. Care is taken to ensure electrical isolation of the heater legs from the X-ray tube.

4. OPERATIONAL CHARACTERISTICS

The oven is controlled from outside the spectrometer by means of an isolation transformer, a Variac and a temperature gauge attached to the thermocouple. In tests outside the spectrometer, temperatures of 650° C were observed. Typically, to attain a temperature of 400° C, the Variac is operated at 20 volts and approximately 1.5 amperes. Temperature rise times depend upon the initial setting of the Variac, but a 400° rise in 15 minutes has been observed. Stability at equilibrium temperatures is on the order of ±2° at 400° C, over a period of several hours. Prolonged heating has an effect on the color and characteristics of the ceramic core. The paper takes on a charred appearance and the paste becomes excessively brittle. In addition, the ceramic-to-metal cements used to attach the thermocouple lines to the oven also become brittle.

5. FUTURE IMPROVEMENTS

Four areas of design improvement have become apparent. First, the ceramic core made from paper-paste components takes longer to construct than is desirable and the lifetime of the core is limited. It would be advantageous to try to use a ceramic-coated wire that can be wrapped directly around the inner sleeve. Second, improved sample resident times in the oven are of great concern. As constructed, the leak rate from the slits is too fast to allow rapid measurement. Third, a better method of attaching the thermocouple legs to the outside of the oven should be used. Perhaps a clamp that holds the ceramic tubing in place, so long as the clamp does not protrude into the sample cell. Last, the heat shield must be attached in a manner that prevents allow slippage of the shield as the oven moves past.

APPENDIX D. PROGRAMS

In the course of this research, three computers have been employed and programs have been written for each of them. The more important of these programs and notation of their uses and functions are outlined in this appendix, in sections according to the machine that the program was written on.

1. CYBER

The campus computer, a Control Data Corporation CYBER 70, is primarily used for CNDO/2[1] calculations and curve fitting of Gaussian functions (GAMET[2]) to complicated spectra. For the latter purpose, two programs have been written to facilitate data input. Two data-taking computers are currently used and the card punching program that must be employed to convert the output from these computers to input for the CYBER programs are different only in input format. Additionally, the CYBER computer was used to aid in the calculation of EXAFS attenuation coefficients for inclusion in the paper of Appendix E, Part 2.

a. CARDPUN

Output from the Digital PDP-9 computer is predominantly in the form of a paper tape. The format of the output is; title, light pen points, data, and the number of scans. All but the title are in I6 format. If the first

light pen point is modified to reflect the number of data channels, CARDPUN will output a file in a format that the GAMET program can accept. A title card, data cards and the number of channels are punched on cards for this purpose. Note that additional cards are required before GAMET can be run from batch and that detailed instructions on both this program and GAMET are available in the CNDO/GAMET log[3].

b. MINCARD

Output from the Digital MINC-11 computer is on disk with a title, light points, number of channels, data, number of scans, date and time, scan conditions and calibrations. The MINCARD program will output a file in the format demanded by GAMET, with the same information as the previous program. Methods for transferring data from disk or paper tape are also outlined in the CNDO/GAMET log[3].

c. EXAFS Programs

In the course of the work on the EXAFS attenuation coefficient, a large variety of programs were written to calculate the attenuation factor as a function of photon energy. In general, these programs were named EXAFSn, where n was either a number (one to nine) or a number-letter combination, e. g. 5C. The programs that follow were not written on the PDP-9, as the first two EXAFS programs were, because of read-in errors from both paper

tape and magnetic tape where one or more data points would get "lost" in the read process.

Data are read in from a data file in PDP-9-type format and output onto a data file that includes the photon energy and the attenuation factor for that energy. Photon energy step size is 0.25 atomic units, k.

All programs ignore 30 channels at the beginning of the data file. The position of the primary photoelectron process is also inherent in the programming. In addition, all programs include a correction for the variation of intensity with kinetic energy that is inherent in our constant resolution spectrometer.

i. EXAFS3

EXAFS3 was written to perform the amplitude attenuation calculation and to include an Al $K\alpha_{3,4}$ X-ray satellite correction to the data. The energy separation (KASEP) and percent contribution (PCKA) of the satellites are written into the program (although any higher-kinetic-energy satellite may be removed by replacing these values). A constant background (JBAC) is assumed.

ii. EXAFS4

EXAFS4 modifies EXAFS3 by performing the amplitude attenuation calculations iteratively with differing constant backgrounds. The backgrounds are all supplied

internally and the output is modified so that each listing of the attenuation factors is preceded by the value of the background that produced it.

iii. EXAFS5, EXAFS5A, EXAFS5B and EXAFS5C

A sloping background is included in EXAFS5. The slope is inherent in the program. In addition, three nearly identical versions of this program were created; EXAFS5A, EXAFS5B and EXAFS5C. These differ only in the "cutoff value" of k, the photon energy. As discussed in the paper in Appendix E, Part 2, a threshold value for the onset of shake was assumed and these three programs reflect differing onset values. 5A has a threshold of 0.75 k, 5B has a threshold of 4.0 k and 5C has a threshold of 25.0 k.

iv. EXAFS6

The background function in the EXAFS6 program is a step function. The step occurs at a fixed channel near the primary peak and a constant background is maintained on both sides of the step with data to lower channels having the higher background.

v. EXAFS7

An exponential tail is included in the EXAFS7 program on top of a constant background. In addition, a 15 channel cutoff rather than a limit on k is used.

vi. EXAFS8

EXAFS8 is a modifed version of EXAFS7. A 20 channel cutoff is employed, so that if the photon energy was within 12 electron volts the attenuation factor was not calculated.

vii. EXAFS9, EXAFS9A, EXAFS9B and EXAFS9C

The EXAFS9 programs require data in a format different from the preceding programs. A modified data file must be prepared. The light pen points must be removed and all background corrections, satellite corrections and constant resolution corrections incorporated into the file. The modified format allows the use of any corrected data file with any modification, so long as the final file has no light pen points. It requires only that the number of data channels be known.

The four versions differ only in their cutoff value for k. 9 has a limit of 0.75 k, 9A of 4.0 k, 9B of 10.0 k and 9C has no threshold value.

The programs that were of most importantance for the calculations reported in the paper of Appendix E, Part 2 are 5, 5A, 5B, 5C, 9, 9A, 9B and 9C. The other programs were relatively unimportant.

2. PDP-9

Most of the data reported in this dissertation were taken on a PDP-9. In addition, a number of programs were written for use on this machine, primarily for the manipulation of data. The first two EXAFS programs are included in this section, along with programs that will compute total counts under a portion of the experimental curve, calculate the average energy over a spectrum, compare total counts between two regions and convert data in octal to decimal.

a. EXAFS

The first two versions of the EXAFS programs were written on the PDP-9. EXAFS1 is the initial version and does not include an X-ray satellite correction. A constant background correction is requested by the program. EXAFS2 does include the satellite correction and is identical to EXAFS3 on CYBER except that all information is entered from a terminal rather than being internal to the program.

b. ADD

This program will add two or more data tapes together, provided that they both have the same number of channels. Output consists of a new data tape. This program is particularly useful when data acquisition must be interrupted.

If the data are punched out and a second run is begun when the computer is once again available for data taking, the two outputs can be summed, saving the time required by the first run. The statistical improvement of summing two or more independent runs is advantageous.

c. BACSUB

BACSUB will use a data tape containing information about the background in a spectrum and remove this contribution from a second data tape. A multiplicative factor is requested by the program. This factor may be used to adjust differences in total counts, number of scans or to normalize peak height of a background peak to the peak height of the same peak in the second tape.

d. COMPAR and CMPARE

CMPARE is identical to COMPAR except that CMPARE requires data tapes without a title or any light pen points. Both programs will sum over two different regions of a data tape and report the total counts in these two regions. A ratio of the two regions is also reported.

Input consists of a request by the program for the channel numbers at the beginning and end of the first region (called the shakeup region by the program), followed by a request for the beginning and end channels of the second region (the peak region). A background will be

subtracted, if the user so desires. Output consists of the total counts in region one, the total counts in region two and the ratio of counts in region one to region two.

e. FOLD

The FOLD manipulation has the effect of creating a new peak with half the intensity of any existing peak in the data, simulating a p photoionization process when performed on a single peak. The program incorporates the second spectrum, at lower kinetic energies, into a data tape. New data is computed by adding half the counts of the old data to the counts in a channel of the old data that is removed from the original data by a channel separation that is determined by the user and requested by the program.

f. LIGHTS

LIGHTS is designed to allow the user to incorproate light pen points onto a tape that does not have them. The program is stored on the PESCAN magnetic tape and is started by calling the loader then commanding the loader as follows:

←LIGHTS,TDAT3,DACTW,SCAN3(ALT MODE)

The number of channels are requested, then the program displays the spectrum on the oscilloscope. Light pen points may now be added, in the ususal manner. However,

since light points without the voltages that accompany them are often meaningless, this program is of limited value.

g. OCTAL

On occasion, a QAREA dump is required to save data on the PDP-9. When recovery of the scanning conditions is impossible because of computer error, it is possible, via DUMP, to recover the raw data. The information recovered in this manner is output as octal rather than as decimal numbers. OCTAL will convert octal numbers into decimal numbers.

It is first necessary to get a paper tape of the DUMP region that contains the data. Because of the format of the DUMP output, some numbers at the beginning and end of this tape may have to be ignored. The program compensates for the DUMP format, requests the number of lines of data that must be read and asks how many points at the beginning and end of the DUMP tape are not part of the data. These point are ignored and a paper tape, in the format of a PDP-9 data tape, is output, with the values in decimal. Light pen points are included.

3. MINC-11

Programs written for use on the MINC computer are also predominantly used for data manipulation. Most of the programs require data in the format that the PDP-9 outputs.

Programs that manipulate data include constant and linear background subtractions, X-ray satellite correction and the merging or counting of data files. Other programs will compute difference spectra, calculate the average energy of a data file and create exponential curves.

a. BACK and SLOPE

These two programs are background correction routines. BACK subtracts a constant background from a data file while SLOPE will subtract a linear background. Both programs require a PDP-9-type data file that has been stored on a disk. The programs request the name of the input file and the number of channels in the data. BACK requests the average background for subtraction while SLOPE asks for the value of the background to be subtracted from the leftmost point in the data then asks for the value to be subtracted from the rightmost point in the data. A sloping background correction is calculated from these two values. SLOPE makes BACK obsolete since entering equal values at both points has the same effect as a constant background subtraction. (However, BACK is faster to run under those circumstances.) In SLOPE, one may exclude some of the channels of the data from the output file.

b. KALPHA

KALPHA subtracts the X-ray satellite contribution from a PDP-9-type data file stored on disk. The file name and number of channels in the file are input from the terminal and the computer will ask for the satellite separation, in channels, and the percent contribution that the satellite makes to the total spectrum. The generated data is output onto disk.

c. MERGEI, MERGEF and MERG2F

These three programs will merge two PDP-9-type data files. MERGEI forms one output file from two integer-formatted data files, MERGEF creates one file from an integer-formatted data file followed by a real-formatted data file, and MERG2F makes one file from two real-formatted data files. Output from all three programs is in real format.

The computer requests the file name and number of channels in each input file, then outputs the title, light pen points and data of the first file followed by the data of the second file. The number of scans in both files and the title and light pen points of the second file do not appear in the output.

The three differing formats of these programs allow usage with raw data in a PDP-9-type data file stored on

disk (MERGEI), one raw data file and one manipulated file (MERGEF) or two manipulated files (MERG2F) in similar formats.

d. COUNT and COUNTF

These programs count the number of data channels in a real (COUNTF) or integer (COUNT) PDP-9-type data file on a disk. Since most of the programs outlined here request the number of channels of data, these programs may be of some use. A major improvement in all of these programs would be to avoid such a request by the computer, analogous to the manner used in the graphing programs written by T. D. Thomas[4].

e. DIFF and DIFFKT

Both of these programs take difference spectra by subtracting one PDP-9-type data file from another. File names and number of data channels for both data files are requested, as are the peak positions (for matching the two spectra). The second file can be manipulated by including a multiplicative factor that compensates for differences in the two data files.

Output from both programs consists of the data calculated by the subtraction of the second data file (with its multiplier) from the first. (The normalization of both data files is carefully done to ensure proper representa-

tion of the data.) DIFFKT will then calculate the average number of counts in the first few channels (the actual number of channels is entered from the terminal), subtract this value, if required, calculate the average energy of the difference spectrum and report it, in electron volts.

f. KOOPTH

KOOPTH computes the weighted average energy of a spectrum from a PDP-9-type data file that has been stored on disk. The file name, number of data chennels and peak position are requested by the program and there is an option to ignore data at the beginning of the file, if required. Once the volts per channels have been entered, the average energy over the spectrum is calculated and reported, in electron volts.

g. EXP10, EXP10B and EXP10F

These programs calculate exponential curves for use with the data manipulation or difference spectrum programs. The values for the slope of the exponential that are input for all three programs are to be in base ten (10^x) rather than the Naperian base (e^x).

EXP10 will match an exponential to the existing data at the leftmost edge of the data if the slope and matching value are entered. A lower limit on the acceptable values for the generated data is also requested, as is the channel

number of the peak in the data being matched. Output consists solely of the total number of added counts, the average energy of these counts (relative to the peak of the matched data) and the number of added channels generated by this program.

EXP10B does nearly the same thing, except that the generated data is output as a file on disk and the average energy is not reported. However, the number of generated data channels is reported.

EXP10F generates output in the same manner as EXP10B, except that the file created by this program starts at its maximum value and decreases to higher channel numbers. EXP10F is used to help smooth the region of the data that once contained the X-ray satellite.

h. COMPAR

Analogous to the PDP-9 program of the same name, COMPAR will compare two regions of a PDP-9-type data file stored on disk. If desired by the user, this program allows the comparison of two overlapping regions. The program requests start and stop channels for each of the regions then outputs the total counts in region one, the total counts in region two, and the ratio of counts in region one to the counts in region two. No background correction is made in this version of the program.

4. REFERENCES AND FOOTNOTES

1. The CNDO/2 program is based upon that of J. A. Pople and D. L. Beveridge, "Approximate Molecular Orbital Theory", McGraw-Hill, San Francisco, 1970.

2. The GAMET program was obtained from B. E. Mills of the Lawrence Berkeley Laboratory.

3. This unpublished log is a record of how to use the programs of Reference 1 and Reference 2.

4. T. D. Thomas, unpublished programs.

APPENDIX E

1. Core-Ionization Energies and the Anomalous Basicity of Arsabenzene and Phosphabenzene.

Journal of the American Chemical Society / 101:7 / March 28, 1979

Core-Ionization Energies and the Anomalous Basicity of Arsabenzene and Phosphabenzene

A. J. Ashe, III*,[1a] M. K. Bahl,[1b] K. D. Bomben,[1b] W.-T. Chan,[1a] J. K. Gimzewski,[1b] P. G. Sitton,[1b] and T. D. Thomas*[1b]

Contribution from the Department of Chemistry, University of Michigan, Ann Arbor, Michigan 48109, and the Department of Chemistry, Oregon State University, Corvallis, Oregon 97331. *Received October 2, 1978*

Abstract: To help understand the anomalously low basicity of arsabenzene and phosphabenzene we have investigated the correlation between the core-ionization energies and proton affinities for arsabenzene, phosphabenzene, arsine, trimethylarsine, phosphine, and the methylphosphines. The results support the view that the low basicity is due to the inability of the aromatic compounds to undergo geometric rearrangement on protonation. Comparison of the Auger kinetic energies with core-ionization energies gives an estimate of 0.45 eV for the stabilization energy due to the resonance delocalization of the charge on phosphine following core ionization. Further comparison of these quantities indicates that a methyl group and an aromatic ring are both electron donating compared to hydrogen.

Introduction

The recent synthesis[2-4] of the pyridine homologues shown below has made it possible to see how the properties of heterobenzenes vary with changes in the heteroatom. A variety of spectral techniques[5-7] indicate that there are similar aromatic properties throughout the series. Structural studies show that **1**–**4** have planar C_{2v} rings with typical aromatic C–C bond lengths (1.40 ± 0.03 Å).[8]

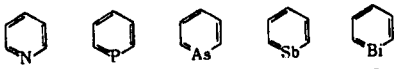

1 **2** **3** **4** **5**

In contrast, chemical studies have shown the heavier heterobenzenes to be markedly different from pyridine. The chemistry of pyridine is dominated by its basicity. However, in solution **2**–**5** show no basic properties.[5] These qualitative solution-phase observations are reflected in the gas-phase proton affinities of phosphabenzene and arsabenzene.[9] For nitrogen compounds, the proton affinity (or gas-phase basicity) increases in the order NH_3, CH_3NH_2, $(CH_3)_2NH$, pyridine, $(CH_3)_3N$, whereas for phosphorus the order is PH_3, phosphabenzene, CH_3PH_2, $(CH_3)_2PH$, $(CH_3)_3P$. For arsenic the complete series has not been studied, but the proton affinity of arsabenzene is only slightly greater than that of arsine. A quantitative comparison of the proton affinities of these compounds indicates that the proton affinities of phosphabenzene and arsabenzene are about 80 kJ/mol less than would be expected from the systematic behavior of the other compounds.

The source of this anomalously low basicity is uncertain. It has been suggested that the phosphorus lone pair may be too diffuse to form a strong bond to a proton.[10] Alternatively it has been argued that the ring structure of phosphabenzene prevents necessary changes in geometry on protonation.[5] These two explanations are, however, closely related to one another. In phosphine, for instance, the HPH bond angle is 93°; the corresponding bond hybridization is predominantly p^3 with little s participation. The lone pair is almost pure s and is, therefore, diffuse, that is, spread over a wide range of angles. For a strong bond to form with an added proton, the lone pair must become more directed and, hence, must acquire additional p character. The P–H bonds must take on more s character and the bond angles shift to the tetrahedral angle (as required also by the symmetry of the PH_4^+ ion). In phosphabenzene, however, the rigidity of the rest of the ring prevents a change in the CPC angle and prevents a decrease in the diffuseness of the lone pair through rehybridization. A strong bond cannot form.

A number of correlations have established that proton affinities (basicities) are closely related to core-ionization energies.[11-17] Since core ionization is a vertical process, it is sensitive only to the electronegativity of the atom ionized (that is, to its electronic ability to accept positive charge), to the electronegativity of the surrounding atoms, and to the ability of the surrounding atoms to delocalize the positive charge. Protonation, on the other hand, is adiabatic and depends not only on the factors just mentioned, but also on the ability of the molecule to undergo geometric rearrangement. The failure of the proton-affinity–core-ionization point for a compound to fall on the correlation line established by other compounds suggests that it undergoes different geometric rearrangements than do the reference compounds.[14] A comparison of the proton-affinity and core-ionization data for phosphabenzene and arsabenzene with those for phosphines and arsines should give information on the importance of geometric rearrangement in the protonation of these substances. We report here on such a comparison.

Experimental Section

Sample Preparation. Arsabenzene and phosphabenzene were synthesized according to methods described by Ashe.[2] Phosphine was prepared by reaction of calcium phosphide with water and purified by distillation under vacuum. Trimethylarsine was purchased from Strem Chemicals, Inc., and used without further purification. Arsine was obtained from one of our colleagues.

Measurements. X-ray photoelectron spectra and Auger spectra of the gaseous substances were measured in the Oregon State University cylindrical mirror analyzer.[18] Aluminum Kα radiation was used to excite the arsenic samples. For the phosphorus samples we used an anode containing both aluminum and silver. The aluminum X-rays provided the phosphorus 2p photoelectron spectra while the silver Lα X-rays excited the KLL Auger transitions.

For the arsenic measurements the sample gases were mixed with argon for calibration.[19] The argon 2p line is close to the arsenic $L_2M_{4,5}M_{4,5}$ Auger peaks and to the arsenic 3s photoemission peak, and, consequently, the spectrum for calibrant and sample could be run in one sweep. Typical results for the three arsenic compounds are shown in Figure 1. The value of the spectrometer constant was determined by comparison of the positions of the argon 2p and LMM Auger peaks, which were run simultaneously. The spectra were also run without argon, in order to establish the shape of the Auger spectrum without interference from the Al K$\alpha_{3,4}$ satellite of the argon spectrum.

The phosphorus samples were run mixed with neon; the neon Auger

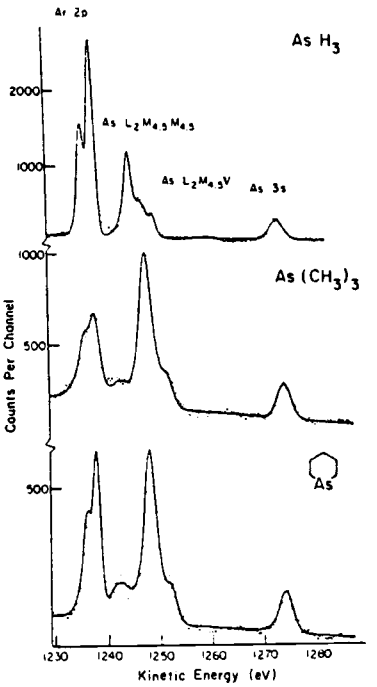

Figure 1. Argon 2p, arsenic LMM Auger, and arsenic 3s electron spectra for arsine, trimethylarsine, and arsabenzene. The argon was included for calibration purposes. The solid lines represent least-squares fits to the data.

(^1D) line[19] and the neon 1s line[19] excited by silver $L\alpha_1$ radiation (2984.31 eV[20]) were used for calibration.

Peak positions were determined by least-squares fits of Gaussian functions to the data; the solid lines in Figure 1 represent these fits. The ionization potentials and Auger kinetic energies are summarized in Table I. Except for arsine, each result is the average of at least two measurements; the root mean square difference between duplicate measurements is 0.1 eV.

Discussion

There are well-established linear correlations between core-ionization potentials and proton affinities (or Lewis basicities) for oxygen, nitrogen, and phosphorus compounds.[11-17] In general, the slope of these lines is close to minus one. The reason for this relationship is that removal of an electron from an atom is electrically equivalent to addition of a proton; the principal difference between the two processes is that electron removal is vertical whereas proton addition is adiabatic. If, however, there is no change in geometry during protonation, or if all molecules of a given series of compounds undergo similar geometrical changes on protonation, then we expect to find good correlations between proton affinities and core-ionization energies. For molecules containing oxygen and nitrogen the geometry of the protonated species is similar to that of the neutral species. A good linear correlation with slope minus one has been reported by Cavell and Allison[16] for nitrogen compounds, including pyridine. For the phosphines[14] the slope of the correlation has been reported to be −0.6; the deviation from unity has been attributed to the substantial geometric change that occurs on protonation of the phosphines.

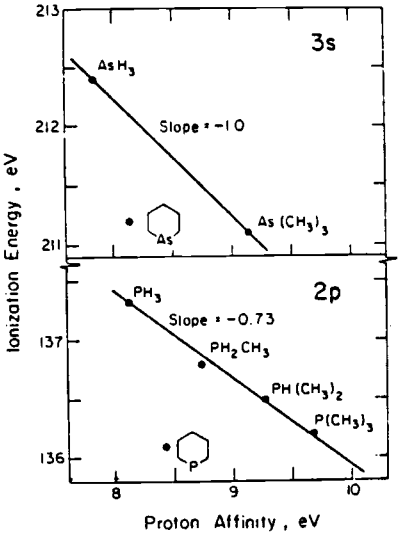

Figure 2. Correlation between core-ionization energy and proton affinity for arsenic and phosphorus compounds. The arsenic data and the points for phosphabenzene and phosphine are from this work. The other phosphorus points are from ref 14, normalized to our data at phosphine.

Table I. Core-Ionization Energies and Auger Kinetic Energies for Arsenic and Phosphorus Compounds

compd	core-ionization energy, eV[a]	Auger kinetic energy, eV[b]
AsH_3	212.4	1245.1
$As(CH_3)_3$	211.1	1247.9
arsabenzene	211.2	1248.2
PH_3	137.3	1841.4
phosphabenzene	136.1	1845.3

[a] 3s for arsenic, 2p multiplet average for phosphorus. [b] $L_2M_{4,5}M_{4,5}(^1G)$ for arsenic, KLL (^1D) for phosphorus.

The correlations between proton affinity and core-ionization potential for arsenic and phosphorus compounds are shown in Figure 2. For proton affinities we have used the data reported by Hodges, Beauchamp, and Ashe.[9,21] The arsenic core-ionization energies are those we have measured. For the phosphorus compounds we have used the shifts reported by Mills, Martin, and Shirley,[14] normalized to our absolute value for phosphine. We note first that the data for phosphines and arsines fall on lines with slopes −0.73 and −1.0, respectively. The difference between the slope of −0.73 given here and that of −0.6, reported by Mills, Martin, and Shirley, arises from our use of more recent values of the proton affinities. The difference in slope between the phosphorus and arsenic compounds is surprising, since the arsines and phosphines both undergo the same sort of geometric change on protonation.

The significant point to be noted in Figure 2 is the large deviation of the arsabenzene and phosphabenzene points from the lines established by the arsines and phosphines. In particular, the proton affinities are substantially lower than would be expected from the core-ionization energies. The situation here is in contrast to that for the corresponding nitrogen compounds, where the aliphatic and aromatic amines all fall on the same correlation line.[16]

For the nitrogen compounds, the bond angles (HNH, HNC,

Table II. Relative Relaxation Energies for Arsenic Compounds Derived from Auger and Core-Ionization Energies

compd	ΔR, eV
AsH_3	0
$As(CH_3)_3$	0.75
arsabenzene	0.95

and CNC) in the unprotonated species are close to those of the protonated species. No geometric rearrangement takes place and, hence, the data for the aliphatic and aromatic compounds are on the same line. For the phosphorus and arsenic compounds, the bond angles change significantly on protonation of the aliphatic species; a stabilization of the protonated species results from this rearrangement. A similar rearrangement is not possible for arsabenzene and phosphabenzene, with the result that their proton affinities and basicities are anomalously low compared to those of the arsines and phosphines. Comparison of the data for arsabenzene and phosphabenzene with the correlation lines indicates that this molecular rearrangement energy is about 0.9 eV for the arsines and about 1.4 eV for the phosphines. These numbers are only approximate, since, as has been noted by Mills, Martin, and Shirley,[14] the molecular rearrangement energy varies as hydrogen is replaced by methyl in the phosphine series.

For an order of magnitude theoretical estimate of this rearrangement energy, we have done CNDO/2 calculations of the energy of a PH_4^+ ion in two configurations. The first is the tetrahedral geometry, representing the ground state of the ion. In the second, three hydrogens have HPH bond angles of 93.3°, as in neutral phosphine. The fourth hydrogen is at the position of an added proton. This species represents the ion before geometric rearrangement has taken place. For both species the bond length was 1.42 Å. The difference in energy between these two species is 0.5 eV, significantly smaller than our experimental estimate, but of the same magnitude.

Additional information about the source of the basicity can be obtained from a comparison of core-ionization energies with Auger energies.[22-29] The proton affinity depends on three factors: the charge distribution in the original molecule (initial-state effect), charge rearrangement after protonation (final-state effect—the positive charge is delocalized over the molecule), and geometric rearrangement (as discussed above). Since core ionization is a vertical process, the core-ionization energy depends only on the first two of these. The shift in core-ionization energy, ΔE, relative to that in some reference compound, can be written as

$$\Delta E = \Delta E_I - \Delta R \qquad (1)$$

where ΔE_I is the shift due to the initial-state charge distribution and ΔR is that due to the rearrangement of the valence electrons to redistribute the positive charge. The Auger kinetic energies also depend on these two quantities. For the Auger kinetic energy, K, the corresponding expression is approximately

$$\Delta K = -\Delta E_I + 3\Delta R \qquad (2)$$

The sum of the core-ionization-energy shift, ΔE, and the Auger kinetic-energy shift, ΔK, is equal to $2\Delta R$, or twice the contribution of electronic relaxation to the core-ionization shift. It should be noted that the factor 2 depends on an assumption of constant polarizability of the surrounding medium (in the classical derivation of expressions 1 and 2) or on an assumption that certain different Coulomb matrix elements are equal to one another (in the quantal derivation). Experimental evidence suggests that it might be as large as 3.

Inspection of the positions of the various peaks in Figure 1 shows that the Auger 3s spacing is noticeably greater for arsine than for either trimethylarsine or arsabenzene. Values of ΔR (relative to arsine) derived from comparison of the Auger energies and core-ionization energies (using the factor of 2 discussed above) are given in Table II. The electronic relaxation energy for trimethylarsine and arsabenzene is significantly greater than that for arsine. This is the expected result; the species attached to arsenic in trimethylarsine and arsabenzene are much more polarizable than the hydrogens of arsine. It is also to be noted that the relaxation energy for arsabenzene is about 0.2 eV higher than that for trimethylarsine. This result presumably reflects the possibility of resonance delocalization of the positive charge in arsabenzene that is not possible for trimethylarsine. The relaxation due to resonance structures is probably greater than this 0.2-eV difference, since there are three carbons attached to the arsenic in trimethylarsine and only two in arsabenzene. A more appropriate comparison would be between arsabenzene and dimethylarsine. By linear interpolation between arsine and trimethylarsine, we estimate the electronic relaxation-energy shift between dimethylarsine and arsabenzene to be 0.45 eV. This energy represents approximately the extra stability gained by the protonated arsabenzene through resonance delocalization of the positive charge. This value, which corresponds to about 43 kJ/mol, is reasonable. It is large enough to be chemically significant but still small compared to the total resonance stabilization energy of the benzene ring (151 kJ/mol).[30] Phosphabenzene and arsabenzene provide a unique opportunity to measure this effect directly, since (1) they incorporate a readily identifiable heteroatom into the ring, and (2) the Auger transition (which is core to core in second- and third-row atoms) can be used to measure the relaxation.

Equations 1 and 2 can also be solved to give ΔE_I, the part of the shift that is due to the initial state charge distribution. From these equations we have

$$\Delta E_I = (3\Delta E + \Delta K)/2$$

For trimethylarsine and arsabenzene, relative to arsine, the values of ΔE_I are −0.55 and −0.25 eV, respectively. From this we conclude that in the neutral molecule the methyl group or the aromatic ring is relatively electron donating compared to hydrogen. Although this result is at odds with the usual ideas about the relative electronegativities of hydrogen and carbon, the same conclusions are reached from similar considerations of germanium compounds,[29] from theoretical calculations on gas-phase acidities and basicities,[31] and from comparisons of experimental core-ionization potentials with gas-phase acidities and basicities.[17]

Summary

For phosphabenzene and arsabenzene the data on the core-ionization energy and proton affinity fall well off the correlation line for the phosphines and arsines. This result is consistent with the belief that the low basicity of phosphabenzene and arsabenzene is due to the inability for these molecules to change their configuration after protonation. From the experimental data it is possible to estimate that the phosphines gain 1.4 eV on rearrangement after protonation and the arsines 0.9 eV.

Comparison of the Auger kinetic energies with the core-ionization energies makes it possible to estimate the relative extra-atomic relaxation energy for the various compounds. Of particular interest is the comparison between arsabenzene and dimethylarsine, which gives a measure of the extra relaxation associated with the resonance delocalization of charge in the aromatic ring.

Acknowledgments. We are indebted to J. W. Nibler for providing us with the arsine and some of the trimethylarsine used in these experiments and to R. G. Cavell and D. A. Allison

for helpful comments. This work was supported in part by the National Science Foundation. Acknowledgment is made to the donors of the Petroleum Research Fund, administered by the American Chemical Society, for partial support of this research.

References and Notes

(1) (a) University of Michigan; (b) Oregon State University.
(2) A. J. Ashe, III, *J. Am. Chem. Soc.*, 93, 3293 (1971).
(3) A. J. Ashe, III, *J. Am. Chem. Soc.*, 93, 6690 (1971).
(4) A. J. Ashe, III, *Tetrahedron Lett.*, 415 (1976); A. J. Ashe, III, and M. D. Gordon, *J. Am. Chem. Soc.*, 94, 7596 (1972).
(5) A. J. Ashe, III, *Acc. Chem. Res.*, 11, 153 (1978).
(6) C. Batich, E. Heilbronner, V. Hornung, A. J. Ashe, III, D. T. Clark, U. T. Cobley, D. Kilcast, and I. Scanlan, *J. Am. Chem. Soc.*, 95, 928 (1973); J. Bastide, E. Heilbronner, J. P. Maier, and A. J. Ashe, III, *Tetrahedron Lett.*, 411 (1976); A. J. Ashe, III, F. Burger, M. Y. El-Sheikh, E. Heilbronner, J. P. Maier, and J.-F. Muller, *Helv. Chim. Acta*, 59, 1944 (1976).
(7) A. J. Ashe, III, R. R. Sharp, and J. W. Tolan, *J. Am. Chem. Soc.*, 98, 5451 (1976).
(8) T. C. Wong and L. S. Bartell, *J. Chem. Phys.*, 61, 2840 (1974); T. C. Wong, A. J. Ashe, III, and L. S. Bartell, *J. Mol. Struct.*, 25, 65 (1975); R. L. Kuczkowski and A. J. Ashe, III, *J. Mol. Spectrosc.*, 42, 457 (1972); R. P. Lattimer, R. L. Kuczkowski, A. J. Ashe, III, and A. L. Meinzer, *ibid.*, 57, 428 (1975); R. L. Kuczkowski, G. Fong, and A. J. Ashe, III, *ibid.*, 70, 197 (1978).
(9) R. V. Hodges, J. L. Beauchamp, and A. J. Ashe, III, to be published.
(10) H. Oehling and A. Schweig, *Phosphorus*, 1, 203 (1971); H. Oehling and A. Schweig, *Tetrahedron Lett.*, 4941 (1970); D. T. Clark and I. W. Scanlan, *J. Chem. Soc., Faraday Trans. 2*, 70, 1222 (1974).
(11) R. L. Martin and D. A. Shirley, *J. Am. Chem. Soc.*, 96, 5299 (1974).
(12) D. W. Davis and J. W. Rabalais, *J. Am. Chem. Soc.*, 96, 5305 (1974).
(13) T. X. Carroll, S. R. Smith, and T. D. Thomas, *J. Am. Chem. Soc.*, 97, 659 (1975).
(14) B. E. Mills, R. L. Martin, and D. A. Shirley, *J. Am. Chem. Soc.*, 98, 2380 (1976).
(15) F. M. Benoit and A. G. Harrison, *J. Am. Chem. Soc.*, 99, 3980 (1977).
(16) R. G. Cavell and D. A. Allison, *J. Am. Chem. Soc.*, 99, 4203 (1977).
(17) S. R. Smith and T. D. Thomas, *J. Am. Chem. Soc.*, 100, 5459 (1978).
(18) P. H. Citrin, R. W. Shaw, Jr., and T. D. Thomas in "Electron Spectroscopy", D. A. Shirley, Ed., North-Holland Publishing Co., Amsterdam, 1972, p 105.
(19) T. D. Thomas and R. W. Shaw, Jr., *J. Electron Spectrosc. Relat. Phenom.*, 5, 1081 (1974).
(20) J. A. Bearden, *Rev. Mod. Phys.*, 39, 78 (1967).
(21) It is not clear that protonation takes place at the heteroatom. If not, the proton affinities for protonation at the heteroatom are presumably smaller than the values given in *ref* 9. The points for arsabenzene and phosphabenzene would then lie even further from the correlation line for the arsines and phosphines.
(22) C. D. Wagner and P. Biloen, *Surf. Sci.*, 35, 82 (1973).
(23) S. P. Kowalczyk, R. A. Pollak, F. R. McFeely, L. Ley, and D. A. Shirley, *Phys. Rev. B*, 8, 2387 (1973).
(24) S. P. Kowalczyk, L. Ley, F. R. McFeely, R. A. Pollak, and D. A. Shirley, *Phys. Rev. B*, 9, 381 (1974).
(25) C. D. Wagner, *Faraday Discuss., Chem. Soc.*, 60, 291 (1975).
(26) H. Siegbahn and O. Goscinski, *Phys. Scr.*, 13, 225 (1976).
(27) L. Asplund, P. Kelfve, H. Siegbahn, O. Goscinski, H. Fellner-Feldegg, K. Hamrin, B. Blomster, and K. Siegbahn, *Chem. Phys. Lett.*, 40, 353 (1976).
(28) M. K. Bahl, R. O. Woodall, R. L. Watson, and K. J. Irgolic, *J. Chem. Phys.*, 64, 1210 (1978).
(29) W. B. Perry and W. L. Jolly, *Chem. Phys. Lett.*, 23, 529 (1973).
(30) R. T. Morrison and R. N. Boyd, "Organic Chemistry", 3rd ed., Allyn and Bacon, Boston, 1973, p 324.
(31) D. W. Davis and D. A. Shirley, *J. Am. Chem. Soc.*, 98, 7898 (1976).

2. Extended x-ray-absorption fine-structure amplitude attenuation in Br_2: Relationship to satellites in the x-ray photoelectron spectrum.

PHYSICAL REVIEW A VOLUME 20, NUMBER 6 DECEMBER 1979

Extended-x-ray-absorption fine-structure amplitude attenuation in Br_2: Relationship to satellites in the x-ray photoelectron spectrum

K. D. Bomben, M. K. Bahl, J. K. Gimzewski, S. A. Chambers, and T. D. Thomas
Department of Chemistry and Radiation Center, Oregon State University, Corvallis, Oregon 97331
(Received 24 July 1979)

That observed amplitudes of extended-x-ray-absorption fine structure (EXAFS) are less than those calculated theoretically has been attributed to the failure of the theory to take into account multielectron excitations during core ionization. To investigate this possibility, the authors have measured the satellite spectrum accompanying ionization of 3*d* electrons from Br_2 by aluminum x rays. There is approximate agreement between the amplitude attenuation calculated from these experiments and that determined from EXAFS data, provided one assumes that shakeup occurs only if the outgoing photoelectron has a kinetic energy of several hundred eV, and makes allowance for a small contribution from high-energy satellites in the shakeup spectrum that would not be observed in the present experiments.

INTRODUCTION

Extended-x-ray-absorption fine structure (EXAFS) has become an important tool for the investigation of molecular structure[1] and has provided information on chemical and biological systems that is not available through the use of other techniques. Although theory has been successful in describing the overall shape of the EXAFS spectra, the predictions of the EXAFS amplitude are not in quantitative agreement with those found experimentally.

In a study of the EXAFS spectrum of Br_2, Kincaid and Eisenberger[2] found the experimental amplitude of the EXAFS oscillations to be about half of that calculated theoretically. More recent measurements by Stern, Heald, and Bunker[3] show that there is no discrepancy for photon energies close to the absorption edge ($k < 5$ Å^{-1}) but that the experimental amplitude is 20% lower than the theoretical value at higher photon energies.

It was suggested[2,4,5] that the theoretical amplitudes are higher than those observed experimentally because the theory did not include multielectron processes—valence-shell excitation during core-hole production. Two types of such excitations are possible. If, in addition to the excitation of a core electron into the continuum, a second electron is excited into an unoccupied bound state, that process is termed "shakeup." If the second electron populates a continuum level, then that is termed "shakeoff." These effects are seen as satellite structure in the photoelectron spectrum.

Lee and Beni[5] pointed out that shakeup and shakeoff will give rise to EXAFS spectra of their own, which are shifted in energy from the main spectrum by an amount equal to the excitation energy of the ion. The total EXAFS is a sum of these individual contributions; there should, therefore, be a relationship between the satellites of the photoelectron spectrum and the amplitude attenuation of the EXAFS spectrum. They suggested that shakeoff electrons are spread over such a wide range of energies that any EXAFS feature associated with this process will be smeared out. Using shakeup data from neon, they concluded that the contribution to the EXAFS spectrum from shakeup is negligible. Their overall conclusion was that the calculated EXAFS amplitude should be multiplied by the relative weight of the main peak (0.74 for Ne) before comparison is made to experimental data. Empirically, they found that a factor of 0.62 gives reasonably good agreement between theory and the experimental results for Br_2 available at the time.

Rehr, Stern, Martin, and Davidson[4] have considered the role of shakeup and shakeoff in the EXAFS spectrum of bromine in more detail. From Hartree-Fock-Roothaan calculations, they conclude that only 64% of the core ionizations in Br_2 lead to the ground state of the ion. Although this result is in good agreement with the empirical factor of 0.62 found by Lee and Beni, they note that there is no compelling argument for ignoring the contributions from multielectron excitations. When they include estimates for shakeup and shakeoff, the calculated EXAFS attenuation factor becomes 0.7 ± 0.04, somewhat higher than Lee and Beni's value and lower than the most recent experimental results.

To provide experimental evidence on the role of valence-shell excitations in the attenuation of an EXAFS spectrum, we have measured the x-ray photoelectron spectrum for Br_2. The observed shakeup and shakeoff spectrum accounts reasonably well for the EXAFS amplitude providing that we allow for excitation of electrons from the $n = 3$ shell, which would not be observed in our mea-

surements but which might be present in the EXAFS experiments, and for the fact that there will be no shakeup or shakeoff if the outgoing electron has very low energy. The fraction of the photoionization leading to shakeup and shakeoff is about 0.38, in agreement with the value of 0.36 calculated by Rehr *et al.*

EXPERIMENTAL PROCEDURE AND RESULTS

Br_2 was obtained commercially and used without further purification. Vapor was introduced into the Oregon State University cylindrical-mirror electrostatic analyzer[7] sample chamber and irradiated with Al $K\alpha$ x rays. For comparison with the EXAFS spectrum, it would have been more appropriate to look at the bromine 1*s* photoelectron spectrum; however, the high K-shell ionization energy precludes measurement of these electrons in our system. It is possible to ionize the 2*s* and 2*p* levels using a gold anode; the resolution is, however, poor, especially for the 2*s* level. Furthermore, the $2p_{1/2}$ and $2p_{3/2}$ levels are separated by 46 eV, so that the $2p_{1/2}$ spectrum interferes with the shakeoff spectrum for the $2p_{3/2}$ level. Similar problems exist for the 3*s* and 3*p* levels. We have chosen the 3*d* level, with an ionization energy of 77.8(2) eV, for our measurements. The spin-orbit splitting is small enough that we observe one reasonably sharp line. Since the 3*d* level is not a deep core level, we can expect that some features of satellite structure that would be present in the 1*s* spectrum will be absent from the 3*d* spectrum. The 3*d* spectrum should, however, contain most of the valence-shell excitations. Data we have taken for the 2*p* and 3*p* levels are consistent with those for the 3*d* level, but less well resolved.

The shakeup and shakeoff satellites arise from processes that are intrinsic to the photoemission event. The spectrum as measured, however, contains contributions from other processes. During the measurement, it is necessary to keep the sample pressure low in order to eliminate or minimize contributions from inelastic scattering to the low-energy portion of the spectrum. In addition, it is necessary to correct for a background that arises from photoelectrons produced by bremsstrahlung and inelastically scattered electrons from other parts of the spectrum. We have studied the pressure dependence of the spectrum from 0.1 to 8 Pa (as measured using a McLeod gauge connected to the sample chamber). Below about 3 Pa, the spectra were independent of pressure. The data reported here were taken at pressures of about 1 Pa.

The EXAFS amplitude calculated from the photoelectron spectrum is somewhat sensitive to the background corrections that are made to the data. We have made this correction in two steps. First, a constant background equal to the average number of counts on the high-energy side of the $K\alpha_{3,4}$ satellite was assumed. That this method is approximately correct is shown in Fig. 1, where we compare our measurements of the neon 1*s* satellite spectrum, after such a background subtraction, with that reported by Gelius.[8] Except for differences in resolution, there is excellent agreement between the two sets of data. The bromine spectrum is shown in Fig. 2, with the satellite region magnified for clarity. A constant background of 920 counts is shown as the horizontal solid line in this figure.

Second, it was necessary to allow for inelastic

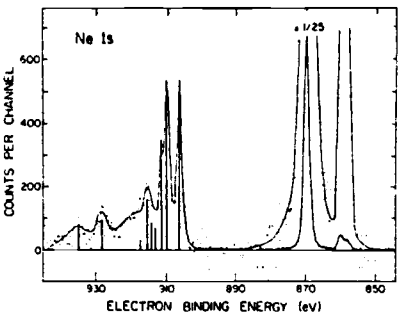

FIG. 1. X-ray photoelectron spectrum of 1*s* electrons from neon excited by aluminum x rays. A background equal to the average intensity on the high-energy side of the $K\alpha_{3,4}$ satellite has been subtracted from the data. The vertical lines show the positions and intensities reported by Gelius (Ref. 8).

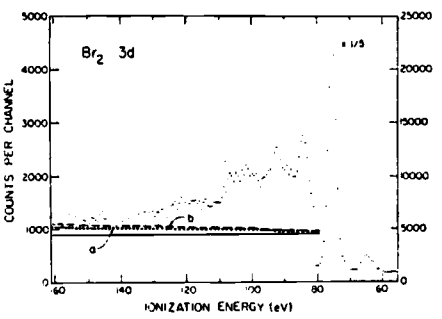

FIG. 2. X-ray photoelectron spectrum of 3*d* electrons from Br_2 excited by aluminum K x rays. The satellite region is amplified relative to the main peak. The line *a* represents our best estimate of the background.

processes associated with the bromine $3d$ peak that are not accounted for by our pressure-dependence measurements. In particular, there is the possibility of inelastic scattering from the walls of the gas cell and analyzer slits, which should give rise to a broad background on the low-kinetic-energy side of the main peak. Such a background is indistinguishable from shakeoff. We have taken this background to be represented by the dotted line (labeled a) in Fig. 2, which begins at 920 counts on the right and rises to the left with a slope determined by the following method. The average energy over the photoelectron spectrum (taking the main peak as zero) is, according to the Manne-Åberg sum rule,[9] equal to the difference between the Koopmans-theorem energy and the true ionization energy. Desclaux's[10] value for the Koopmans-theorem energy and that of Huang, Aoyagi, Chen, Craseman, and Mark[11] for the fully relaxed energy give 9.0 eV for the atomic relaxation energy. We add to this 1.5 eV, calculated by Martin and Davidson,[12] for the extra-atomic relaxation in Br_2. The slope of line a was then chosen so that the spectrum remaining after background subtraction gives an average energy of 10.5 eV. The intersection of this line with our data falls in a region where the shakeoff spectrum from the $3d$ line is obscured by the $K\alpha_{3,4}$ satellite of the $3p$ line (slightly to the left of the data shown in Fig. 2). To account for this part of the spectrum, which we cannot measure, we have added 185 channels (115 eV) of exponential tail to the data, normalized to the leftmost point in Fig. 2. The slope of the added tail is the same as that for the data, which fall exponentially. Different theoretical estimates of the relaxation energy vary by as much as 1 eV. Line b (dashed) shows the background that gives a relaxation energy of 9.6 eV. The effect of these different choices on the EXAFS amplitude is discussed below.

The data shown result from the excitation by both the $K\alpha_{1,2}$ and $K\alpha_{3,4}$ x rays. Under the conditions of our experiment, the $K\alpha_{3,4}$ peak is 9.4% of the main peak at a separation of 10.5 eV. To correct for this, we subtracted from each channel 9.4% of the counts in the channel 10.5 eV lower in kinetic energy. This correction on our analysis of the EXAFS amplitude is about 1%.

Furthermore, for a spectrometer such as ours, with fixed $\Delta E/E$ (where ΔE is the resolution and E is the kinetic energy of the detected electron), the measured intensities must be divided by the energy to obtain correct relative intensities. This correction has been made, but has only a small effect on our calculations of EXAFS amplitudes (about 1% over the energy range we have considered).

TABLE I. Relative intensities and energies in the Br_2 $3d$ photoelectron spectrum

Peak	Relative intensity	Relative energy (eV)
Main	0.62	0
1	0.064	8.6
2	0.092	16.8
3	0.059	25.0
4	0.045	30.4
5[a]	0.12	

[a] Shakeup and shakeoff greater than 33 eV.

The relative energies and intensities of the primary peak and four shakeup peaks were determined by using least-squares fitting of Gaussian functions. The first two columns of Table I give peak position and relative intensities determined from the data shown in Fig. 2 together with the exponential extension to lower energies described above. Without this extension, the relative intensity of the main peak is 0.63; with it, 0.62. Both are in agreement with a value of 0.64 ± 0.04 calculated by Rehr *et al.* for Br_2. Their calculation includes shakeup and shakeoff from core as well as valence levels, with about 6% of the $1s$ ionizations being accompanied by other inner-shell excitations.[13] Since no core shakeup would be likely in our experiments, their number should be corrected for this difference. The comparison is then between 0.68 (theoretical) and 0.62 (experimental).

DISCUSSION

The normalized EXAFS spectrum χ is defined by Stern[14] in terms of the x-ray-absorption coefficient μ as

$$\chi = (\mu - \mu_0)/\mu_0 , \tag{1}$$

where μ_0 is the atomic absorption coefficient. For molecules with only one significant interatomic distance (i.e., Br_2 and $GeCl_4$) a number of authors[15-18] have shown that χ may be represented as

$$\chi_0(k) = (|f_a|/kR^2)\sin[2kR + 2\delta_0(k)] \times \exp(-\gamma R - 2\sigma^2 k^2) , \tag{2}$$

where k is the wave vector of the outgoing electron, R is the interatomic distance, f_a is the backscattering amplitude, σ^2 is the mean-square fluctuation of the distance R due to molecular vibration, $\delta(k)$ is an appropriate phase shift, and $e^{-\gamma R}$ is a decay factor that accounts for absorption of the electron as it travels through the molecule.

Rehr *et al.* have modified Eq. (2) to take account of multielectron excitations, each of which leads

to a new EXAFS spectrum $\chi_n(k)$. The primary effect of these processes is a shift ΔE_n in the energy of the EXAFS oscillations. This shift can be used to calculate $\chi_n(k)$ if the EXAFS of the primary process $\chi_0(k)$ is known

$$\chi_n(k) \simeq \chi_0(k^2 - 2\Delta E_n)^{1/2}. \tag{3}$$

The total EXAFS χ is

$$\chi = \sum_n S_n^2 \chi_n(k), \tag{4}$$

where S_n^2 is the probability of occurrence of $\chi_n(k)$.[19]

If one assumes that only the sine factor of Eq. (2) varies rapidly with k and that all other terms remain essentially constant, then one may approximate the attenuation of the EXAFS amplitude with the attenuation of the sine factor. Then setting $\delta_n(k) = \delta_0(k)$, as Rehr *et al.* have done, and defining a relative phase shift

$$\phi_n(k) = 2R[(k^2 - 2\Delta E_n)^{1/2} - k], \tag{5}$$

χ can be written

$$\chi = |A(k)|(|f_s|/kR^2)\sin[2kR + 2\delta_0(k) + \phi(k)] \times \exp(-\gamma R - 2\sigma^2 k^2), \tag{6}$$

where the amplitude-reduction factor $|A(k)|$ and the phase shift are determined from the expression

$$|A(k)|e^{i\phi(k)} = \sum_n S_n^2 e^{i\phi_n(k)}. \tag{7}$$

If the S_n^2 values are known as a function of ΔE_n, then $|A(k)|$ can be calculated from Eq. (7). Values of $|A(k)|$ determined with this expression and our data using several different assumptions (discussed below) are shown in Fig. 3. Also shown as the dashed curve are the recent experimental results of Stern *et al.*[3]

The simplest approach to evaluating the S_n^2 from the experimental data is to set them equal to the counts in each channel divided by the total number of counts in the spectrum. This is the principal method we have used. It is, however, more accurate to recognize that the true widths of the main peak and the shakeup satellites are narrower than we have observed experimentally. To investigate the effect of correction for the resolution, we have also done the calculations using a spectrum in which the counts for each peak have been collected into a single channel at the appropriate energy. The shakeoff continuum is left unchanged. Comparison of results obtained by the two methods shows that this effect is negligible.

The most important corrections are for background and for the high-ionization-energy portion of the shakeoff spectrum that was undetectable in our experiments because of interference from the bromine $3p$ photopeaks and their satellites. As discussed above, we have extended our data into the unmeasurable region using an exponential tail and have chosen the background so that the observed spectrum is consistent with the Manne-Åberg sum rule.

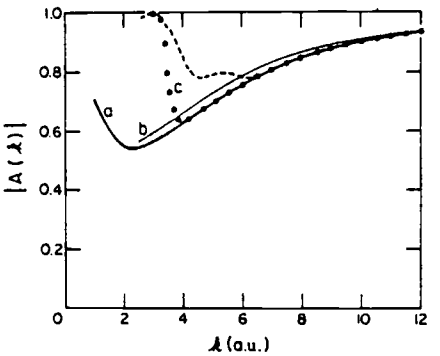

FIG. 3. EXAFS amplitude reduction factor as a function of k. The dashed curve represents the experimental results of Stern, Heald, and Bunker (Ref. 3). Curves a and b are calculated from the data of Fig. 2 with no threshold for shakeup, a being based on background curve a of Fig. 2 and b on background curve b. For curve c, the threshold is 225 eV ($k = 4$).

The first calculation of the EXAFS amplitude is based on the assumption that the shake spectrum is given by the data of Fig. 2 (corrected for background a), but is zero if the outgoing electron has zero or less kinetic energy. The corresponding result is shown as curve a of Fig. 3, where it is compared with the recent data of Stern *et al.*[3] (dashed curve). Also shown, as curve b, is the calculated amplitude assuming that the background is given by curve b of Fig. 2 or, equivalently, that the relaxation energy is 9.6 eV instead of 10.5 eV. We see that the amplitude is relatively insensitive to assumptions about the relaxation energy. The agreement between either line a or line b and the curve given by Stern *et al.* is poor, presumably because of our choice of zero energy as the threshold for shake to occur.

In the simplest view of shakeup and shakeoff, if the outgoing electron has a velocity less than or comparable to the velocities of the valence electrons, then the valence electrons should adjust adiabatically to the disappearance of the core electron and no shakeup or shakeoff should occur. There should, therefore, be no attenuation of the EXAFS spectrum at low-k values, a point that has been noted also by Stern *et al.*[3] Taking 25 eV as a typical kinetic energy of the valence electrons in

core-ionized Br_2 and assuming that the velocity of the outgoing electron should be at least three times the velocity of the electrons, we have 225 eV as the approximate threshold for shakeup and shakeoff. This value corresponds to $k \simeq 4$ a.u. Curve *c* of Fig. 3 has been calculated using this approximation. The agreement between this result and that of Stern *et al.* is reasonable, except that the calculated curve falls too sharply at threshold, and then rises more rapidly with increasing k than do the experimental results.

It is important to note, however, that core ionization of the 1*s* orbital, as in the EXAFS experiments, may include shakeup and shakeoff involving the $n=2$ and $n=3$ orbitals. On the other hand, in our experiments, core ionization of the 3*d* electrons, there should be little excitation of these inner orbitals. To investigate the effects of such inner-shell excitation, we have added an additional feature to our measured spectrum in the following way. First, the EXAFS experiments are below the threshold for simultaneous emission of a 1*s* electron and excitation of an $n=2$ electron. We expect, therefore, no contributions from $n=2$ excitations. The satellite spectrum for 1*s* ionization should, at these energies, be the same as for 2*s* or 2*p*. The energy averaged over this shake spectrum should, according to the Manne-Åberg sum rule, correspond to the relaxation energy associated with 2*s* or 2*p* ionization. From comparison of the calculations of Huang *et al.*[11] with those of Desclaux,[10] we calculate this relaxation energy to be 32 eV, of which 9 eV arises from valence shell excitations and the rest from excitations from $n=3$ orbitals.

Taking a weighted average of the ionization energy of the Br_2 3*s*, 3*p*, and 3*d* orbitals plus about 20 eV (to allow for the positive charge remaining after core ionization), we estimate an average shake energy from these levels to be 156 eV. Combining this with a relative intensity of 0.15 gives the desired relaxation energy of 32 eV. This satellite spectrum should begin at about 100 eV, the approximate ionization energy for 3*d* electrons from core-ionized Br_2. Our simulated $n=3$ shake spectrum rises sharply at 100 eV, and then falls exponentially with a slope chosen to give an average energy of 156 eV. The height of the initial rise is chosen to give a total relative intensity of 0.15.

Comparison between the experimental EXAFS amplitude and that calculated using this modification is shown in Fig. 4. As in Fig. 3, the dashed curve represents the data of Stern *et al.*,[3] the solid curve (*a*) is calculated with no threshold for shake, and the dotted curve (*b*) with a threshold of about 225 eV. We see, as expected, that the additional higher-energy satellites cause the calculated amplitude to level off at about 0.7, somewhat lower than the lowest value observed by Stern *et al.*

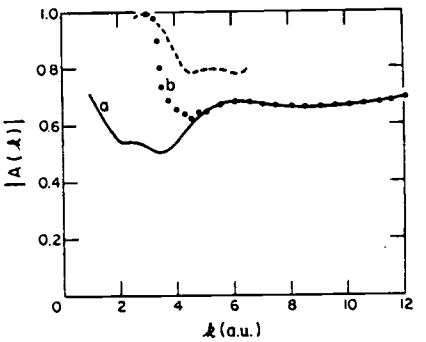

FIG. 4. EXAFS amplitude reduction factor as a function of k. The dashed curve represents the experimental results of Stern, Heald, and Bunker (Ref. 3). Additional structure has been added to the data of Fig. 2 to allow for shakeup and shakeoff from the $n=3$ shell, which should be present in the EXAFS experiments but not in ours. For curve *a*, a threshold of zero is taken for shakeup. For curve *b*, the threshold is 225 eV ($k=4$).

The threshold behavior we have chosen is unrealistic in that the shake processes do not come on abruptly as we have assumed in our calculations. As a result, the EXAFS amplitude should not drop so sharply as do the calculated curves of Figs. 3 and 4. Furthermore, the threshold for the $n=3$ processes should be much higher than the 225 eV we have chosen for valence electrons. The contribution of the $n=3$ satellites to the amplitude attenuation should, therefore, be less pronounced than is indicated by the curves of Fig. 4. Both of these corrections should bring the calculated EXAFS amplitude in closer agreement to that reported by Stern *et al.* We conclude, therefore, that the measured EXAFS amplitude and the bromine satellite spectrum are consistent with one another.

ACKNOWLEDGMENTS

We are indebted to both P. S. Bagus and R. L. Martin for suggesting this problem, to R. L. Martin for a number of helpful discussions, and to E. A. Stern, both for supplying us with his latest results before publication and for helpful comments. This work was supported in part by the National Science Foundation. Acknowledgment is made to the Donors of the Petroleum Research Fund, administered by the American Chemical Society, for partial support of this research.

[1]P. Eisenberger and B. M. Kincaid, Science 200, 1441 (1978).
[2]B. M. Kincaid and P. Eisenberger, Phys. Rev. Lett. 34, 1361 (1975).
[3]E. A. Stern, S. M. Heald, and B. Bunker, Phys. Rev. Lett. 42, 1372 (1979).
[4]J. J. Rehr, E. A. Stern, and M. Brown (unpublished).
[5]P. A. Lee and G. Beni, Phys. Rev. B 15, 2862 (1977).
[6]J. J. Rehr, E. A. Stern, R. L. Martin, and E. P. Davidson, Phys. Rev. B 17, 560 (1978).
[7]P. H. Citrin, R. W. Shaw, Jr., and T. D. Thomas, in *Electron Spectroscopy*, edited by D. A. Shirley (North-Holland, Amsterdam, 1972), p. 105.
[8]U. Gelius, J. Electron. Spectrosc. Relat. Phenom. 5, 985 (1974).
[9]R. Manne and T. Åberg, Chem. Phys. Lett. 7, 282 (1970).
[10]J. P. Desclaux, At. Data Nucl. Data Tables 12, 312 (1973).
[11]K.-N. Huang, M. Aoyagi, M. H. Chen, B. Craseman, and H. Mark, At. Data Nucl. Data Tables 18, 243 (1976).
[12]R. L. Martin and E. R. Davidson, Phys. Rev. A 16, 1341 (1977).
[13]R. L. Martin (private communication).
[14]E. A. Stern, Phys. Rev. B 10, 3027 (1974).
[15]D. E. Sayers, F. W. Lytle, and E. A. Stern, in *Advances in X-Ray Analysis*, edited by B. L. Henke, J. B. Newkirk, and G. R. Mallett (Plenum, New York, 1970), Vol. 13, p. 248.
[16]D. E. Sayers, E. A. Stern, and F. W. Lytle, Phys. Rev. Lett. 27, 1204 (1971).
[17]C. A. Ashley and S. Doniach, Phys. Rev. B 11, 1279 (1975).
[18]P. A. Lee and J. B. Pendry, Phys. Rev. B 11, 2795 (1975).
[19]The use of S_n^2 for probability follows the notation of Ref. 6. S_n is the monopole matrix element between the Koopmans-theorem state and the final ionic state. The probability for population of the state is the square of this matrix element.

3. Electron Spectroscopic Investigations of the Influence of Initial- and Final-State Effects on Electronegativity.

J. Am. Chem. Soc. 1980, 102, 4873-4879

Electron Spectroscopic Investigations of the Influence of Initial- and Final-State Effects on Electronegativity

E. J. Aitken, M. K. Bahl, K. D. Bomben, J. K. Gimzewski, G. S. Nolan, and T. D. Thomas*

Contribution from the Department of Chemistry and Radiation Center, Oregon State University, Corvallis, Oregon 97331. *Received January 14, 1980*

Abstract: Chlorine KLL Auger energies and 2p ionization energies in a variety of compounds have been used to investigate the role of initial- and final-state effects on electronegativity. Compounds studied are HCl, CH_3Cl, C_2H_5Cl, *n*-C_3H_7Cl, *i*-C_3H_7Cl, *t*-C_4H_9Cl, $CH_{4-n}Cl_n$, $CF_{4-n}Cl_n$, Cl_2, and ClF. The results obtained (together with similar data on phosphorus and germanium) agree with chemical experience and with theoretical calculations. They show that substituent polarizability (the final-state effect) increases in the order H ≈ F < CH_3 ≳ Cl < Br. The ability of the substituent to create a positive potential at a nearby site (initial-state effect) increases in the order CH_3 < H < Br < Cl < F if the substituent is directly attached to the site and CH_3 < H < Br ≈ Cl ≈ F if the substituent is remote from the site. These results together with related studies of carboxylic acids show that the influence of an alkyl group arises from its ability to disperse charge in the final state and that alkyl groups are either electron donating or electron withdrawing, as their environment demands.

Introduction

The concept of electronegativity, defined by Pauling[1] as the power of an atom in a molecule to attract electrons to itself, has been very useful to chemists. However, an exact, quantitative description of electronegativity remains elusive.

As an example of this elusiveness, it is notable that in the aqueous phase[2] the acidity of CH_2XCOOH decreases as X is varied from F to I, in keeping with the Pauling electronegativities[3] of the halogens, whereas in the gas phase[4] the order is reversed. In the latter case, the predicted order based on electronegativity clearly conflicts with the measured gas-phase acidities. A similar reversal between gas phase and aqueous phase is found in the acids RCOOH. The aqueous-phase acidities decrease as R is varied from CH_3 to C_3H_7, in keeping with the concept that alkyl groups are electron releasing and become more so with increasing size. In the gas phase, however, the order is once again reversed.[5]

These apparently contradictory observations can be reconciled if we assume that electronegativity arises from two, somewhat related, effects. On the one hand, the atoms compete with one another for electrons; on the other, the atoms are able to accept charge, either positive or negative. In the first, the atoms play an active role. This view is close to the usual concept of electronegativity—the power of an atom to attract electrons to itself. In the second, the atoms are passive; a large, polarizable atom lowers the total energy of the system by either contributing electrons to or receiving electrons from the rest of the molecule.

As an example, consider the substituents fluorine, chlorine, and an alkyl group. The electronegativity of fluorine is dominated by the first factor; it draws electrons strongly to itself but is only slightly polarizable. Chlorine also attracts electrons strongly, but, because of its large size it is more polarizable. In bonding terminology, chlorine is a σ acceptor and a π donor. Alkyl groups do not attract electrons, but are polarizable; the polarizability increases with size. They can, therefore, either give or receive electrons from the surroundings. In this respect, Ingold[6] has noted that "alkyl groups will exert essentially those polar effects which are impressed on them by the other polar groups present in the molecule".

The ability of a molecule to accept additional charge at a given site, through ionization, protonation, proton removal, or other chemical reactions, is influenced by these two factors in different ways. Conceptually we divide such processes into two steps, (1) the interaction of the new charge with the ground-state, or initial-state, charge distribution of the molecule and (2) the rearrangement of that distribution to accommodate the new charge. Since the ground-state charge distribution is dominated by the competition between the atoms for electrons, it is influenced most strongly by the first of the factors that determine electronegativity, and only to a lesser extent by the second. The rearrangement, or relaxation, of the charge distribution upon arrival of new charge is, on the other hand, determined entirely by the second factor. We can, therefore, approximately equate a substituent's electron-withdrawing power to an initial-state effect and its polarizability to a final-state effect.

This separation of energies into two parts, one due to the initial-state charge distribution and the other to the final-state rearrangement, is similar to that used in theoretical analyses of hydrogen bond energies.[7] In particular, Kollman and Allen[7a] have proposed a decomposition of the hydrogen bond energy into an electrostatic-plus-exchange contribution (which depends only on initial-state properties) and a polarization-plus-charge-transfer contribution (which depends on the difference between initial- and final-state properties).

Using these concepts, we can readily account for the relative gas-phase acidities mentioned above. For the acids RCOOH, the initial-state effect is approximately independent of the size of the R group, and the final-state effect, which stabilizes the anion, increases with the size of R.[5,8] As a result, the predicted anion stabilities and gas-phase acidities are in the order acetic < propionic < butyric, in agreement with experiment. For the halogenated acids, the explanation is essentially the same.[4] The initial-state effect, though large, is nearly the same for fluorine, chlorine, and bromine. However, the polarizability increases with atomic size, and the acidity increases with the polarizability of the substituent.

In solution, the final-state effect arises from the polarization of the solvent in addition to polarization of the substituent. The solvent effect will be greatest for the smallest substituent, since, in this case, the solvent molecules are closest to the carboxyl anion.

(1) Pauling, L. C. "The Nature of the Chemical Bond", 2nd ed.; Cornell University Press: Ithaca, NY, 1948; p 58.
(2) Morrison, R. T.; Boyd, R. N. "Organic Chemistry", 3rd ed.; Allyn and Bacon: Boston, MA, 1973; p 600.
(3) Reference 1, pp 64–66.
(4) Hiraoka, K.; Yamdagni, R.; Kebarle, P. *J. Am. Chem. Soc.* **1973**, *95*, 6833.
(5) Yamdagni, R.; Kebarle, P. *J. Am. Chem. Soc.* **1973**, *95*, 4050.
(6) Ingold, C. K. "Structure and Mechanism in Organic Chemistry", 2nd ed.; Cornell University Press: Ithaca, NY, 1969; p 80.
(7) (a) Kollman, P. A.; Allen, L. C. *Theor. Chim. Acta* **1970**, *18*, 399. (b) Morokuma, K. *J. Chem. Phys.* **1971**, *55*, 1236. (c) Dreyfus, M.; Pullman, A. *Theor. Chim. Acta* **1970**, *19*, 20. (d) Kollman, P. A. "Modern Theoretical Chemistry", Schaefer, H. F., III, Ed.; Plenum Press: New York, 1977; Vol. 4, pp 109–151.
(8) (a) Brauman, J. I.; Blair, L. K. *J. Am. Chem. Soc.* **1968**, *90*, 6561. (b) *Ibid.* **1970**, *92*, 5986.

[Reprinted from the Journal of the American Chemical Society, 102, 4873 (1980).]

The effect on acidity of the solvent is, therefore, F > Cl > Br > I, which is the reverse of the effect of the substituent itself. In aqueous solution, the polarizability of the solvent dominates and the order of acidity is reversed from that in the gas phase. An alternate but equivalent view is that replacement of a small fluorine atom with a larger halogen also involves displacement of nearby solvent molecules by the halogen. If the halogen is less polarizable than the solvent (as is the case for aqueous solutions), the acidity is lowered. If the halogen were more polarizable, then the acidity would be raised.

Core-ionization energies, measured by X-ray photoelectron spectroscopy (XPS), provide a probe by which these effects can be studied. Early works[9-12] in this field have shown that there are systematic correlations between the core-ionization energies of a particular atom in a molecule and quantities related to the electronegativities of the substituents. In particular, Thomas[12] showed that the carbon 1s ionization energy in halogenated methanes varies linearly with the electronegativity of the substituents. Later research,[13-20] in particular that by Martin and Shirley[13] and by Davis and Rabalais,[14] pointed out similar correlations between gas-phase proton affinities (basicities) and core-ionization energies and established the importance of relaxation, or final-state effects, in determining both core-ionization energies and basicities. This approach has been extended to gas-phase acidities by Davis and Shirley[21] (theoretically) and by Smith and Thomas[19] (experimentally). From comparison of gas-phase acidities and basicities with core-ionization energies, Smith and Thomas determined the relative contributions of initial-state and final-state effects to the gas-phase acidity of a number of carboxylic acids. Their conclusions are in accord with the concepts outlined above.

The core-ionization energies are, like the other chemical properties, affected by both the initial-state charge distribution and the final-state relaxation. Only when other information, such as gas-phase acidities, is available, is it possible to sort out the relative importance of these effects. One source of such information is the Auger kinetic energies for the same atom for which the core-ionization energies have been measured. It has long been recognized that whereas the absolute magnitude of the core-ionization energies and Auger kinetic energies are about equally affected by initial-state effects, the Auger energies are considerably more responsive to final-state effects than are the core-ionization energies.[22,23] As a first approximation we may express the shift, ΔI, in core-ionization energy between two compounds as

$$\Delta I = \Delta V - \Delta R \tag{1}$$

where ΔV represents the initial-state effect and ΔR the final-state effect. The corresponding expression for the shift in Auger kinetic energies, ΔK, is

$$\Delta K = -\Delta V + 3\Delta R \tag{2}$$

The Auger parameter α, as defined by Gaarenstroom and Winograd,[24] is the sum of the core-ionization energy and Auger kinetic energy. Thus

$$\Delta\alpha = 2\Delta R \tag{3}$$

If I and K are measured simultaneously, then charging and reference level effects cancel out in the determination of ΔR. Because of this cancellation, this technique can be, and has been, used to determine relative relaxation energies in solids,[25,26] even though the relative shifts ΔI and ΔK may be uncertain. The evaluation of ΔV from eq 1 and 2 requires a correct knowledge of both ΔI and ΔK, referenced to the vacuum level, with the result that full exploitation of this technique is limited to gas-phase studies. Few gas-phase measurements of the Auger parameter have been reported,[20,25,27,28] and, in general, these have focused on ΔR and have not been concerned with ΔV.

We report here the measurement of I and K for chlorine in a variety of compounds RCl and XCl (R = H, CH_3, C_2H_5, n-C_3H_7, i-C_3H_7, t-C_4H_9, CH_2Cl, $CHCl_2$, CCl_3, CF_3, CF_2Cl, $CFCl_2$; X = F, Cl). The purpose of this work has been to obtain, through eq 1-3, quantitative information on initial- and final-state effects (ΔV and ΔR), to show that these results are consistent with chemical intuition and simple theory, and further, to determine the relative importance of these two effects on electronegativity. Chlorine is a particularly suitable element for this investigation, since it can be incorporated into a wide variety of molecules.

Table I. Chlorine 2p Core-Ionization and KLL (^1D) Auger Kinetic Energies (eV)

	compd	$2p_{1/2}$	$2p_{3/2}$	KLL
1	CH_3Cl	207.90	206.26	2374.51
2	CH_2Cl_2	208.25	206.62	2375.15
3	$CHCl_3$	208.50	206.86	2375.52
4	CCl_4	208.73	207.04	2375.72
5	CCl_3F	208.81	207.20	2374.93
6	CCl_2F_2	209.10	207.47	2374.18
7	$CClF_3$	209.44	207.83	2373.30
8	Cl_2	209.45	207.82	2373.72
9	ClF	210.83	209.18	2370.73
10	HCl	209.01	207.38	2371.98
11	C_2H_5Cl	207.56	205.92	2375.46
12	n-C_3H_7Cl	207.45	205.81	2375.77
13	i-C_3H_7Cl	207.25	205.62	2376.17
14	t-C_4H_9Cl	207.00	205.38	2376.64

Experimental Section

All samples were obtained from commercial sources and used without further purification. Measurements on Cl_2 and ClF were made after enough gas had passed through the sample cell so that no evidence of impurities remained. Without such pretreatment, reaction of the sample gas with substances adsorbed on the spectrometer surfaces would give rise to impurity peaks in the spectrum.

X-ray photoelectron and Auger spectra were measured in the Oregon State University cylindrical mirror analyzer.[29] Neon was included with the sample gas to provide calibration lines. Aluminum Kα X-rays were used to excite the chlorine 2p electrons of the sample and the neon 1s and 2s calibration lines.[30,31] For the Auger measurements, X-rays from a silver anode were used to excite chlorine KLL Auger electrons, and the calibration was based on the neon KLL (^1D) Auger line[30] and the neon 1s line excited by silver Lα_1 radiation (2984.31 eV[32]). In all of the

(9) Siegbahn, K.; Nordling, C.; Fahlman, A.; Nordberg, R.; Hamrin, K.; Hedman, J.; Johansson, G.; Bergmark, T.; Karlsson, S.-E.; Lindgren, I.; Lindberg, I. "ESCA, Atomic, Molecular and Solid State Structure Studied by Means of Electron Spectroscopy"; Almqvist and Wiksell: Uppsala: Sweden, 1967; pp 101-139.
(10) Hamrin, K.; Johansson, G.; Fahlman, A.; Nordling, C.; Siegbahn, K. *Chem. Phys. Lett.* **1968**, *1*, 557.
(11) Nordberg, R.; Albridge, R. G.; Bergmark, T.; Ericson, U.; Hedman, J.; Nordling, C.; Siegbahn, K.; and Lindberg, B. J. *Ark. Kemi* **1968**, *28*, 257.
(12) Thomas, T. D. *J. Am. Chem. Soc.* **1970**, *92*, 4184.
(13) Martin, R. L.; Shirley, D. A. *J. Am. Chem. Soc.* **1974**, *96*, 5299.
(14) Davis, D. W.; Rabalais, J. W. *J. Am. Chem. Soc.* **1974**, *96*, 5305.
(15) Carroll, T. X.; Smith, S. R.; Thomas, T. D *J Am. Chem. Soc.* **1975**, *97*, 659.
(16) Mills, B. E.; Martin, R. L.; Shirley, D. A. *J. Am. Chem. Soc.* **1976**, *98*, 2380.
(17) Benoit, F. M.; Harrison, A. G. *J. Am. Chem. Soc.* **1977**, *99*, 3980.
(18) Cavell, R. G.; Allison, D. A. *J. Am. Chem. Soc.* **1977**, *99*, 4203.
(19) Smith, S. R.; Thomas, T. D. *J. Am. Chem. Soc.*, **1978**, *100*, 5459.
(20) Ashe, A. J., III; Bahl, M. K.; Bomben, K. D.; Chan, W.-T.; Gimzewski, J. K.; Sitton, P. G.; Thomas, T. D. *J. Am. Chem. Soc.* **1979**, *101*, 1764.
(21) Davis, D. W.; Shirley, D. A. *J. Am. Chem. Soc.* **1976**, *98*, 7898.
(22) Wagner, C. D.; Biloen, R. *Surf. Sci.* **1973**, *35*, 82.
(23) Shirley, D. A. *Phys. Rev. A* **1973**, *7*, 1520.
(24) Gaarenstroom, S. W.; Winograd, N. *J. Chem. Phys.* **1977**, *67*, 3500.
(25) Wagner, C. D. *Faraday Discuss. Chem. Soc.* **1975**, *60*, 291.
(26) (a) Bahl, M. K.; Woodall, R. O.; Watson, R. L.; Irgolic, K. J. *J. Chem. Phys.* **1976**, *64*, 1210. (b) *Ibid.* **1978**, *68*, 3272.
(27) Perry, W. D.; Jolly, W. L. *Chem. Phys. Lett.* **1973**, *23*, 529.
(28) Asplund, L.; Kelfve, P.; Siegbahn, H.; Gusczinski, O.; Fellner-Feldegg, H.; Hamrin, K.; Blomster, B.; Siegbahn, K. *Chem. Phys. Lett.* **1976**, *40*, 353.
(29) Citrin, P. H.; Shaw, R. W., Jr.; Thomas, T. D. In "Electron Spectroscopy"; Shirley, D. A., Ed.; North-Holland Publishing Co.: Amsterdam, 1972; p 105.
(30) (a) Thomas, T. D.; Shaw, R. W., Jr. *J. Electron Spectrosc. Relat. Phenom.* **1974**, *5*, 1081. (b) Johansson, G.; Hedman, J.; Berndtsson, A.; Klasson, R. *J. Electron Spectrosc. Relat. Phenom.* **1973**, *2*, 295.
(31) Moore, C. E. *Natl. Bur. Stand. (U.S.) Cir.* **1949**, No. 469.
(32) Bearden, J. A. *Rev. Mod. Phys.* **1967**, *39*, 79.

measurements small corrections were made for the recoil energy of the residual ion and for relativistic effects in the analyzer.[30a] Peak positions were determined by least-squares fits of Gaussian or Voigt functions to the data.

Results

The ionization energies and Auger kinetic energies are summarized in Table I. Each result is the average of at least two measurements. On the basis of the differences between duplicate measurements, we estimate a precision of 0.04 eV for the ionization energies and 0.05 eV for the Auger energies. Particular attention was given to the determination of the Cl_2 and ClF core-ionization energies in order to resolve apparent discrepancies between earlier measurements from this laboratory[33] and later ones by Perry and Jolly.[34] Our reported results for these two substances are the average of eight measurements for Cl_2 and six for ClF, of which about half were taken several years ago.[35] The value given in Table I for the Cl_2 $2p_{3/2}$ ionization energy (207.82 eV) is in excellent agreement with that reported by Perry and Jolly[36] and corrected by Jolly[37] (207.81 eV). For the 2s ionization energy, the new value of 278.71 eV is in good agreement with 278.66 eV given by Carroll and Thomas[33] and 278.74 eV by Holmes.[38] For ClF the new value of the chlorine 2s ionization energy (280.08 eV) is in substantial disagreement with the earlier[33] value of 279.23 eV. We cannot account for this discrepancy except to note that ClF reacts readily with adsorbed substances in the spectrometer, giving other chlorine-containing compounds. It is possible that Carroll and Thomas measured the photoelectron spectrum for these reaction products rather than that of ClF.

The $2p_{3/2}$ ionization energies in Table I for CH_3Cl, CCl_4, Cl_2, ClF, HCl, and $(CH_3)_3CCl$ are in excellent agreement with those given by Perry and Jolly[36] and corrected by Jolly.[37] The accuracy of our measurements is further supported by a series of six measurements of the argon $2p_{3/2}$ ionization energy we have made during the course of these experiments. The value of 248.59 eV is in excellent agreement with the value of 248.60 ± 0.05 eV reported by Thomas and Shaw[30a] and that of 248.62 ± 0.08 eV given by Johansson et al.[30b] Our value for the Auger kinetic energy in HCl agrees with that given by Cavell and Sodhi[39] well within their uncertainties of 0.5 eV.

Theoretical Framework

Equations 1 and 2, upon which our analysis is based, have been derived using both quantal[23,40] and classical[25] approaches. The physical principles involved can be demonstrated by a simple classical model, which is outlined below. A different approach, which includes higher order corrections, is presented elsewhere.[41]

The core-ionization energy is the difference between the energy of the initial species (with no core vacancies) and that of the final, core-ionized species. For a neutral free atom we take the first of these energies to be zero and, then, with use of the frozen-orbital approximation, the second is $-\epsilon_i$, where ϵ_i is the orbital energy of the ionized electron in the neutral free atom. For a free atom with valence charge[42] q (in units of the electron charge), we still take the first to be zero; the second becomes $-\epsilon_i + k_i q$, where k_i is a constant.

The orbitals are, however, not frozen, and, for cases of interest here, the atoms are not free. To account for these conditions, we assume that the initial atom is imbedded in a polarizable medium that produces a potential V'/e at this atom. Its energy becomes qV'. If no additional polarization took place upon core ionization, V' would remain constant, and the energy of the final state would be $-\epsilon_i + k_i q + (q + \Delta Z)V'$, where ΔZ is the change in total charge on core ionization ($\Delta Z = 1$). This change in charge does, however, cause an additional polarization of the medium with a lowering of the total energy by $\alpha'(\Delta Z)^2/2$, where α' is proportional to the polarizability of the medium.[43] The final state energy[44] is, then

$$E_f = -\epsilon_i + k_i q + (q + \Delta Z)V' - \alpha'(\Delta Z)^2/2 \quad (4)$$

Subtracting the initial-state energy, qV', and setting $\Delta Z = 1$, the ionization energy, I, is

$$I = -\epsilon_i + k_i q + V' - \alpha'/2 \quad (5)$$

The first three terms on the right represent properties of the initial atom and its interaction with the initial-state charge distribution. We combine $k_i q + V'$ into a single potential energy, V. The last term of eq 5 represents the relaxation energy, R. Thus

$$I = -\epsilon_i + V - R \quad (6)$$

The Auger transition goes from an initial state with vacancy i to a final state with two vacancies j and k. The initial-state energy is given by eq 4, which is the final-state energy for the photoemission process. The final-state energy for the Auger process, E_f', is

$$E_f' = -\epsilon_j + k_j q - \epsilon_k + k_k q + F_{jk} + (q + 2\Delta Z)V' - \alpha'(2\Delta Z)^2/2 \quad (7)$$

The first pair of terms represents the energy to remove electron j from the free atom with charge q; the second pair represents the energy for the same process involving electron k. F_{jk} is the interaction energy between these two electrons. The three terms $-\epsilon_k + k_k q + F_{jk}$ thus give the energy to remove electron k from an atom that has already lost electron j (in the frozen-orbital approximation). Interaction with the surroundings and relaxation of the passive electrons are accounted for by the remaining terms. It is assumed that the polarizability α' is independent of the total charge on the atom.

We further assume that $k_i = k_j = k_k$. This assumption is valid if all of the electrons are in the core, as is the case for the systems we have studied. Once again setting $\Delta Z = 1$ and subtracting eq 7 from eq 4 to give the Auger kinetic energy, K, we have

$$K = -\epsilon_i + \epsilon_j + \epsilon_k - F_{jk} - k_i q - V' + 3\alpha'/2 \quad (8)$$

The first three terms of eq 8 are properties of the free neutral atom, and the fourth is independent of chemical state for core electrons. Combining the first four terms into a single constant, K_0, and comparing the remaining terms with those of eq 5 we have

$$K = K_0 - V + 3R \quad (9)$$

In comparisons of core-ionization and Auger energies between different compounds, the constant terms $-\epsilon_i$ and K_0 cancel out, giving eq 1 and 2, $\Delta I = \Delta V - \Delta R$ and $\Delta K = -\Delta V + 3\Delta R$, respectively.

The key assumptions in deriving these expressions are (1) that orbital energies shift linearly with valence charge, (2) that the proportionality constants for these shifts are independent of the core level, (3) that the Coulomb interaction energy, F_{jk}, between pairs of core electrons is independent of chemical state, and (4) that the polarizability of the medium is independent of the atomic charge. This last assumption is equivalent to that made by

(33) Carroll, T. X.; Thomas, T. D. *J. Chem. Phys.* 1974, *60*, 2186.
(34) Perry, W. B.; Jolly, W. L., unpublished results.
(35) Avanzino, S. C.; Jen, J. S.; Jolly, W. L.; Thomas, T. D., unpublished results.
(36) Perry, W. B.; Jolly, W. L. *Inorg. Chem.* 1974, *13*, 1211.
(37) Jolly and Perry measured their ionization energies relative to argon $2p_{3/2}$, for which they took a core-ionization energy of 248.45 eV. More recent measurements[30] show that this value is too low by 0.15–0.17 eV. In an unpublished compilation of core-ionization energies, Jolly has corrected the original data of ref 36 for this difference.
(38) Holmes, S. A. M.S. Thesis, Oregon State University, 1974.
(39) Cavell, R. G.; Sodhi, R. *J. Electron Spectrosc. Relat. Phenom.* 1979, *15*, 145.
(40) Siegbahn, H.; Goscinski, O. *Phys. Scr.* 1976, *13*, 225.
(41) Thomas, T. D. *J. Electron Spectrosc. Relat. Phenom.*, in press.
(42) Valence charge is equal to the number of valence electrons in the ground-state neutral atom minus the number of valence electrons in the atom of interest. It does not include any contribution from core holes.
(43) The quantity α' is closely related to but not identical with the Auger parameter α. The relationship is established in the subsequent discussion. The factor of 2 has been included to reflect the fact that the total change in energy is half the interaction energy between the charge and the induced field and to eliminate a factor of 2 that would otherwise appear in the relationship between α and α'.
(44) Further refinements to the theory, discussed in ref 40 and 41, take into account that the valence charge q changes during core ionization.

Table II. Relaxation Energies and Initial-State Potentials Derived from the Auger Parameter Relative to CH_3Cl (eV)

compd	ΔR	ΔV
HCl	−0.71	0.41
CH_3Cl	0	0
CH_2Cl_2	0.50	0.86
$CHCl_3$	0.81	1.41
CCl_4	0.99	1.77
$CClF_3$	0.19	1.76
CCl_2F_2	0.44	1.65
CCl_3F	0.69	1.65
CCl_4	0.99	1.77
Cl_2	0.39	1.95
ClF	−0.43	2.49
CH_3Cl	0	0
C_2H_5Cl	0.31	−0.03
n-C_3H_7Cl	0.36	−0.08
i-C_3H_7Cl	0.52	−0.12
t-C_4H_9Cl	0.63	−0.25

Shirley,[23] in the corresponding quantum mechanical derivation, that V^*-V, the polarization potential due to a transition from 0 to 1 core vacancies, is equal to $V^{**}-V^*$, the polarization potential due to a transition from 1 to 2 vacancies.

In eq 6 and 9, R includes both atomic and extraatomic relaxation. It is assumed that the atomic relaxation is constant as an atom is shifted from one environment to another; consequently, ΔR of eq 1 and 2 depends only on the extraatomic relaxation, which in turn reflects the polarizability of the surrounding molecules.

As was noted in the introduction, combination of eq 1 and 2 leads to the relationship between the Auger parameter, α, and the relaxation energy, R, $\Delta\alpha \equiv \Delta I + \Delta K = 2\Delta R = \Delta\alpha'$ (eq 3). We see here that the relative Auger parameter is identical with the relative polarizability, $\Delta\alpha'$. The relationship between $\Delta\alpha$ and ΔR, eq 3, has not been verified experimentally. Adams[45] has theoretically calculated both $\Delta\alpha$ and ΔR for a number of chlorine-containing compounds and found that these values scatter fairly close to the line predicted by eq 3. The average difference between ΔR and $\Delta\alpha/2$ is 0.24 eV.

Siegbahn and Goscinski[40] have proposed further refinements to this model, taking into account that the relaxation during core ionization transfers charge to the ionized atom (in addition to polarizing the surroundings). In this case, the q's of eq 4 and 7 are not equal to one another nor to the charge of the original atom. Thomas[41] has considered the same problem from a different point of view. According to his results, the relationship between the Auger parameter and the relaxation energy is

$$\Delta\alpha = 2\left[\Delta R - \frac{2}{3}\Delta\frac{dk}{dN}\frac{dq}{dN}\right] \qquad (10)$$

where N is the number of core electrons, k is the proportionality constant between valence charge and potential energy of an electron (as in eq 4), and q is the valence charge. A very similar expression is given by Siegbahn and Goscinski, who also note that this additional term is large in some cases, amounting to 2.5 eV between CS_2 and SF_6. It will be seen below, however, that this correction is relatively small for the systems we are considering.

Discussion

The values of ΔR and ΔV (relative to those for CH_3Cl) determined from our measurements of ΔI and ΔK together with eq 1 and 2 are given in Table II. The entries are grouped to facilitate comparisons between similar compounds.

Hydrogen–Methyl Shift. The comparison of HCl with CH_3Cl and the series of compounds $(CH_3)_{3-n}CH_nCl$ show the effect of hydrogen vs. methyl. As expected, ΔR for hydrogen is negative compared to that of methyl, reflecting the greater polarizability of methyl. The sign of ΔV is positive for HCl. Both of these results agree with those obtained by Smith and Thomas[19] from comparisons of core-ionization energies with gas-phase acidities of carboxylic acids, and with those obtained by Ashe et al.[20] from comparison of AsH_3 with $As(CH_3)_3$. It is important to note that a positive ΔV does not necessarily imply that, in the ground state, hydrogen gives up negative charge to chlorine less readily than does methyl. V/e is the potential at the chlorine center and reflects not only the charge on the chlorine but also the field caused by surrounding charges. In methyl chloride, the positive charge is more delocalized and less effective at producing a positive potential at the chlorine than is the charge on hydrogen in HCl. CNDO/2 calculations indicate that the charge on chlorine in the two compounds is nearly the same and the ΔV arises largely from such delocalization. Recent calculations by Wiberg,[46] which indicate that the carbon in methyl chloride is negative, also support this view. (A similar situation exists for CF_3, which appears to be slightly electron donating but which produces a strong positive potential at an adjacent atom.[47])

Hydrogen–Fluorine Shift. The effect of replacing hydrogen with fluorine can be seen by comparing HCl with ClF or by comparing CH_3Cl with CF_3Cl. In each case we see that the change in ΔR is relatively small, +0.28 eV for the first comparison and +0.20 eV for the second. This small ΔR is consistent with the results obtained by Smith and Thomas. There is apparently little difference between the polarizability of H and F in these substances. This result explains why models that ignored relaxation could be applied to fluorinated hydrocarbons successfully.[12,48,49] The differential relaxation effects in such substances are small. The ΔV term is, as expected, large and positive. The presence of the fluorine atoms produces a positive potential at chlorine, either by direct withdrawal of electrons from the chlorine (as in ClF) or by withdrawal of electrons from the adjacent carbon (as is probably the case in CF_3Cl[47]).

Hydrogen–Chlorine Shift. The comparison between HCl and Cl_2 and comparison within the series of compounds $CH_{4-n}Cl_n$ show the effect of replacing hydrogen by chlorine. Because of the high polarizability of chlorine there is a large increase in relaxation energy between HCl and Cl_2 and also through this series. Similarly, because chlorine attracts electrons more strongly than does hydrogen, there is a corresponding increase in ΔV. These conclusions agree with those obtained by Smith and Thomas[19] in a comparison of the core-ionization energy and gas-phase acidity of CH_3COOH with those of $CH_2ClCOOH$.

The overall relaxation per chlorine is less in the halogenated methanes than in Cl_2, presumably because of the greater chlorine–chlorine distances in the methanes. The positive charge on the core-ionized atom in these compounds is less effective at polarizing the neighboring chlorines and interacts less effectively with the induced field than does the charge on the corresponding chlorine in Cl_2. According to a simple model,[8b] the total interaction energy should fall off as the fourth power of the distance. We note also that there is an apparent saturation of the relaxation energy in the chloromethanes. Although ΔR and ΔV increase with the number of chlorine atoms, the first spectator chlorine (in CH_2Cl_2) is nearly twice as effective as additional chlorines. Such saturation is in disagreement with the model given by Bahl et al.,[26b] which predicts a linear relationship between the total relaxation energy and the number of chlorines.

Chlorine–Fluorine Shift. Information on the chlorine–fluorine shift comes from the series $CCl_{4-n}F_n$, in which chlorines are replaced by fluorines, and from the comparison of Cl_2 with ClF. The relaxation energies are unambiguous: replacement of fluorine by more polarizable chlorine increases the relaxation energy. The effect is largest when the chlorine–chlorine distance is smallest.

(45) Adams, D. B. *J. Electron Spectrosc. Relat. Phenom.* 1977, *10*, 247.

(46) Wiberg, K. B. *J. Am. Chem. Soc.* 1979, 101, 1718.

(47) Holmes, S. A.; Thomas, T. D. *J. Am. Chem. Soc.* 1975, *97*, 2337.

(48) Davis, D. W.; Shirley, D. A.; Thomas, T. D. In "Electron Spectroscopy"; Shirley, D. A., Ed.; North-Holland Publishing Co.: Amsterdam, 1972; p 707.

(49) Davis, D. W.; Shirley, D. A.; Thomas, T. D. *J. Am. Chem. Soc.* 1972, *94*, 6565.

as is the case for replacing hydrogen with chlorine. Saturation of ΔR is not apparent in this series.

The values of ΔV for these compounds are of particular interest. Between Cl_2 and ClF there is a significant increase in ΔV, indicating that fluorine withdraws electrons from chlorine, in keeping with chemical intuition. There is, however, almost no effect on the value of ΔV from exchanging chlorine for fluorine on the halogenated methanes. A similar result has been reported by Smith and Thomas,[19] who found from studies of halogenated carboxylic acids (CH_2XCOOH) that $\Delta V_F = \Delta V_{Cl} = \Delta V_{Br} = 0.45$ eV.

We see from foregoing observations that the relative effects of halogen substituents depend on whether they are attached directly to the atom of interest, as in ClF, or remotely, as in CX_3Cl or CH_2XCOOH. In the first case, the relaxation contribution increases and the initial-state effect decreases as we go from F to Cl. If, however, the halogen is remote to the atom of interest, then the initial-state effect is the same for fluorine, chlorine, and bromine, and only the relaxation effect varies. This conclusion is completely in accord with the view expressed by Hiraoka et al.,[4] that the relative gas-phase acidities of the halogenated carboxylic acids are dictated by the relative polarizabilities of the halogens.

Chlorine–Methyl Shift. Comparison of CH_3Cl with Cl_2, of C_2H_5Cl with CCl_2H_2, of i-C_3H_7Cl with CCl_3H, and of t-C_4H_9Cl with CCl_4 shows that the relaxation energy for chlorine is greater than that for methyl. The difference is, however, small except in the first case, where the substituent is close to the atom of interest. The results of Smith and Thomas[19] for $CH_2ClCOOH$ and C_2H_5COOH indicate that chlorine and methyl have about the same relaxations. The same set of comparisons shows that ΔV is much larger for chlorine than for methyl.

Fluorine–Methyl Shift. The fluorine–methyl shift can be determined by comparison of ClF with CH_3Cl and $CClF_3$ with t-C_4H_9Cl. ΔR for methyl is greater than that of fluorine and ΔV is less, as expected.

Alkyl Groups. The series of compounds RCl with R = CH_3, C_2H_5, n-C_3H_7, i-C_3H_7, and t-C_4H_9 shows that ΔR increases with the size of the alkyl group. There is, however, only a slight variation in ΔV through the series. Both of these results agree with those obtained by Smith and Thomas from a comparison of CH_3COOH with C_2H_5COOH.

In a theoretical investigation of the proton affinities of alkyl halides,[50] Jorgensen has found that "the proton affinities of alkyl chlorides are controlled by the ability of the alkyl group to accommodate (the) positive charge" of the additional proton. Since protonation and core ionization both correspond to addition of a positive charge at the halogen and the subsequent redistribution of that charge over the molecule, there is a close correspondence between the factors that govern proton affinities and those that govern core-ionization energies.[13-20] What Jorgensen describes as the ability of the alkyl group to accomodate positive charge, we describe as the contribution of the alkyl group to the relaxation energy. Since the variation of ΔV through the series of alkyl halides is negligible our conclusion is the same as that of Jorgensen.

The effect of an alkyl group on the gas-phase acidity of carboxylic acids is, as noted in the introduction and verified by the measurements of Smith and Thomas, to stabilize the anion by dispersing the negative charge over itself. In this case, the alkyl group acts as an electron acceptor. During core ionization, as studied here, or in protonation,[13] the alkyl group stabilizes the final state by dispersing a positive charge over itself. Here the alkyl group acts as an electron donor. Thus, depending on the environment, alkyl groups act readily as either electron donors or electron acceptors. They generally behave as electron donors because, as Ingold[51] has pointed out, "the majority of commonly encountered substituents are attractors of electrons".

Comparisons with Other Work. Perry and Jolly[27] have measured the Auger parameter for a series of substituted germanes and have analyzed the results in terms of relaxation energies. Their data together with values of ΔV, which were not included in their work, are summarized in Table III.

Table III. Final-State Relaxation Energies (ΔR) and Initial-State Potentials (ΔV) for Germanium and Phosphorus Compounds (eV)

compd	ΔR	ΔV
	Germanium[a]	
GeH_4	0	0
$GeH_3(CH_3)$	0.30	−0.16
$GeH(CH_3)_3$	0.94	−0.33
GeH_3Br	0.53	1.28
GeH_3Cl	0.39	1.26
$GeBr_4$	1.44	3.49
$GeCl_4$	1.10	3.80
GeF_4	−0.29	4.36
	Phosphorus[b]	
PH_3	0	0
PCl_3	1.6	4.4
PF_3	0.1	4.8
$SPCl_3$	2.2	6.0
SPF_3	1.3	6.8
$OPCl_3$	1.7	5.7
OPF_3	0.4	6.3
PF_5	0.8	9.1

[a] Data from ref 27. [b] Data from ref 39 using phosphorus 2p core-ionization energies.

The conclusions to be drawn from the germanium results are very similar to those based on our measurements. The first three lines of Table III show the greater polarizability of methyl compared to hydrogen and that hydrogen creates a more positive environment at the germanium atom than does methyl. Comparison between GeH_4 and GeF_4 shows that the relaxation difference between hydrogen and fluorine is small (although of opposite sign to what we have observed). The relaxation differences between the halogens are large whereas the differential effects on the initial-state potential are relatively small. There is some evidence for the saturation of relaxation energy mentioned above. Some of these conclusions were noted by Perry and Jolly, who also pointed out that the order of polarizabilities derived from their results (F < H < CH_3 < Cl < Br) is consistent with optically determined polarizabilities. This is the same order as determined in our measurements except that we find H ≳ F.

Also summarized in Table III are values of ΔV and ΔR calculated from the phosphorus KLL Auger kinetic energies and 2p core-ionization energies reported by Cavell and Sodhi.[39] The conclusions are basically the same. The order of polarizabilities is H ≈ F < Cl. The values of ΔV for chlorine are, however, about the same as those for fluorine. We note that ΔR for sulfur is slightly greater than ΔR for oxygen, as might be expected.

Measurements of the Auger parameter for tellurium compounds have been reported by Bahl et al.[26b] Since the measurements were made in the solid phase, no ΔV information is available. The order of relaxation energies is hydrocarbon < OH < Cl ≳ O < Br < I, which agrees with the order we have found.

Comparison with Theoretical Models

Adams[45] has calculated total relaxation energies for chlorine in several compounds by using a contracted Gaussian basis set. Relative to CH_3Cl, these calculations give extraatomic relaxation energies of −0.77 eV for HCl and −0.50 eV for ClF, which compare favorably with the corresponding experimental values of −0.71 and −0.43 eV from Table II. The overall shifts in 2p ionization energies calculated by Adams are 1.48 eV for HCl and 2.84 eV for ClF, compared with experimental values of 1.12 and 2.92 eV, respectively.

Potential models have been developed by Davis and Shirley[52] with which it is possible to calculate ΔR and ΔV and, hence, ΔI and ΔK. Using these models and the CNDO/2 approximation (without d orbitals), we have calculated these quantities.

(50) Jorgensen, W. L. *J. Am. Chem. Soc.* **1978**, *100*, 1049.
(51) Reference 6, p 81.

(52) Davis, D. W.; Shirley, D. A. *J. Electron Spectros. Relat. Phenom.* **1974**, *3*, 137.

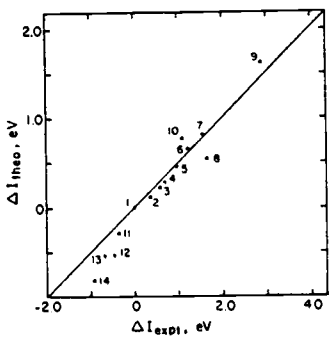

Figure 1. Chlorine core-ionization energy shifts calculated by using the relaxation-potential model and CNDO/2 wave functions plotted against the experimental shifts.

Figure 1 shows the theoretical shifts ($\Delta V - \Delta R$, or relaxation-potential model, RPM), relative to CH_3Cl, vs. the experimental shifts. The line has a slope of 1.00. Although there is some scatter about this line, it is clear that the theoretical model predicts the trend of the data. A least-squares fit to these points has a slope of 1.23.

A similar comparison has been made by Cavell and Sodhi[39] of phosphorus 1s and 2p experimental core-ionization energies with values from RPM calculations. A plot similar to that of Figure 1, with use of their data, shows comparable scatter and least-squares slopes of 1.13 for the 1s electron and 1.34 for the 2p. Cavell and Sodhi attribute the difference between these two slopes to "the more pronounced interaction of the 2p electrons with the valence shell electrons as compared to the 1s electrons". A similar effect might be important for the chlorine 2p electrons. These, however, have significantly higher ionization energies than do the phosphorus 2p electrons (207 eV for HCl compared with 137 eV for PH_3) and, therefore, are more corelike. This view is supported by the theoretical calculations of Adams,[45] which show that the chlorine 1s shifts are about 6% greater than the chlorine 2p shifts. The corresponding difference in phosphorus is 16% from the data of Cavell and Sodhi. An analysis we have presented elsewhere[41] suggests that, to correct for this effect, the chlorine 2p shift should be reduced by 6% before calculating $\Delta\alpha$. The effect of this correction of ΔR is about 0.09 eV for ClF and is less for all of the other compounds.

A comparison between experimental relaxation energies (relative to CH_3Cl) and those from RPM and GPM (ground-state potential model[32]) calculations using CNDO/2 wave functions is shown in Figure 2. Except for HCl the agreement is reasonably good, although the data deviate slightly from the line of unit slope. Consideration of higher order corrections[41] to eq 3 indicates that this method will give relaxation energies that are too high in proportion to the relaxation energy (eq 10 of this work). The deviation of the data (except for HCl) from the calculated values is in this direction.

A more quantitative analysis of the higher order terms[41] gives eq 10. The quantity dk/dN is negative and dq/dN is positive. The overall error is positive. The second factor, dq/dN, is the change in valence charge on core ionization and is easily obtained from the CNDO/2 calculations for the initial molecule and the core-ionized species (using the equivalent-cores approximation).

We can estimate values of k for Cl and its core-ionized species Cl^{*+} with the equivalent-cores approximation,[53] giving dk/dN = −4 eV/atomic charge unit. Siegbahn and Goscinski[40] have obtained values of k by using the orbital exponents ζ for the appropriate Slater orbital. For $n = 2$ orbitals $k = \zeta/2$ and ζ increases by $^1/_2$ as the core charge changes by 1. Hence, dk/dN = $-^1/_4$ au = −7 eV. Taking the first estimate, −4 eV, which is based on experimental quantities, we obtain the correction term for ΔR as $^8/_3\Delta(dq/dN)$.

(53) Jolly, W. L. In "Electron Spectroscopy"; Shirley, D. A., Ed.; North-Holland Publishing Co.: Amsterdam, 1972; p 629.

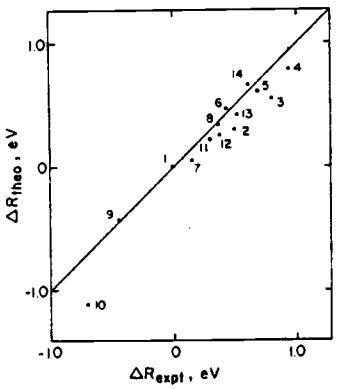

Figure 2. Theoretical relaxation energies plotted against those determined from the Auger parameter.

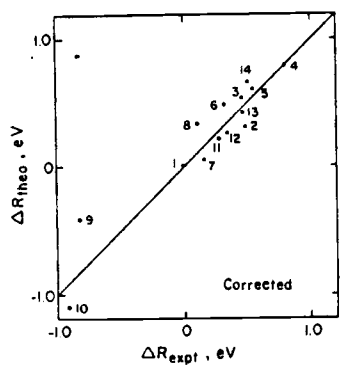

Figure 3. Theoretical relaxation energies plotted against those determined from the Auger parameter with higher order corrections.

We have applied the correction to the relative relaxation energies determined from the Auger parameter by using values of dq/dN from the CNDO/2 calculations. The results are compared with the theoretical calculations in Figure 3; the slope is now much closer to 1. The absolute values of the corrections are significant, about 0.4 eV for CCl_4. The relative corrections are, however, small, ΔR for CCl_4 changing from 0.99 to 0.80. The qualitative conclusions are unchanged.

It is interesting to note that the theory predicts the general trend of the relaxation energies (Figure 3) more accurately than it does the shifts in ionization energy (Figure 1). The former depend only on changes in the potential during ionization, whereas the latter depend also on the absolute value of the potential. Presumably, there are systematic errors in the absolute potentials that cancel when the changes in the potential are calculated.

Conclusions

The chemical effects that are included within the qualitative concept of electronegativity arise from two sources. First, a substituent affects the ground-stage charge distribution in the molecule by its ability to attract electrons to itself. Second, the ability of a molecule to accept charge (through protonation, proton removal, or ionization, for example) is influenced by the ability of the substituent to delocalize this charge.

Core-ionization energies and Auger kinetic energies can be combined to give direct and quantitative measurements of these

properties. The results obtained are in good agreement with chemical experience and simple theory. In particular, they show that the relaxation effect increases in the order H ≈ F < CH_3 ≳ Cl < Br. For alkyl groups the contribution increases with the size of the group. The relaxation energy decreases with distance between the substituent and the site at which the charge is being changed. For the initial state, the effect depends on whether the substituent is attached directly to the atom of interest or is more remote in the molecule. In the first case, the order is CH_3 < H < Cl < Br < F; in the second, CH_3 < H < Cl ≈ Br ≈ F. The striking results here are that hydrogen produces a more positive environment than does methyl and that halogens in remote positions affect the ground-state potential about equally.

The influence of an alkyl group on the initial-state charge distribution is, by definition,[9] essentially neutral. The effect of alkyl groups arises from their polarizability, or, equivalently, their ability to disperse charge. Comparison of the results obtained here with those from studies of carboxylic acid shows that an alkyl group can act either as an electron acceptor or as an electron donor, depending on the sign of the charge that must be dispersed.

Acknowledgments. This work was supported in part by the National Science Foundation. Acknowledgment is made to the donors of the Petroleum Research Fund, administered by the Americal Chemical Society, for partial support of this research. We are indebted to Leon Ungier for valuable comments.